

Connectivity-aware Synthesis of Quantum Algorithms

Florian Dreier,^{1, 2,*} Christoph Fleckenstein,^{2,*} Gregor Aigner,¹ Michael Fellner,^{1, 2}
Reinhard Stahn,³ Martin Lanthaler,^{1, 2} and Wolfgang Lechner^{1, 2, 3}

¹*Institute for Theoretical Physics, University of Innsbruck, A-6020 Innsbruck, Austria*

²*Parity Quantum Computing GmbH, A-6020 Innsbruck, Austria*

³*Parity Quantum Computing Germany GmbH, 20095 Hamburg, Germany*

(Dated: January 31, 2025)

We present a general method for the implementation of quantum algorithms that optimizes both gate count and circuit depth. Our approach introduces connectivity-adapted CNOT-based building blocks called Parity Twine chains. It outperforms all known state-of-the art methods for implementing prominent quantum algorithms such as the quantum Fourier transform or the Quantum Approximate Optimization Algorithm across a wide range of quantum hardware, including linear, square-grid, hexagonal, ladder and all-to-all connected devices. For specific cases, we rigorously prove the optimality of our approach.

I. INTRODUCTION

Quantum computers [1–5] promise a computational speedup for classically intractable problems ranging from efficient and accurate simulation of quantum systems [6, 7] over quantum chemistry [8] to financial modeling [9] and solving real world large scale optimization problems [10–12]. Recently, both quantum hardware and software experienced enormous leaps of improvements putting modern quantum hardware in the range of state-of-the art classical computing systems for specialized tasks [3, 5]. However, unlike for classical computation, present day quantum resources of near-term quantum hardware systems [13] are sparse which is why efficient quantum algorithms are crucial to leverage quantum advantage.

The efficiency of quantum algorithms can be measured by various means such as the total execution time [14, 15], the number of involved quantum operations [16], or the total count of specific costly operations [17]. Optimizations, measured according to these metrics, can be distinguished by dividing them into two groups: (i) hardware agnostic optimizations aiming to find more efficient algorithms, and (ii) optimizations improving the compilation of algorithms to fit the specific connectivity constraints of corresponding quantum devices. In fact, current quantum hardware rarely fits the algorithmic connectivity requirements so that ab initio implementations of (multi-body) quantum operations are often infeasible. Although there exist ion-based quantum computers that provide intrinsic all-to-all connectivity [18, 19], these are usually limited to a few tens of qubits. In many cases, quantum devices, in particular those where the position of the information carriers is physically fixed, provide two-dimensional grids of qubits with nearest-neighbor connectivity [20], like for example square [1, 5], hexagonal [3, 21] or octagonal [22] lattices. On such platforms, arbitrary connectivity is

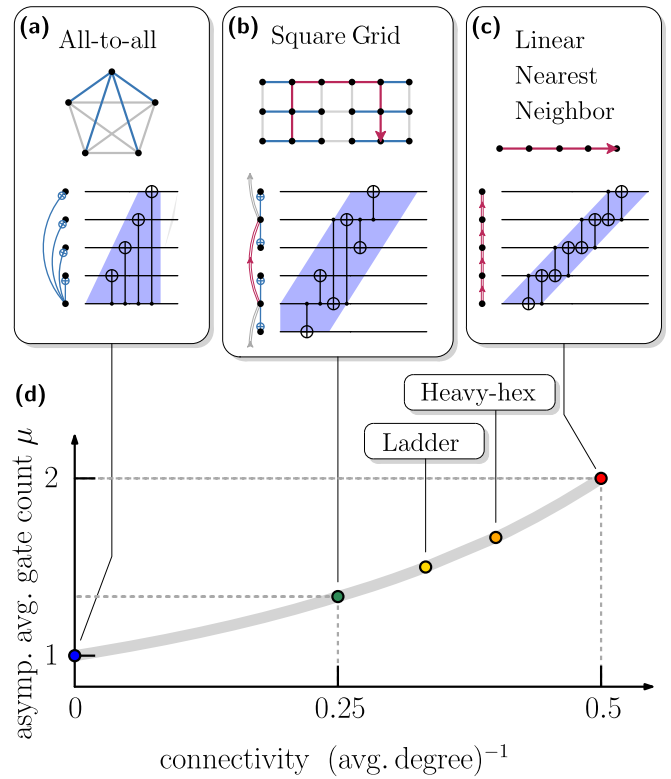


FIG. 1. The average asymptotic gate count as a function of connectivity ranging from linear nearest neighbor, square grid, heavy hexagon, ladder to all-to-all for algorithms considered in this work. The depicted Parity Twine chain constitute basic building blocks used throughout the article. The resulting average gate counts per interaction are schematically indicated as a function of the qubit layout connectivity. Connectivity gains lead to significant reductions in gate count approaching the theoretical optimum for all-to-all connected devices.

* These two authors contributed equally;
c.fleckenstein@parityqc.com
f.dreier@parityqc.com

typically emulated by costly SWAP networks [23–28] or shuttling operations [2, 29–32], maneuvering quantum states or physical qubits, respectively. Recently, parity label tracking was introduced as a compelling alternative to SWAP networks enabling the redesign of established

algorithms using heuristic routing algorithms [33, 34] and exact solutions [35]. In particular, the approach introduced in Ref. [35] utilizes aspects of the ZX-calculus [36] and combines them with the Lechner-Hauke-Zoller (LHZ) architecture for universal quantum computing [37–39]: Every physical qubit carries a logical parity label which can be altered by Clifford operations. Tracking of these labels throughout a circuit provides a means to understand the corresponding information flow and enables the design of efficient quantum algorithms.

Based on the parity label tracking approach, in this work we focus on optimizations of type (ii) for designing efficient, connectivity-aware quantum algorithms that implement logical many-body operators. More specifically, we propose a constructive approach for the design of gate-count- and depth optimized algorithms implementing logical many-body operators. Our approach is generic and easily adaptable to a wide range of contemporary quantum hardware. We present a generic construction recipe to implement quantum algorithms on specific hardware and we showcase the efficiency of our approach in five different exemplary platforms: linear nearest-neighbor (LNN) systems, all-to-all connected systems, square grids, heavy hexagon and ladder architectures. As a metric for the efficiency, we introduce the asymptotic measures μ and ν , where μ determines the average number of CNOT gates necessary to generate a single logical k -body operator and ν represents a normalized depth for an arbitrarily large number of qubits. To synthesize algorithm implementations, we use connectivity-adapted variations of so-called *Parity Twine* chains depicted in Fig. 1(c) for LNN devices and schematically indicated for all-to-all and square grids in (a) and (b). As connectivity of the underlying graph increases, we obtain reductions in the corresponding asymptotic average gate counts μ [see Fig. 1(d)], where eventually on all-to-all connected devices, our approach yields the provable optimal value $\mu = 1$. Tabs. I and II compare the results for implementations of quantum approximate optimization algorithms (QAOA) for quadratic unconstrained binary optimization (QUBO) problems (Tab. I) and the quantum Fourier transform (QFT, Tab. II) obtained within our formalism to the best known implementations outside our framework. Our approach outperforms alternative implementations on all the investigated platforms in gate count. Simultaneously, circuit depths are, at most, equivalent to the best known alternatives. Recursive extensions of Parity Twine chains allow us to synthesize logical k -body operators (with $k > 2$). Thereby the corresponding circuits for $k > 2$ inherit the average count from lower order leading to the results summarized in Tab. III.

The article is organized as follows. In Sec. II we introduce and recapitulate the label-tracking formalism used throughout the article. In Sec. III we introduce the quantities μ and ν and investigate fundamental properties regarding gate count and depth regarding the algorithms of interest. This is followed by Sec. IV A where we discuss in depth the different building blocks of our approach

Connectivity graph	QAOA ours				QAOA best known [27]			
	count	depth	μ	ν	count	depth	μ	ν
LNN	n^2	$2n(1 + \frac{1}{p})$	2	$2(1 + \frac{1}{p})$	$\frac{3}{2}n^2$	$3n$	3	3
heavy hexagon	$\frac{5}{2}n^2$	$\frac{5}{2}n(1 + \frac{1}{p})$	$\frac{5}{3}$	$\frac{5}{2}(1 + \frac{1}{p})$	$\frac{3}{2}n^2$	$3n$	3	3
ladder	$\frac{3}{4}n^2$	$\frac{3}{2}n(1 + \frac{1}{p})$	$\frac{3}{2}$	$\frac{3}{2}(1 + \frac{1}{p})$	$\frac{3}{2}n^2$	$3n$	3	3
square grid	$\frac{2}{3}n^2$	$3n(1 + \frac{1}{p})$	$\frac{4}{3}$	$3(1 + \frac{1}{p})$	$\frac{3}{2}n^2$	$3n$	3	3
all-to-all	$\frac{1}{2}n^2$	$n(1 + \frac{1}{p})$	1	$1 + \frac{1}{p}$	n^2	$2n$	2	2

TABLE I. Summary of the leading order terms of gate count and depth as well as the asymptotic average gate count μ , defined in Eq. (4), and the asymptotic normalized depth ν , defined in Eq. (5), of different implementations of QAOA (with p QAOA cycles) for various connectivity graphs. All provided values refer to count and depth per QAOA cycle. Our results refer to an odd number of QAOA cycles p . For even p we obtain slightly lower depth (cf. Sec. V A). We compare our results to the best known algorithms. As noted in Ref. [27] a linear chain represents the best known approach also for two-dimensional connectivity graphs. For heavy hexagon architectures, where no Hamiltonian path exists, this implies that not all qubits are used. Instead, the provided numbers are only valid for a sub-graph of the heavy hexagon layout. This is also the case in our approach, although with a different sub-graph (compare App. F for details).

exemplified on LNN devices. In Secs. IV B and Sec. IV C we generalize the concepts of Sec. IV A to a wide range of qubit-connectivity graphs and explicitly discuss complete graphs (Sec. IV B) as well as a number of planar graphs such as square grids and heavy hexagons (Sec. IV C). In Secs. V A and V B we apply our approach to optimization problems within the QAOA framework and the QFT. We conclude with a summary and an outlook in Sec. VI.

II. PARITY LABEL TRACKING AND k -BODY OPERATORS

Quantum computers inherently rely on entangling gates to systematically distribute information and perform computations. A typical (Clifford) gate utilized for this purpose is the CNOT gate. The logical action of a CNOT can be understood as encoding the parity information of the two qubits involved, the target and the control qubit, on one qubit. In the z -basis, a CNOT encodes the z parity information on the target qubit, while in the x basis a CNOT gate encodes the x parity information on the control qubit. To capture this abstract notion of the action of a CNOT on a set of physical qubits $Q = \{1, \dots, n\}$, we attribute to each qubit $j \in Q$ a logical parity label ℓ_j . If not explicitly stated differently, we interpret the labels ℓ_j as the logical z parity encoded on the qubit j . In this language the action of the CNOT gate $\text{CX}_{c,t}$ on the sequence of labels $\ell = (\ell_1, \dots, \ell_n)$ is given by

$$(\ell_1, \dots, \ell_n) \text{CX}_{c,t} = (\ell_1, \dots, \ell_{t-1}, \ell_t \Delta \ell_c, \dots, \ell_n), \quad (1)$$

where Δ denotes the symmetric difference operator. We adopt the notation that operators act from the right onto

Connectivity graph	QFT ours				QFT best known (count-optimized) [16]				QFT best known (depth-optimized) [40]			
	count	depth	μ	ν	count	depth	μ	ν	count	depth	μ	ν
LNN	n^2	$4n$	2	4	n^2	n^2	2	n	$\frac{3}{2}n^2$	$6n$	3	6
heavy hexagon	$\frac{5}{6}n^2$	$5n$	$1 + \frac{2}{3}$	5	n^2	n^2	2	n	$\frac{3}{2}n^2$	$6n$	3	6
ladder	$\frac{3}{4}n^2$	$3n$	$1 + \frac{1}{2}$	3	n^2	n^2	2	n	$\frac{3}{2}n^2$	$6n$	3	6
square grid	$\frac{2}{3}n^2$	$6n$	$1 + \frac{1}{3}$	6	n^2	n^2	2	n	$\frac{3}{2}n^2$	$6n$	3	6
all-to-all	$\frac{1}{2}n^2$	$2n$	1	2	n^2	$4n$	2	4	n^2	$4n$	2	4

TABLE II. Summary of the leading order terms of gate count and depth as well as the asymptotic average gate count μ , defined in Eq. (4), and the asymptotic normalized depth ν , defined in Eq. (5), of different implementations of the QFT for various connectivity graphs. We compare our results to the best known algorithms which amounts to the use of a linear chain approach for all the investigated connectivity graphs [27] (compare caption of Tab. I).

Connectivity graph	ours for $k > 2$	
	μ	ν
LNN	2	k
heavy hexagon	$1 + \frac{2}{3}$	$\frac{5}{3}k$
square grid	$1 + \frac{1}{3}$	$\frac{25}{12}k$ for $k = 3$ $\frac{7}{3}k$ for $k > 3$
all-to-all	1	$k/2$

TABLE III. Summary of the average CNOT count μ , defined in Eq. (4), and the normalized depth ν , defined in Eq. (5), for generator circuits \mathcal{G}_k (see Sec. IV A 2) with $k > 2$ for the different connectivity graphs investigated.

sequences of labels. In the following, we denote the symmetric difference of two labels with shorthand notation $\ell_c \ell_t := \ell_c \Delta \ell_t$ as well as we waive the set notation. For example, if the logical parity label ℓ_i contains the labels p and q we denote $\ell_i = pq$. Moreover, if not explicitly stated differently, we assume an initial state with logical parity labels $\ell_j = j$ for all $j \in Q$.

The logical parity labels together with the symmetric difference operation as an addition form a vector space V over $\text{GF}(2)$ where the empty set is the zero vector. Interpreting the $\text{CX}_{c,t}$ gate as an operator on the n -fold direct product V^n , the $\text{CX}_{c,t}$ operator is a bijective operator which maps label sequences that form a basis in V to another label sequences that are again a basis in V . Hence, starting with a label sequence which is a basis in V , the logical parity labels form a basis at any moment within a CNOT circuit. In particular, none of the labels will be empty. Moreover, transforming the $\text{CX}_{c,t}$ operator to an operator on $\text{GF}(2)^{n \times n}$, $\text{CX}_{c,t}$ can be viewed as a Gauss operation performing an addition of rows on matrices.

We define a *circuit* as a sequence of time steps - called *moments* - enumerated from 1 to d . Each of these moments contains a number of non-overlapping gates where we require for non-empty circuits at least one gate in the first and in the last moment. The *depth* of the circuit is d and the *gate count* or *size* is the number of gates contained in the circuit. To emphasize that a circuit C acts on n qubits we write $C^{(n)}$ and if the circuits only act on a subset of qubits $\{p, \dots, q\}$ we denote it with $C^{(p,q)}$. Moreover, $A \odot B$

denotes (a possibly shifted) concatenation of two circuits A and B , and C^\dagger the *adjoint circuit* of some unitary circuit C . Circuits may be used to map between two label sets ℓ and ℓ' : if ℓ and ℓ' both form a basis in V , then there exists a Clifford circuit C so that $\ell C = \ell'$ and $\ell' C^\dagger = \ell$.

In general, circuits can be described by specifying the unitaries to be implemented without detailing the actual implementation in terms of gates available on a quantum computer. However, this abstract description omits details that could be crucial for optimizations. Therefore, it is important to consider circuits composed solely of gates native to the quantum computer. Moreover, the fact that different circuits with various gate count and depths can produce the same unitary operator highlights another key reason why distinguishing between circuits and their corresponding unitary operators is essential. Consider for example a logical many-body rotation $\exp(-i\alpha \prod_{j \in \ell} Z_j)$: A concrete implementation on quantum hardware with access to CNOT and single-body rotation gates is given by

$$\exp \left(-i\alpha \prod_{j \in \ell} Z_j \right) = C \odot \text{RZ}_i(\alpha) \odot C^\dagger, \quad (2)$$

where we first use a CNOT circuit C to encode the label ℓ on, say, qubit i . This is followed by a single-body z rotation applied to qubit i , $\text{RZ}_i(\alpha) = \exp(-i\alpha Z_i)$, which in effect implements a logical many-body rotation associated with all qubits $j \in \ell$. Eventually, to regain the initial label sequence we use a decoding circuit C^\dagger . Note that in Eq. (2), the right-hand side is interpreted as the induced operator of the circuit composed of C , $\text{RZ}_i(\alpha)$ and C^\dagger . We emphasize that RZ gates act as the identity on the z parity labels which follows from the fact that RZ gates commute with each other. This in turn implies that the logical effect of a single RZ gate does not depend on other RZ gates in a circuit composed of CNOT and RZ gates.

Similarly, a series of logical operators can be encoded

with

$$\begin{aligned} \prod_{\ell \in L} \exp \left(-i\alpha_\ell \prod_{j \in \ell} Z_j \right) \\ = \bigodot_{(\ell, k) \in S} \left(C_{\ell, k} \odot \text{RZ}_k(\alpha_\ell) \odot C_{\ell, k}^\dagger \right), \end{aligned}$$

where L is a set of desired labels and S is set of tuples containing the labels of L paired with physical qubits k . The circuit $C_{\ell, k}$ produces the label ℓ at qubit k : The output label set just after $C_{\ell, k}$ contains label ℓ on physical qubit k . Note that the left hand side has no dependence on the physical qubits (specified only on the right-hand side by k). This reflects the fact that a logical operator is not aware of the device on which eventually it is implemented.

The inverse Clifford circuits $C_{\ell, k}^\dagger$ are used to decode the produced logical parity label to return to the initial label sequence after each application of a physical non-Clifford gate. This is where parity label tracking can yield an advantage: instead of decoding after every logical non-Clifford gate, the parity labels can be tracked and the next parity label can be encoded using potentially shorter CNOT circuits. Eventually, the decoding is applied once after the last physical non-Clifford gate

$$\begin{aligned} \prod_{\ell \in L} \exp \left(-i\alpha_\ell \prod_{j \in \ell} Z_j \right) \\ = \left(\bigodot_{p=1}^{|L|} C_p \odot \text{RZ}_{k(p)}(\alpha_{\ell(p)}) \right) \odot C_{\text{clean}} \quad (3) \end{aligned}$$

where $\bigodot_{i=1}^p C_i$ generates label $\ell(p)$ at qubit $k(p)$. The $\ell(p)$ enumerate the elements of L . Moreover,

$$C_{\text{clean}} = \bigodot_{p=1}^{|L|} C_{|L|-p+1}^\dagger.$$

Note that due to potential cancellations, the actual size and depth of the circuit C_{clean} can be significantly smaller than the above formula seems to imply. Furthermore, as long as the sequence of logical operators to encode [on the left-hand side of Eq. (3)] forms a pairwise commuting set, their order is irrelevant. However, depending on the order of physical operators [right-hand side of (3)], the corresponding CNOT circuits C_p can drastically differ in depth and count. Optimizing the order of physical operators with respect to the total gate count or depth of the corresponding CNOT circuits C_p is in general a NP-hard problem akin to the traveling salesman problem. A formal mathematical approach to parity labels, their properties and manipulation via circuits is provided in App. A.

III. AVERAGE GATE COUNT AND NORMALIZED DEPTH

In this article, we are mainly interested in z -diagonal non-Clifford gates, which leave the logical parity labels in the z basis unchanged. As long as we maintain the label tracking, relevant non-Clifford gates can always be inserted at corresponding moments of the circuit (i.e., just after a circuit C_p produced a logical label of interest). Thus, in the following we focus solely on the Clifford parts that *generate* the desired labels. Furthermore, throughout this article, we assume that Clifford circuits constitute CNOT circuits.

Consider n qubits and a set $L^{(n)}$ of non-trivial labels over these qubits. We say that a CNOT circuit $C^{(n)}$ *generates* the labels $L^{(n)}$ from a starting configuration $\ell = (\ell_1, \dots, \ell_n)$ if each label in $L^{(n)}$ appears at least in one moment of the circuit $C^{(n)}$. Note that if $C^{(n)}$ generates the labels $L^{(n)}$ from ℓ it also generates any subset of $L^{(n)}$. For such a generator circuit $C^{(n)}$ of the label set $L^{(n)}$ we define the *average CNOT count* as

$$\mu_n(C^{(n)}, L^{(n)}) = \text{size} \left(C^{(n)} \right) / |L^{(n)}|$$

with the total CNOT count size $(C^{(n)})$ of $C^{(n)}$. Furthermore, we define the *asymptotic average CNOT count* of some generator circuit family C and some label family L , where C contains circuits $C^{(n)}$ and L some label sets $L^{(n)}$ on n qubits, as

$$\mu(C, L) = \liminf_{n \rightarrow \infty} \mu_n(C^{(n)}, L^{(n)}). \quad (4)$$

A similar measure can be defined for the CNOT depth of the generator circuit family C . We recognize that every moment of $C^{(n)}$ allows at most $\lfloor n/2 \rfloor$ CNOT gates applied in parallel. Thus, we define

$$\nu(C, L) = \liminf_{n \rightarrow \infty} \frac{\text{depth} (C^{(n)}) n}{2|L^{(n)}|}, \quad (5)$$

where $\text{depth} (C^{(n)})$ denotes the depth of the CNOT circuit $C^{(n)}$ (see App. A.12). We leave out single-body gates in the gate count and depth analysis since they typically require significantly shorter execution times than two-body gates [41] and are not subject of the applied optimizations.

From Eq. (3) it is evident that every logical many-body operator can be associated with one pair of Clifford CNOT circuits combined with a physical single-body (non-Clifford) gate. The encoding of many-body operators thus requires at least one CNOT gate per many-body operator since we demand all many-body operators and the associated labels in $L^{(n)}$ to be different and generating logical parity labels can only happen via application of CNOT gates (or related two-body entangling gates). Thus, we conclude that for any generator circuit $C^{(n)}$ of $L^{(n)}$ we expect $\mu_n(C^{(n)}, L^{(n)}) \geq 1$ (see also App. A.14).

For efficient generator circuits with low average gate count of large enough label sets, expressed in the property $\lim_{n \rightarrow \infty} |L^{(n)}|/n = \infty$, we can draw some fundamental conclusions. For that, let us assume we find a generator circuit $C^{(n)}$ of $L^{(n)}$ with $\mu_n(C^{(n)}, L^{(n)}) = 1 + \gamma$, i.e., using only $(1 + \gamma)|L^{(n)}|$ CNOT gates. Then, using generic counting arguments, one can demonstrate that at least $(1 - \gamma)|L^{(n)}|$ of all $(1 + \gamma)|L^{(n)}|$ CNOT gates of $C^{(n)}$ transform labels $\ell \in L^{(n)}$ into other labels $\ell' \in L^{(n)}$, where ℓ' has not been generated in prior moments of $C^{(n)}$. For small $\gamma > 0$ almost all gates of $C^{(n)}$ have to act in this way. By this property, we call CNOT gates implementing the above mapping *typical* CNOT gates. With this in mind we can employ further counting arguments for LNN devices to find lower bounds for possible values of γ in the limit $n \rightarrow \infty$. In particular, in case the label set $L^{(n)}$ consists of labels which cannot be pairwise combined to form other labels of $L^{(n)}$, i.e., if $\ell_i \ell_j \notin L^{(n)}$ with $\ell_i, \ell_j \in L^{(n)}$, then $\gamma \geq \frac{1}{9}$ for $n \rightarrow \infty$ holds. This is notable since label sets with this property appear frequently in the subsequent sections. As an example, consider the set of all three-body labels for n qubits on a LNN device: combinations of two three-body labels cannot yield another three-body label. Similar considerations hold for all odd-bodied label sets or label sets where all labels share (at least) one constituent. In all these cases, an increased theoretical lower bound of $\mu \geq 1 + \frac{1}{9}$ holds. A detailed proof of the concepts outlined above can be found in App. I.

IV. CONNECTIVITY-OPTIMIZED k -BODY GENERATORS

A. LNN connectivity

1. Generator circuits for two- and three-body operators

In this section we recapitulate the circuit construction introduced in Ref. [35]. There, the authors present a *scalable* quantum circuit for LNN chains that generates *all* two-body labels with significantly reduced gate count and depth compared to established algorithms. When combined with corresponding physical non-Clifford single-qubit operators, this approach can be used to implement all relevant logical two-body operators diagonal in the z basis. As the authors demonstrate, this can be useful for algorithms like QAOA [11] or QFT.

The most prominent building block of the circuit outlined in Ref. [35] is a *double-controlled NOT (DCNOT)* gate [42], $\text{DX}_{c,t} = \text{CX}_{c,t} \odot \text{SW}_{c,t}$, which combines a CNOT gate with a corresponding SWAP gate acting on the same qubits. Using trivial operator identities, we observe for the induced operators

$$\begin{aligned} \text{DX}_{c,t} &= (\text{CX}_{c,t} \odot (\text{CX}_{c,t} \odot \text{CX}_{t,c} \odot \text{CX}_{c,t})) \\ &= (\text{CX}_{t,c} \odot \text{CX}_{c,t}). \end{aligned}$$

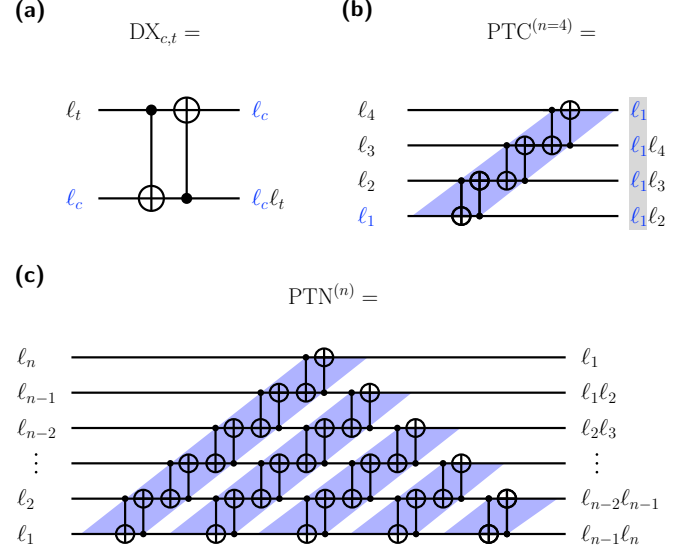


FIG. 2. (a) Schematic of a DCNOT gate. (b) Concatenations of DCNOT gates forming a Parity Twine chain. (c) Concatenated Parity Twine chains acting on a decreasing number of qubits and forming the Parity Twine network $\text{PTN}^{(n)}$, generating all possible two-body terms.

The $\text{DX}_{c,t}$ gate is depicted in Fig. 2(a). Note that the DCNOT gate shares aspects with an iSWAP gate, native to many state-of-the-art hardware platforms [43, 44].

Logically, the action of a $\text{DX}_{c,t}$ gate can be understood as swapping the parity information of the two qubits involved and a subsequent encoding of the combined parity on qubit c . These two features are essential for an efficient encoding of many-body operators on the LNN chain, where the location of logical parity information on the devices plays a pivotal role. Concatenations of DCNOT gates, which we call a *Parity Twine chain*, allow to systematically distribute logical parity information from one physical qubit to all other qubits

$$(\ell_1, \dots, \ell_n) \text{PTC}^{(n)} = ((\ell_2, \dots, \ell_n) \ell_1, \ell_1) \quad (6)$$

where the Parity Twine chain is given by

$$\text{PTC}^{(n)} = \text{DX}_{1,2} \odot \text{DX}_{2,3} \odot \dots \odot \text{DX}_{n-1,n}. \quad (7)$$

Fig. 2(b) schematically depicts a Parity Twine chain for $n = 4$ qubits. Here and in the following, we use the shorthand notation $((\ell_2, \dots, \ell_n) \ell_1, \ell_1) = (\ell_2 \ell_1, \ell_3 \ell_1, \dots, \ell_n \ell_1, \ell_1)$. Note that a simple CNOT chain is not able to accomplish the same encoding. CNOT chains either encode an increasing number of logical labels or just pair the logical labels of neighboring qubits when applying their adjoint operation. In contrast, $\text{PTC}^{(1,n)}$ encodes the logical parity information originally located on the first physical qubit with the logical parity information of *all* other physical qubits. Consequently, starting from the label sequence (ℓ_1, \dots, ℓ_n) , $\text{PTC}^{(n)}$ generates all

logical two-body parity labels that include the label ℓ_1 . Interestingly, we obtain the generator circuit for all two-body labels containing ℓ_1 and all two-body labels containing ℓ_2 from a concatenation of PTC circuits, since

$$((\ell_2, \dots, \ell_n)\ell_1, \ell_1)\text{PTC}^{(1,n-1)} = ((\ell_3, \dots, \ell_n)\ell_2, \ell_2\ell_1, \ell_1).$$

Similarly, we can construct the generator circuit of all two-body labels just from repeated application of Parity Twine chains on a shrinking set of qubits

$$\text{PTN}^{(n)} = \text{PTC}^{(n)} \odot \text{PTC}^{(1,n-1)} \odot \dots \odot \text{PTC}^{(1,2)}. \quad (8)$$

We call the circuit $\text{PTN}^{(n)}$ a *Parity Twine network of type I*. Application of $\text{PTN}^{(n)}$ on a label set (ℓ_1, \dots, ℓ_n) yields

$$(\ell_1, \dots, \ell_n)\text{PTN}^{(n)} = (\ell_n\ell_{n-1}, \ell_{n-1}\ell_{n-2}, \dots, \ell_2\ell_1, \ell_1).$$

Fig. 2(c) illustrates the building block $\text{PTN}^{(n)}$. As outlined in Ref. [35], the circuit $\text{PTN}^{(n)}$ can be interpreted as a spatio-temporal version of the LHZ encoding where certain spanning tree lines of an extended LHZ code can be mapped to a moment of the circuit $\text{PTN}^{(n)}$.

Following $\text{PTN}^{(n)}$, a CNOT chain $\overline{\text{CXC}}^{(n)} = \text{CX}_{n,n-1} \odot \text{CX}_{n-1,n-2} \odot \dots \odot \text{CX}_{2,1}$ acts as a decoding circuit and may be used to restore the original labels (in reversed order)

$$(\ell_n\ell_{n-1}, \ell_{n-1}\ell_{n-2}, \dots, \ell_2\ell_1, \ell_1)\overline{\text{CXC}}^{(n)} = (\ell_n, \dots, \ell_1).$$

With \overline{O} we denote the *reversed circuit* of a circuit O , which simply maps each $\text{CX}_{i,j}$ to $\text{CX}_{n-i+1,n-j+1}$ (see App. A.3). The concatenation

$$\mathcal{G}_2^{(n)} = \text{PTN}^{(n)} \odot \overline{\text{CXC}}^{(n)} \quad (9)$$

constitutes a generator circuit for all two-body labels which maps an input sequence of single body labels to an output of single-body labels. In the subsequent sections we call generator circuits with this property *clean* generator circuits. For a more detailed analysis of the above circuits and their properties, we refer to App. C.

Our strategy for a circuit that generates all three-body logical parity labels $\mathcal{L}_3^{(n)}$ builds on the two-body generator circuit. Here, the central idea is to encode an additional label ℓ_s repeatedly on physical qubit 2 just before every application of a Parity Twine chain (starting at physical qubit 2). The corresponding modified building block is thus a *modified Parity Twine chain*

$$\text{PTC}'^{(n)} = \text{CX}_{1,2} \odot \text{PTC}^{(2,n)}.$$

Concatenations of modified Parity Twine chains yield a *modified Parity Twine network of type I*

$$\begin{aligned} \text{PTN}'^{(n)} &= \text{PTC}'^{(n)} \odot \text{PTC}'^{(1,n-1)} \odot \dots \\ &\dots \odot \text{PTC}'^{(1,3)} \odot \text{CX}_{1,2}. \end{aligned} \quad (10)$$

The application of $\text{PTN}'^{(n)}$ on the label sequence $(\ell_s, \ell_1, \dots, \ell_{n-1})$ yields

$$\begin{aligned} (\ell_s, \ell_1 \dots, \ell_{n-1})\text{PTN}'^{(n)} \\ = (\ell_s, \ell_{n-1}\ell_{n-2}, \ell_{n-2}\ell_{n-3}, \dots, \ell_2\ell_1, \ell_1\ell_s), \end{aligned} \quad (11)$$

where $\text{PTN}'^{(n)}$ is generating the label set

$$\{\ell_s\ell_i\ell_j \mid 1 \leq i < j \leq n-1\}$$

from the label sequence $(\ell_s, \ell_1 \dots, \ell_{n-1})$, i.e. all logical three-body labels that include ℓ_s . By this property the label ℓ_s is a *special label* wherefore we also call the modified Parity Twine network of type I a *special three-body generator* (in App. E.2, we give a detailed definition of arbitrary special k -body generators).

While $\text{PTN}'^{(n)}$ in Eq. (11) generates all labels containing the special label ℓ_s , the output label set has an inconvenient form as the special label ℓ_s is encoded on physical qubit 1 and n . For a LNN chain with periodic boundary conditions, ℓ_s can be annihilated on qubit n using a single CNOT gate. However, given open boundary conditions, extra SWAP operations would be required to achieve the same. This issue is circumvented recognizing that the circuit $\text{PTN}'^{(n)}$ constitutes a special three-body generator not only from the label sequence $(\ell_s, \ell_1, \dots, \ell_{n-1})$ but also from the label sequence $(\ell_s, (\ell_1 \dots \ell_{n-1})\ell_s)$. Then, application of $\text{PTN}'^{(n)}$ yields

$$\begin{aligned} (\ell_s, (\ell_1, \dots, \ell_{n-1})\ell_s)\text{PTN}'^{(n)} \\ = (\ell_s, \ell_{n-1}\ell_{n-2}, \ell_{n-2}\ell_{n-3}, \dots, \ell_2\ell_1, \ell_1). \end{aligned} \quad (12)$$

The output label sequence of Eq. (12) coincides with that of Eq. (11) except on qubit n which does not anymore contain the special label. The starting label sequence $(\ell_s, (\ell_1 \dots \ell_{n-1})\ell_s)$ [left-hand side of Eq. (12)] can be obtained via two simple CNOT chains. The first CNOT chain prepares a label set similar to the right-hand side of Eq. (12) [see Fig. 3(a)]

$$\begin{aligned} (\ell_s, \ell_1, \dots, \ell_{n-1})(\text{CXC}^{(n)})^\dagger \\ = (\ell_s, \ell_s\ell_1, \ell_1\ell_2 \dots, \ell_{n-2}\ell_{n-1}) \end{aligned} \quad (13)$$

and via a second CNOT chain we can transform the result into the required input of Eq. (12)

$$(\ell_s, \ell_s\ell_1, \ell_1\ell_2 \dots, \ell_{n-2}\ell_{n-1})\text{CXC}^{(2,n)} = (\ell_s, (\ell_1, \dots, \ell_{n-1})\ell_s).$$

The combined building block

$$\text{PTN}_3^{(n)} = \text{CXC}^{(2,n)} \odot \text{PTN}'^{(n)} \quad (14)$$

is depicted in Fig. 3(b) and is called *Parity Twine network of type II*. Note that $\text{PTN}_3^{(n)}$ is also a special three-body generator since it generates all three-body logical labels that include the special label ℓ_s . Importantly, however, $\text{PTN}_3^{(n)}$ maps the input label set (which corresponds to

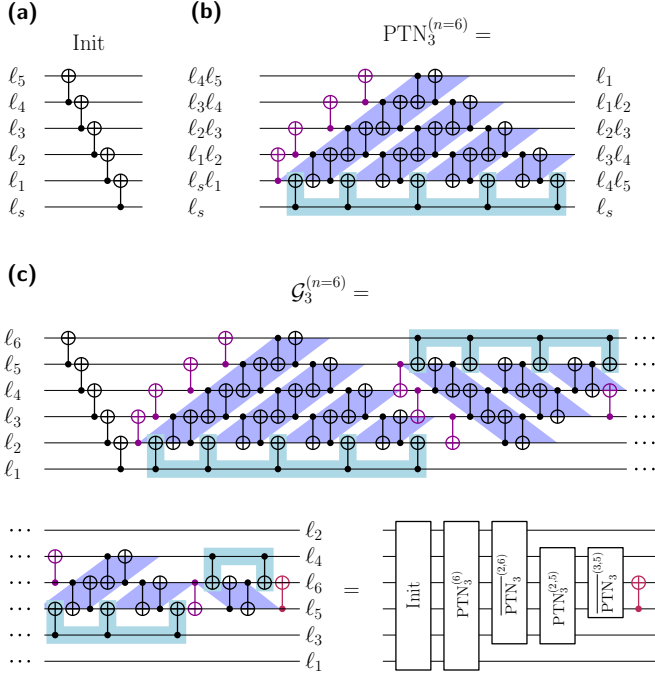


FIG. 3. (a) An initialization circuit preparing the input label set for special three-body generators. (b) Schematic of the special three-body generator circuit $\text{PTN}_3^{(n)}$ for the special label ℓ_s . (c) Schematic of a three-body generator circuit $\mathcal{G}_3^{(n)}$ composed of special three-body generators $\text{PTN}_3^{(n)}$ and $\overline{\text{PTN}}_3^{(n)}$, respectively.

the output label set of Eq. (13)) on an output label set reusable for forthcoming special three-body generators

$$\begin{aligned} (\ell_s, \ell_s \ell_1, \ell_1 \ell_2 \dots, \ell_{n-2} \ell_{n-1}) \text{PTN}_3^{(n)} \\ = (\ell_s, \ell_{n-1} \ell_{n-2}, \ell_{n-2} \ell_{n-3}, \dots, \ell_2 \ell_1, \ell_1) \end{aligned} \quad (15)$$

The label set on the right-hand side of Eq. (15) has the same structure of logical labels encoded on qubits $\{2, \dots, n\}$ (in reversed order) as the input label set has on qubits $\{1, \dots, n\}$. Furthermore, the special label ℓ_s is isolated on physical qubit 1. Thus, in the next step, we can now use ℓ_1 as the special label and apply a reversed $\overline{\text{PTN}}_3^{(2,n)}$ circuit, which is a special three-body generator for the label set $\{\ell_1, \dots, \ell_{n-1}\}$ acting on the physical qubits $\{2, \dots, n\}$. The parity label ℓ_s , which is isolated on qubit 1 remains unaffected by this. Pursuing this strategy on a shrinking set of qubits, we form a clean generator circuit $\mathcal{G}_3^{(n)}$ for all possible logical three-body labels. The corresponding circuit is schematically depicted in Fig. 3(c). After the application of the last Parity Twine network of type II (which only acts on three qubits) and a final CNOT gate that acts as a clean-up step, the output label sequence is given by

$$(\ell_1, \ell_3, \dots, \ell_4, \ell_2). \quad (16)$$

If we demand the input and output label set to coincide with (ℓ_1, \dots, ℓ_n) , this can be achieved with a sorting

network, which has $\mathcal{O}(n)$ depth and $\mathcal{O}(n^2)$ gate count, which is (relatively) cheap in comparison to the $\mathcal{O}(n^2)$ depth and $\mathcal{O}(n^3)$ gate count of $\mathcal{G}_3^{(n)}$. For a comprehensive definition and rigorous analysis of $\mathcal{G}_3^{(n)}$, we refer the reader to App. D.3 and D.4

Our circuit constructions have the neat advantage that building blocks can be partially executed in parallel. Using shifted concatenations as described in App. A.6 in Eq. (8) allows to start each $\text{PTC}^{(1,p)}$ circuit with only a constant delay of four moments [compare Fig. 2 (c)]. In contrast, without shifted concatenation, each $\text{PTC}^{(1,p)}$ circuit would acquire a delay of $2p$ moments. Eventually, shifted concatenations yield a reduction in total depth of $\mathcal{O}(n)$. For $\text{PTN}^{(n)}$ this yields a total depth of $4n + \mathcal{O}(1)$. Similar concatenation shifts can be applied for $\text{PTN}_3^{(n)}$ and $\mathcal{G}_3^{(n)}$. The respective depth-reduced circuits are depicted in Fig. 2 and 3.

With the additional concatenation shifts for consecutive special three-body generators, we obtain for $\mathcal{G}_3^{(n)}$ a reduced total depth of $n^2 + \mathcal{O}(n)$, whereas the total gate count amounts to $\frac{1}{3}n^3 + \mathcal{O}(n^2)$. This result can readily be deduced from the involved building blocks: every special three-body generator is mainly based on DCNOT gates (up to $\mathcal{O}(n^2)$ additional CNOT gates), whereby every DCNOT gate (consisting of two CNOT gates) generates one required three-body label. In total, there are $|\mathcal{L}_3^{(n)}| = \binom{n}{3} = \frac{1}{6}n^3 + \mathcal{O}(n^2)$ three-body labels. Thus, in leading order, we expect a total count of $\frac{2}{6}n^3$ gates. According to Eqs. (4) and (5), this yields an asymptotic average gate count of $\mu(\mathcal{G}_3, \mathcal{L}_3) = 2$ as well as an asymptotic depth of $\nu(\mathcal{G}_3, \mathcal{L}_3) = 3$. The label set $\mathcal{L}_3^{(n)}$ falls into the class of label sets investigated in Sec. III and App. I.1 for which we find a hypothetical lower bound of $\mu \geq 1 + \frac{1}{9}$. We note that for large enough n also most of the special three-body generator circuits must obey the same lower bounds since two labels of the corresponding special label set cannot be combined to form another label from the set. This holds equivalently for every (large enough) special label set in which all labels share at least one constituent. To obtain an average asymptotic gate count smaller than two for LNN chains, this requires a finite fraction of labels from $\mathcal{L}_3^{(n)}$ to be created using (on average) only a single CNOT gate. Constructing such a circuit becomes exceedingly difficult, if not outright impossible, even for moderately large values of n (~ 10).

2. Generator circuits for arbitrary many-body operators

The concepts outlined in Sec. IV A 1 can be used to construct special four-body generators. To do so, we recycle the optimized three-body generator circuit with inserting an extra label on top of the existing ones. This can be achieved using an additional CNOT to encode an additional label $\ell_{s'}$ on the physical qubit that holds the special label ℓ_s . Then, the circuit $\text{CX}_{1,2} \odot \text{PTN}_3^{(2,n)}$

generates all four-body labels that include $\ell_s \ell_{s'}$. However, if we want to utilize the full depth-optimized three-body generator circuit \mathcal{G}_3 via mirroring every second special three-body generator $\text{PTN}_3^{(n)}$, we need to encode the label $\ell_{s'}$ also on the other end of the LNN chain. Let us assume a similar initial label set as used for the special three-body generator $\text{PTN}_3^{(n)}$, $(\ell_{s'}, \ell_s, \ell_s \ell_2, \ell_2 \ell_3, \dots, \ell_{n-2} \ell_{n-1})$ encoded using the tools of the latter section. Next, we apply a CNOT chain to obtain

$$\begin{aligned} & (\ell_{s'}, \ell_s, \ell_s \ell_2, \ell_2 \ell_3, \dots, \ell_{n-2} \ell_{n-1}) \text{CXC}^{(3,n)} \\ & = (\ell_{s'}, \ell_s, \ell_s (\ell_2 \dots \ell_{n-1})) \quad (17) \end{aligned}$$

Now we can use a Parity Twine chain to encode the label $\ell_{s'}$ on physical qubit n

$$\begin{aligned} & (\ell_{s'}, \ell_s, \ell_s (\ell_2 \dots \ell_{n-1})) \text{PTC}^{(n)} \\ & = (\ell_{s'} \ell_s, \ell_{s'} \ell_s (\ell_2 \dots \ell_{n-1}), \ell_{s'}). \end{aligned}$$

Up the label encoded on qubit n , the resulting label sequence has the same structure as the input label sequence in Eq. (12). Therefore, all four-body labels containing $\ell_s \ell_{s'}$ can now be generated using $\text{PTN}'^{(1,n-1)}$ (note that we leave out the very last qubit n where $\ell_{s'}$ is encoded)

$$\begin{aligned} & (\ell_{s'} \ell_s, \ell_{s'} \ell_s (\ell_2 \dots \ell_{n-1}), \ell_{s'}) \text{PTN}'^{(1,n-1)} \\ & = (\ell_{s'} \ell_s, \ell_{n-2} \ell_{n-1}, \ell_{n-3} \ell_{n-2}, \dots, \ell_3 \ell_2, \ell_2, \ell_{s'}). \quad (18) \end{aligned}$$

Importantly, the output label set of Eq. (18) encodes the same label structure (in reversed order) as the input state in Eq. (17). This pattern can be repeated and eventually yields a circuit which generates all four-body labels that containing $\ell_{s'}$ (initially encoded on qubit 1).

As a post-processing step, we add an additional clean-up circuit with $\mathcal{O}(n)$ CNOT count and depth to regain single-bodied labels. The resulting (combined) circuit constitutes a clean special four-body generator $\mathcal{SG}_4^{(n)}$. Fig. 4(a) illustrates the circuit $\mathcal{SG}_4^{(n)}$. A precise definition of the circuit $\mathcal{SG}_4^{(n)}$ and its components as well as their properties can be found in App. A.10 and E.2-E.6.

Similar to the design of the three-body generator $\mathcal{G}_3^{(n)}$, we can build a four-body generator $\mathcal{G}_4^{(n)}$ by concatenating $n - 3$ special four-body generators each with different special labels. Thereby, later clean special four-body generators ignore all previous special labels, until the last clean special four-body generator only acts on four qubits. The circuit design is schematically shown in Fig. 4(b).

The circuit construction for the clean special four-body generator $\mathcal{SG}_4^{(n)}$ can now be utilized to constructively design clean special k -body generators for arbitrary $k > 4$. The strategy here is to recycle the clean special $(k-1)$ -body generator $\mathcal{SG}_{k-1}^{(n)}$ for the construction of a clean special k -body generator $\mathcal{SG}_k^{(n)}$. To do so, we encode the an extra special label $\ell_{s'}$ into each of the special label ℓ_s of the corresponding clean special $(k-1)$ -body generator.

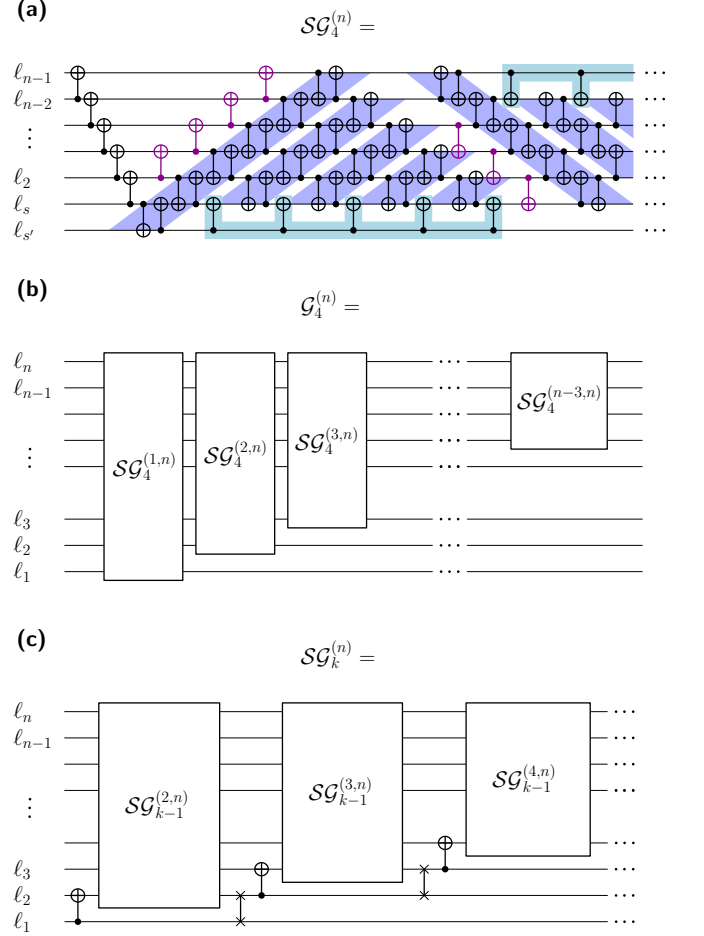


FIG. 4. (a) Schematic of the clean special four-body generator $\mathcal{SG}_4^{(n)}$. (b) Schematic of the four-body generator circuit $\mathcal{G}_4^{(n)}$ from the clean special four-body generator $\mathcal{SG}_4^{(n)}$. (c) Design of a clean special k -body generator $\mathcal{SG}_k^{(n)}$ from the clean special $(k-1)$ -body generator $\mathcal{SG}_{k-1}^{(n)}$. We indicate a SWAP gate by crossed-out qubits connected by a line.

The corresponding circuit then becomes a clean special $(k-1)$ -body generator which generates all k -body labels with the special labels $\ell_{s'} \ell_s$. To proceed with the next clean special $(k-1)$ -body generator, we apply a SWAP gate to exchange the special labels ℓ_s and $\ell_{s'}$ enabling the repetition of the same procedure. Chaining $n - k + 1$ clean special $(k-1)$ -body generators (with the extra special label $\ell_{s'}$) and a subsequent clean-up step then yields a clean special k -body generator (i.e. a generator for all labels that contain $\ell_{s'}$). Concatenations of clean special k -body generators can then be composed into a k -body generator $\mathcal{G}_k^{(n)}$. The recursive construction of our k -body generator $\mathcal{G}_k^{(n)}$ implies that $\mathcal{G}_k^{(n)}$ is also a generator for all $(k-p)$ -body labels with $p < k$. For more details, we refer to App. E.7 - E.10.

An interesting feature of this construction of k -body generators $\mathcal{G}_k^{(n)}$ is that each $\mathcal{G}_k^{(n)}$ inherits the asymptotic average gate count and asymptotic normalized depth from

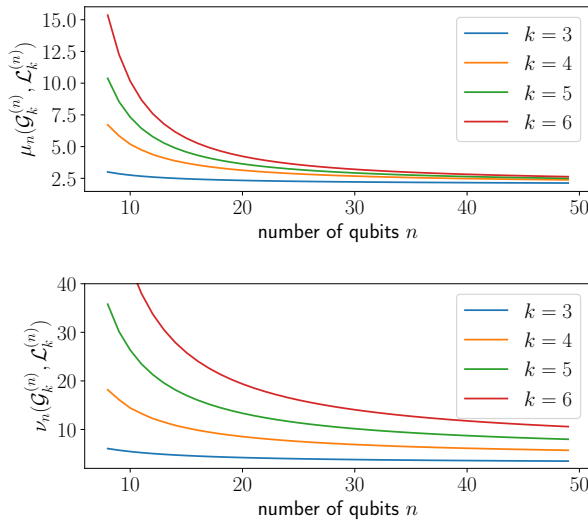


FIG. 5. Average count $\mu_n(\mathcal{G}_k^{(n)}, \mathcal{L}_k^{(n)})$ and normalized depth $\nu_n(\mathcal{G}_k^{(n)}, \mathcal{L}_k^{(n)})$ for different k -body generator circuits on LNN devices as a function of the number of qubits n .

the corresponding clean special k -body generator since for each k we just introduce an asymptotically negligible amount of extra CNOT gates. Recursively, this yields the asymptotic average gate count for the family of k -body generators \mathcal{G}_k with the corresponding family of label sets \mathcal{L}_k to be $\mu(\mathcal{G}_k, \mathcal{L}_k) = 2$. Likewise, for the asymptotic normalized depth we obtain $\nu(\mathcal{G}_k, \mathcal{L}_k) = k$ (see App. E.1 for a detailed gate count and depth analysis). In Fig. 5 we investigate the convergence properties of the average gate count μ_n and the normalized depth ν_n for the different k -body generator circuits as a function of the number of qubits n . The average count shows fast convergence to the expected asymptotic value ($\mu = 2$). In contrast, convergence of the normalized depth slows down with increasing k . This is expected as we do not employ further depth optimizations beyond $k = 4$. Instead higher order terms are recursively constructed using lower order building blocks which amounts to increasing pre-factors in the sub-leading order contributions to the normalized depth.

B. All-to-all connectivity

On all-to-all connected devices, logical information of any qubit is accessible from any other qubit. This is dramatically different to LNN devices where each qubit is connected to (at most) *two* other qubits. On first glance one might assume corresponding generator circuits to reflect these dramatic architectural differences since all-to-all connected devices render the positioning of labels inconsequential and label transportation via Parity Twine chains is unnecessary. However, in this section we present

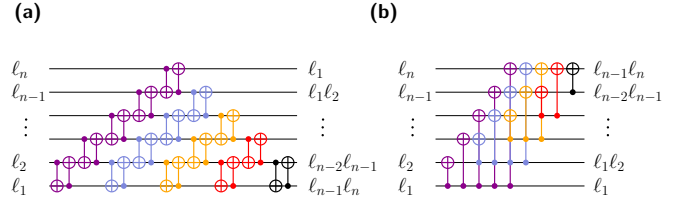


FIG. 6. (a) Circuit diagram of the two-body generator circuit $\text{PTN}^{(n)}$ on LNN devices. (b) Equivalent circuit $\text{PTN}^{(n)}_{\text{all-to-all}}$ for a hardware with all-to-all connectivity. Note that this version uses half the amount of CNOTs and has half the depth.

a simple scheme to map the circuits developed in Sec. IV A to gate count and depth optimized circuits on all-to-all connected devices.

On LNN devices, $\text{DX}_{i,j} = \text{CX}_{i,j} \odot \text{SW}_{i,j}$ constitutes the basis of our circuit constructions, providing two essential features: (i) it encodes the combined parity information on the control qubit i and (ii) it transports the initial logical parity information of the control qubit i to the target qubit j . Since the positioning of logical labels is irrelevant on all-to-all connected devices, this implies that the action of a DCNOT gate can be emulated on an all-to-all connected device with just a single CNOT gate. For that, we replace each SWAP gate with a *virtual* SWAP gate, which virtually swaps the positions of the qubits involved. Virtual SWAP gates are merely a trick to map the output label sequence of a DCNOT gate on the LNN chain to its corresponding counterpart for all-to-all connected devices. One can use classical software to keep track of all virtual SWAP gates applied and, in the end of the circuit, we obtain the actual qubit layout by reverting all virtual SWAP gates.

With this approach, we can now construct $\text{PTC}^{(n)}$ and $\text{PTN}^{(n)}$ circuits for all-to-all systems. For example, Fig. 6(b) shows the circuit $\text{PTN}^{(n)}_{\text{all-to-all}}$ obtained by applying this reverting process of virtual SWAP swaps on the circuit $\text{PTN}^{(n)}$. For comparison, Fig. 6(a) displays the corresponding LNN circuit. For each moment m of the circuit in Fig. 6(b), there exists a bijection which maps the label sequence at m to the corresponding label sequence at moment $2m$ in the circuit of Fig. 6(a). In terms of generated labels, the action of $\text{PTN}^{(n)}_{\text{all-to-all}}$ is identical with that of $\text{PTN}^{(n)}$ (given in Eq. (8)). However, $\text{PTN}^{(n)}_{\text{all-to-all}}$ only requires *half* as many gates and *half* of the depth as compared to $\text{PTN}^{(n)}$.

We can readily extend these ideas to $\text{PTN}'^{(n)}_{\text{all-to-all}}$ and $\text{PTN}^{(n)}_{3,\text{all-to-all}}$ circuits [see Eq. (10) and (14) and Fig. 3(b)]. Their dominant contribution consists of $\text{PTC}^{(n)}_{\text{all-to-all}}$ circuits and, consequently, we achieve (almost) half of the gate count and depth compared to the LNN construction. Likewise, all the generator circuits profit from this inheritance. For the family of k -body generators $\mathcal{G}_{k,\text{all-to-all}}$ with $k > 2$, this yields an asymptotic

average gate count of $\mu(\mathcal{G}_{k,\text{all-to-all}}, \mathcal{L}_k) = 1$ and a normalized depth of $\nu(\mathcal{G}_{k,\text{all-to-all}}, \mathcal{L}_k) = k/2$ (see App. G). Let us emphasize again that $\mu = 1$ corresponds to the theoretical lower bound. Thus, all the (special) k -body generators for any $k \geq 2$ are asymptotically optimal circuits (in gate count) where on average each CNOT in the circuit $\mathcal{G}_k^{(n)}$ creates one label of the label set $\mathcal{L}_k^{(n)}$ for $n \rightarrow \infty$.

C. General connectivity graphs

From the prospective of connectivity, LNN and all-to-all connected devices constitute two extreme cases. LNN devices possess the minimal required connectivity so that every qubit can be reached from any other qubit via residual connections. Except for the first and last qubit, each qubit has two directly connected neighbor qubits, resulting in an average neighbor count of $\eta_n \sim 2$. In all-to-all devices, the qubit connectivity graph is described by a complete graph where all qubits are directly connected resulting in an average neighbor count of $\eta_n = n - 1$. In between these two extremes, we can allocate qubit layouts with connectivity graphs with an average neighbor count $2 < \eta_n < n - 1$. As a prototypical example, here we discuss square grid devices [5, 45], however, our results can be directly transferred to other popular architectures such as hexagonal [21, 27] or octagonal [22] layouts.

If we aim to implement generator circuits on square grid devices, from the results of Secs. IV A and IV B we can already deduce an average gate count $1 \leq \mu \leq 2$. This follows directly from the connectivity graph described by square grid devices, where all qubits can easily be connected in a Hamiltonian path [Fig. 7(a)]. A chosen Hamiltonian path can then be used as an effective LNN model to implement the generator circuits outlined in Sec. IV A with an average gate count of $\mu(\mathcal{G}_k, \mathcal{L}_k) = 2$. Interpreting square grid devices as effective LNN devices might be convenient, however, this neglects a considerable amount of additional connections. To utilize this untapped potential, we pursue a different strategy: instead of laying out a Hamiltonian path, we define a path so that all qubits of the square grid are either within the path or directly neighbor this path. Fig. 7(b) depicts such a path on a 3×3 square grid where the black solid line indicates the path itself and the blue dashed lines represent the connections to path neighbors. Subsequently, we call paths of this kind *Hamiltonian grid paths*. Qubits are either directly part of a Hamiltonian grid path or they are direct neighbors to a Hamiltonian grid path in which case we call them Hamiltonian grid path neighbors. We call a Hamiltonian grid path *minimal*, if the number of qubits directly contained in it is minimal (and, as consequence, the number of Hamiltonian grid path neighbors is maximal). For example, the path depicted in Fig. 7(a) represents a Hamiltonian grid path but it is not minimal. In contrast, Fig. 7(b) shows a minimal Hamiltonian grid path on a 3×3 grid. In the following,

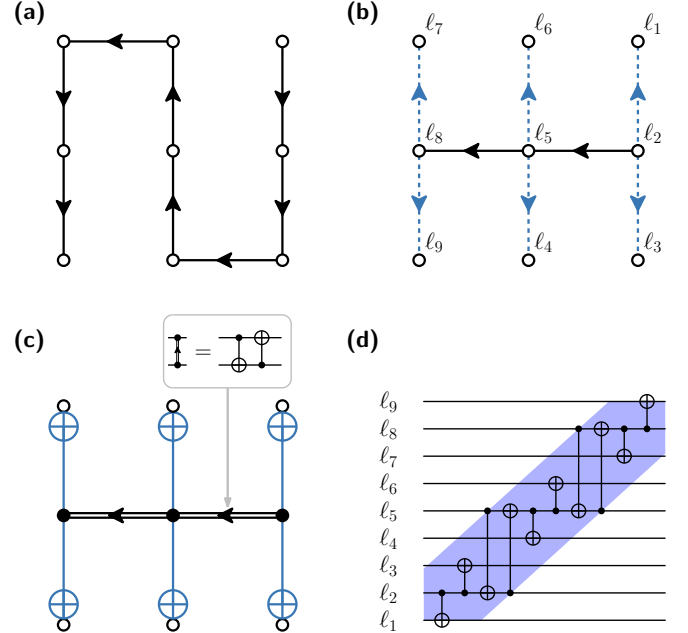


FIG. 7. (a) A Hamiltonian path on a square grid of nine qubits. (b) A Hamiltonian grid path on a square grid of nine qubits. (c) An implementation of $\text{PTC}_{\text{grid}}^{(9)}$ on a square grid of nine qubits based on the Hamiltonian grid path of (b). (d) Same as (c) as a circuit diagram.

we demonstrate how minimal Hamiltonian grid paths can be used to efficiently implement the circuit building blocks of Sec. IV A.

Let us recapitulate the action of $\text{DX}_{i,j}$, which encodes the combined parity information, $\ell_i \ell_j$ of qubit i and j onto qubit i while transporting the (initial) parity information of qubit i onto qubit j . The latter property allows to use concatenations of DCNOT gates, i.e., Parity Twine chains, to encode the label ℓ_i on all qubits of the concatenation. On square grids, we can use the additional connections to implement this even more efficiently: we use concatenations of DCNOT gates, akin to Parity Twine chains on LNN devices, which is applied along a defined minimal Hamiltonian grid path [black arrowed lines in Fig. 7(b)]. However, we intertwine it with CNOT gates that target the direct Hamiltonian grid path neighbors [blue dashed lines in Fig. 7(b)]. In this way, the corresponding circuit, subsequently denoted $\text{PTC}_{\text{grid}}^{(n)}$, encodes the label ℓ_2 of Fig. 7(b) onto all qubits of the square grid. Fig. 7(c) and (d) show a $\text{PTC}_{\text{grid}}^{(n)}$ circuit following a minimal Hamiltonian grid path for a 3×3 square grid. Compared to a corresponding $\text{PTC}_{\text{grid}}^{(n)}$ circuit (along a conventional Hamiltonian path), $\text{PTC}_{\text{grid}}^{(n)}$ saves $\sim 1/3$ of the involved CNOT gates.

Following the construction principles outlined in Sec. IV A, we repeatedly apply $\text{PTC}_{\text{grid}}^{(1,p)}$ circuits on a shrinking set of qubits p for the construction of $\text{PTC}_{\text{grid}}^{(n)}$ circuits. To allow this, after each $\text{PTC}_{\text{grid}}^{(1,p)}$ a final circuit is

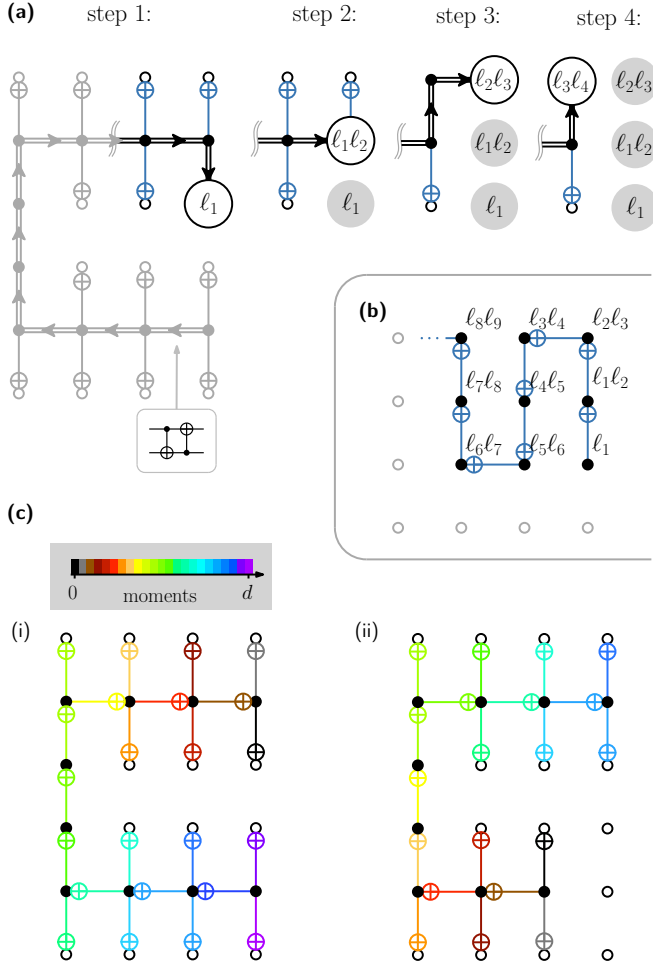


FIG. 8. (a) Schematic of the first four consecutive $\text{PTC}_{\text{grid}}^{(1,p)}$ circuits combined with a respective circuit to pigeonhole labels to corresponding locations to simplify the decoding. (b) Schematic of the decoding step given by a CNOT chain along a conventional Hamiltonian path. Depending on the device dimensions, extra SWAP gate are required along the boundaries. (c) The initializer consisting of two CX chains on a minimal Hamiltonian grid path.

required to pigeonhole labels and allow subsequent circuits to address all relevant labels. In Fig. 8(a) we schematically display the first four consecutive $\text{PTC}_{\text{grid}}^{(1,p)}$ circuits together with the corresponding pigeonhole circuit for a 6×4 square grid. As a general rule for the pigeonhole circuit, we first transport a label to one of the Hamiltonian grid path neighbors, the next label is transported to the corresponding Hamiltonian grid path node while the third label then occupies the second Hamiltonian grid path neighbor.

Concatenation of $n - 1$ $\text{PTC}_{\text{grid}}^{(1,p)}$ circuits (with the final pigeonhole circuits) leaves us with a label pattern depicted in Fig. 8(b). Similar to the LNN circuit construction, we can decode the labels using a chain of CNOT gates [Fig. 8(b)]. Depending on the geometry of the device, extra SWAP gates are necessary to breach the boundaries.

Note that, as a consequence of the employed Hamiltonian grid path, after decoding we do not regain the initial label order, however, labels can be tracked and appear in deterministic positions dictated by the algorithm.

As a whole, the outlined steps yield a clean generator circuit for all two-body labels $\mathcal{G}_{2,\text{grid}}^{(n)}$. In comparison to the corresponding LNN circuit derived in Sec. IV A, here we save $\sim 1/3$ of the involved CNOT gates which leaves us with an asymptotic average CNOT count of $\mu(\mathcal{G}_{2,\text{grid}}, \mathcal{L}_2) = 1 + \frac{1}{3}$. Interestingly, in close analogy to LNN, the $\text{PTC}_{\text{grid}}^{(1,p)}$ and the final pigeonhole circuits can be stacked using shifted concatenations to form a depth-optimized $\text{PTN}_{\text{grid}}^{(n)}$ circuit. Fig. 9 displays the $\text{PTN}_{\text{grid}}^{(12)}$ circuit together with a decoding CNOT chain for a 3×4 square grid. Each of the $n - 1$ $\text{PTC}_{\text{grid}}^{(1,p)}$ circuits starts with a constant delay of six moments which eventually yields a total depth of $6n + \mathcal{O}(1)$ for the combined $\text{PTN}_{\text{grid}}^{(n)}$ circuit.

Beyond two-body generator circuits, we can repeat the steps derived for LNN devices using our adapted building blocks $\text{PTC}_{\text{grid}}^{(n)}$. The only additional building block required is an *initializer* that prepares a label sequence akin to that of Eq. (12), i.e. encoding a special label ℓ_s in all other labels while keeping the label ℓ_s fixed. On a minimal Hamiltonian grid path, this can be done with two CNOT sequences, reaching all Hamiltonian grid path nodes as well as all Hamiltonian grid path neighbors [see Fig. 8(c), note that for the square grid, this can equivalently accomplished with a CNOT chain along a conventional Hamiltonian path with the same count and depth]. With this, special three-body generators are constructed using the initializer of Fig. 8(c)(ii) together with a modified Parity Twine network of type I $\text{PTN}_{\text{grid}}^{(n)}$. $\text{PTN}_{\text{grid}}^{(n)}$ can be derived from the definition of $\text{PTN}'^{(n)}$ [Eq. (10)] by replacing each $\text{PTC}^{(n)}$ circuit with the respective square grid version $\text{PTC}_{\text{grid}}^{(n)}$ (followed by a suitable pigeonhole circuit). Concatenating an initializer according to Fig. 8(c)(ii) with $\text{PTN}_{\text{grid}}^{(n)}$, this yields the special three-body generator $\text{PTN}_{3,\text{grid}}^{(n)}$ adapted to square grids. Similarly, the full three-body generator $\mathcal{G}_3^{(n)}$ can be assembled using concatenations of the initialiser akin to Fig. 8(c)(i) as well as $\text{PTN}_{3,\text{grid}}^{(n)}$ and $\overline{\text{PTN}}_{3,\text{grid}}^{(n)}$ (replacing the building blocks in Fig. 3(c) with the respective square grid adapted version).

In general, to adapt the LNN circuit to the square grid, we need to replace the respective building blocks (see Fig. 2) with the ones suitable for square grids. However, following this recipe, we obtain a depth overhead originating from the misalignment of the special three-body generators $\text{PTN}_{3,\text{grid}}^{(n)}$ and $\overline{\text{PTN}}_{3,\text{grid}}^{(n)}$ [in contrast to the respective case for LNN devices; compare Fig. 3(c)]. The concatenation of the special three-body generator for square grids $\text{PTN}_{3,\text{grid}}^{(n)}$ and its reversed counterpart $\overline{\text{PTN}}_{3,\text{grid}}^{(n)}$ can be shifted at most by $4/3n + \mathcal{O}(\sqrt{n})$. This originates

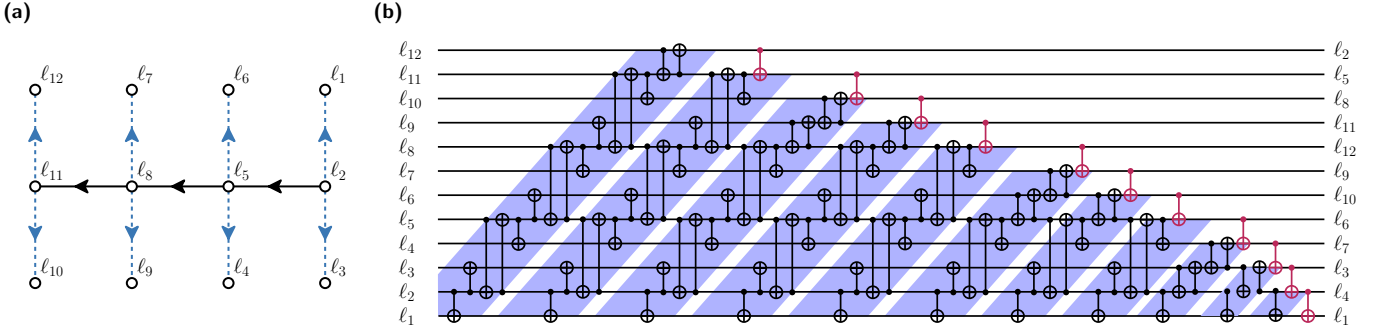


FIG. 9. A clean two-body generator designed for a square grid device. (a) The Hamiltonian grid path used for the design of the clean two-body generator depicted in (b) on a square grid device with 12 qubits together with their initial labels enumerated with ℓ_1, \dots, ℓ_{12} . (b) Two-body generator implementation for the square grid device schematically shown in (a).

from the form of the PTN_{grid} circuits (compare Fig. 9) where each constituent PTC_{grid} circuit is displaced by six moments with a corresponding length of $4n/3 + \mathcal{O}(\sqrt{n})$. The resulting misalignment of $\text{PTN}_{3,\text{grid}}^{(n)}$ and $\overline{\text{PTN}}_{3,\text{grid}}^{(n)}$ then leads to an increased depth of $7/3n^2 + \mathcal{O}(n\sqrt{n})$ for the corresponding three-body generator $\mathcal{G}_3^{(n)}$. To improve on this result, in App. G we investigate a construction based on clean special three-body generators which allows to use Lemma A.16. This has the advantage that we can concatenate not only $\text{PTN}_{3,\text{grid}}^{(n)}$ and $\overline{\text{PTN}}_{3,\text{grid}}^{(n)}$, i.e. a special three body generator and its reversed circuit, but also the adjoint reversed. With this improvement, we obtain a depth of $25/12n^2 + \mathcal{O}(n)$ for the full three body generator. However, starting from special four-body generators, this approach does not yield any depth gains and, eventually, for four-body generators and beyond, we find an asymptotic average CNOT count of $\mu(\mathcal{G}_k, \mathcal{L}_k) = 1 + \frac{1}{3}$ and an normalized asymptotic depth of $\nu(\mathcal{G}_k, \mathcal{L}_k) = 7/3k$ (see App. G).

We emphasize that the procedure outlined above is generic and can be generalized to all connectivity graphs where the qubits can be connected in a Hamiltonian grid path such as ladders, hexagonal layouts [21] but also graphs with non-local and/or non-planar connectivity [2, 4, 46]. For a connectivity graph of interest, we define a (minimal) Hamiltonian grid path. Based on this, we construct the respective building blocks: a PTC circuit which maps the respective input label sets as derived in Eq. (6), a decoding circuit and an initializer circuit. Up to implementation details, we can then readily design any k -body generator of interest. As an additional example of utility, in App. F we demonstrate our approach for heavy hexagon layouts. All results regarding asymptotic normalized depth and asymptotic average CNOT count are collected in Tab. III.

The approach of using Hamiltonian grid paths can also be applied for LNN and all-to-all connected devices, though the respective paths are not recognized as such or do not yield performance gains. In the LNN case, a minimal Hamiltonian grid (almost) coincides with a conventional Hamiltonian path: the Hamiltonian grid

path includes all but the first and the last qubits which are the only Hamiltonian grid path neighbors. For all-to-all connected devices, a minimal Hamiltonian grid path is trivial as it contains just a single qubit with all other qubits being Hamiltonian grid path neighbors.

Using Hamiltonian grid paths allows to convert increments in connectivity into reductions of the total CNOT count. In Fig. 1 we depict the asymptotic average CNOT count μ as a function of the inverse asymptotic average neighbor count $1/\eta$ for the investigated connectivity graphs. With the approach outlined above, for k -body generator circuits this yields a reduction in gate count on the order of $\mathcal{O}(n^k)$. However, this comes at the expense of an increased depth on the order of $\mathcal{O}(n^{k-1})$ as compared to LNN (except for all-to-all, compare Tab. III). Motivated by this observation, in App. H we investigate an alternative approach for a ladder layout, which allows to reduce both, total count and depth (as compared to the LNN approach). Here, the main idea is to use multiple Hamiltonian grid paths in parallel. For the two-body generator circuits, this allows to obtain a CNOT count of $3/4n^2 + \mathcal{O}(n)$ with a total depth of $3n + \mathcal{O}(1)$, which beats the corresponding LNN approach in both metrics.

V. APPLICATIONS

A. Quantum Approximate Optimization Algorithms

QAOA [11, 47] is considered a promising candidate algorithm to solve combinatorial optimization problems using quantum computers. The algorithm follows a quantum-classical protocol to reach the ground state of an (typically) Ising-like problem Hamiltonian. This requires the repeated application of a parameterized problem unitary $U_P(\beta)$, which encodes the problem Hamiltonian, followed by a parameterized driver unitary $U_X(\alpha)$. The concatenation of a driver together with a problem unitary defines a QAOA cycle. The prepared candidate state after p

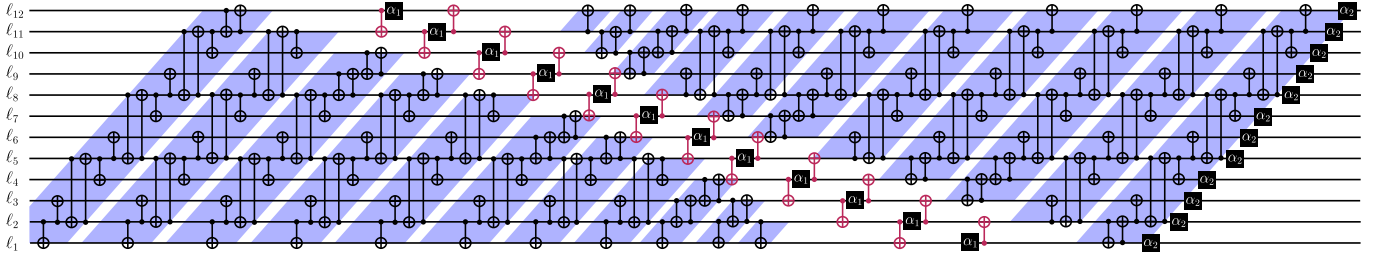


FIG. 10. Two subsequent QAOA cycles for the 3×4 square grid of Fig. 9(a) using shifted concatenation of two-body generators $\mathcal{G}_{2,\text{grid}}^{(12)}$ and $(\mathcal{G}_{2,\text{grid}}^{(12)})^\dagger$ with single-qubit x -rotations of the driver unitary in between, indicated by black rectangular boxes. For illustration purposes we neglect the (many) single-qubit z rotations.

QAOA cycles

$$|\psi(\alpha, \beta)\rangle = \prod_{j=1}^p U_X(\alpha_j) U_P(\beta_j) |+\rangle^{\otimes n}$$

yields a trial energy expectation value which is then used in a quantum-classical feedback loop to optimize the $2p$ parameters α_j, β_j with $j \in [1, p]$. In Ref. [35], the authors discuss the implementation of QAOA for all-to-all connected QUBO problems on LNN devices using parity label tracking. There, the corresponding problem Hamiltonian is described by an all-to-all connected Ising Hamiltonian of the form

$$H_{\text{QUBO}} = \sum_{k=1}^n \sum_{j < k} J_{jk} Z_j Z_k + \sum_{j=1}^n h_j Z_j.$$

The implementation of the problem unitary $U_{\text{QUBO}} = \exp(-i\beta H_{\text{QUBO}})$ thus requires the encoding of all logical two-body rotation operators $\exp(-i\beta J_{ij} Z_i Z_j)$, a task that can be accomplished using the clean two-body-generator $\mathcal{G}_2^{(n)}$ given in Eq. (9) (intertwined with single-body rotation gates wherever corresponding parity labels are available).

Utilizing the circuit building blocks developed in Secs. IV A, IV B and IV C we can generalize this to arbitrary higher order binary optimization (HUBO) problems which we can efficiently implement on a multitude of different connectivity graphs. For example, to encode a problem unitary $\exp(-i\beta H_{\text{HUBO}})$ with a problem Hamiltonian of the form

$$H_{\text{HUBO}} = \sum_{k=1}^n \sum_{j < k} \sum_{l < j} M_{jkl} Z_j Z_k Z_l + \sum_{k=1}^n \sum_{j < k} J_{jkl} Z_j Z_k + \sum_{j=1}^n h_j Z_j$$

we can use the clean three-body generator circuit $\mathcal{G}_3^{(n)}$ (which is automatically also a generator of all two-body terms). Adapting the required building block of $\mathcal{G}_3^{(n)}$ readily yields the corresponding implementation for the connectivity graph of interest.

In Ref. [35] the authors demonstrate a QAOA encoding with a depth of $2n + \mathcal{O}(1)$ per QAOA cycle (up to an initialization encoding circuit). In contrast, a QAOA algorithm for QUBO problems on LNN devices implemented based on $\mathcal{G}_2^{(n)}$ would yield a depth of $4n + \mathcal{O}(1)$ per QAOA cycle. To improve on this, we can employ a similar strategy as used for the design of the three-body generators: Instead of concatenating bare $\mathcal{G}_2^{(n)}$ generators in subsequent QAOA cycles, we use a shifted concatenation of circuits that alternate between the two-body generators $\mathcal{G}_2^{(n)}$ and $\overline{\mathcal{G}}_2^{(n)}$. Moreover, we apply shifted concatenations of the x rotation gates of the driver unitary after each two-body generator. In this way, shifted concatenation of all building blocks achieves a reduction of the total QAOA algorithm depth by a factor ~ 2 . More concretely, with this trick for p QAOA cycles we obtain a normalized depth of $2n(1 + 1/p) + \mathcal{O}(1)$ per cycle on LNN devices. A similar approach can be utilized for all-to-all connected devices, reducing the normalized depth per QAOA cycle from $2n + \mathcal{O}(1)$ to $n(1 + 1/p) + \mathcal{O}(1)$ per QAOA cycle.

For qubit layouts with other connectivity graphs, a depth efficient implementation of QAOA [45, 48, 49] requires more care. As discussed in Sec. IV C, the two-body generator tend to become asymmetric so that shifted concatenations of, for instance, $\mathcal{G}_{2,\text{grid}}^{(n)}$ and $\bar{\mathcal{G}}_{2,\text{grid}}^{(n)}$ do not align properly [compare Fig. 9(b)]. Each $\mathcal{G}_{2,\text{grid}}^{(n)}$, $\bar{\mathcal{G}}_{2,\text{grid}}^{(n)}$, respectively, has a depth of $6n + \mathcal{O}(1)$, while their shifted concatenation allows only for an overlap of $4n/3 + \mathcal{O}(1)$. However, according to Lemma A.16, since $\bar{\mathcal{G}}_k^{(n)}$ is a clean generator circuit for all k -body terms from a sequence of single-body labels, then also the adjoint circuit $(\bar{\mathcal{G}}_k^{(n)})^\dagger$ is a clean k -body generator from a set of single body labels. Thus, instead of concatenating $\mathcal{G}_{2,\text{grid}}^{(n)}$ and $\bar{\mathcal{G}}_{2,\text{grid}}^{(n)}$ for subsequent QAOA cycles, we can also concatenate $\mathcal{G}_{2,\text{grid}}^{(n)}$ and $(\bar{\mathcal{G}}_{2,\text{grid}}^{(n)})^\dagger$. This enables a better alignment and a larger overlap of subsequent QAOA blocks using shifted concatenation. In Fig. 10, we schematically illustrate this approach for two subsequent QAOA cycles on the 3×4 square grid shown in Fig. 9(a). In between the two Hamiltonian encoding blocks a permutation of the

single body labels is available so that we can apply the x rotation of the driver unitary. Shifted concatenation of QAOA blocks built from $\mathcal{G}_{2,\text{grid}}^{(n)}$ and $(\mathcal{G}_{2,\text{grid}}^{(n)})^\dagger$ reduce the total depth by a factor of ~ 2 . More precisely, for an even number of QAOA cycles p we obtain a depth of $3n(p + \frac{4}{9}) + \mathcal{O}(1)$ while for an odd number of QAOA we find $3n(p + 1) + \mathcal{O}(1)$. Thus, eventually we obtain a depth of $3n(1 + 1/p) + \mathcal{O}(1)$ ($3n(1 + \frac{4}{9p}) + \mathcal{O}(1)$) per QAOA cycle given an odd (even) number of cycles. For $p \gg 1$, this is on par with the best known depth, however saving a factor of $9/4$ in gate count compared to established SWAP based approaches [27, 45]. The same approach can be applied to heavy-hexagon and ladder layouts. For all the connectivity graphs we investigate, we obtain a circuit depth that is at most equal to the best known result with a simultaneously significant improvement in gate count. In fact in most cases both metrics outperform existing algorithms. Our results for implementations of QAOA on the different connectivity graphs are collected in Tab. I.

B. Quantum Fourier Transform

The QFT constitutes a major cornerstone algorithm in quantum computing and lays the foundation to a multitude of important algorithms and use cases such as modular exponentiation and phase estimation [50, 51] used in Shor's factoring algorithm, quantum arithmetic [52, 53] or solving linear systems of equations [54]. In recent years, a multitude of algorithms was developed to implement QFT on different connectivity graphs optimizing either depth [15, 55–57] or gate count [16, 40, 58]. Thereby, state-of art approaches typically use architecture optimized SWAP networks. Here we demonstrate how to apply the conclusion drawn in Secs. IV B and IV C for the design of gate count and depth optimized implementations of the QFT adapted to different connectivity graphs.

Recently, some of the authors demonstrated in Ref. [35] how parity label tracking can yield reductions in gate count and depth when implementing the QFT on LNN devices. Up to single-qubit z rotations, the QFT circuit of Ref. [35] can (mainly) be understood as a combination of PTC circuits neatly intertwined with single-qubit Hadamard gates. Fig. 11(a) depicts the corresponding QFT circuit. In between subsequent PTC circuits we add the necessary single-body z rotations and Hadamard gates, which we decompose into z and x rotation gates. Notably, aside from single-qubit gates, the QFT implemented in this way only uses PTC circuits together with a final CNOT chain as a cleanup/decoding step. Thus, by replacing the respective building blocks, we can easily adapt this approach to qubit layouts with other connectivity graphs. In essence, this amounts to replacing each PTC circuit with its corresponding counterpart on the connectivity graph of interest and inserting corresponding single-body z rotation gates. For instance, using the mapping established in Sec. IV B, we can map the circuit

of Fig. 11(a) to a corresponding circuit optimized for all-to-all connected devices shown in Fig. 11(b). By virtue of mapping PTC to $\text{PTC}_{\text{all-to-all}}$, we can directly conclude that the CNOT count and depth of the algorithm halves. Interestingly, the structure of the QFT implementation on all-to-all connected devices readily allows to construct an approximate QFT [55, 59] just from omitting CNOT gates (and corresponding rotations with angles below the approximation threshold).

Analogously to the procedure outlined above for all-to-all connected devices, once a PTC circuit together with a decoding circuit is available for a given connectivity graph, implementing a corresponding QFT circuit is straightforward. In Sec. IV C we discuss in detail how to find PTC circuits using Hamiltonian grid paths. The obtained gate count and depth obtained for PTN circuits can then directly transferred also to the corresponding QFT implementation (up to single-qubit gates). The results for our implementations of QFT on the different connectivity graphs are summarized in Tab. II. Notably, our implementations significantly improve the gate count while the depth is at most the same as that of the best known state-of-the-art implementations.

VI. CONCLUSION AND OUTLOOK

Efficient quantum algorithms constitute a cornerstone for the development of quantum computing. In this work, we have contributed to this development by establishing generic algorithmic tools for the efficient implementation of logical many-body operators on quantum devices with typical contemporary qubit connectivity graphs. Resulting algorithms are highly optimized both in gate count and circuit depth and significantly outperform competing algorithms. Using the developed tools we have constructed generator circuits that are surprisingly close to the provable lower bound for the gate count or – in the case of all-to-all connected devices – even align with it. We have derived a generic framework for the construction of generator CNOT circuits of parity label sets with k -body labels adaptable to a wide range of connectivity graphs and we have analyzed the role of the device connectivity. Thereby, we have found that even moderate increments in connectivity can yield significant efficiency improvements. We have investigated five different qubit layouts in depth: (1) LNN devices with nearest neighbor connectivity, planar connectivity graphs among which are (2) heavy hexagon devices (3) ladder devices (4) square grid devices and (5) all-to-all connected devices with complete connectivity graphs. The average gate count of the derived generator circuits interpolates from LNN ($\mu = 2$) over heavy hexagon ($\mu = 5/3$), ladder ($\mu = 3/2$) and square grids ($\mu = 4/3$) to all-to-all with an optimal asymptotic average gate count of $\mu = 1$. The developed formalism can be understood as a means to map the circuits between graphs of different connectivity. This lets us conjecture that the class of optimal circuits derived within our for-

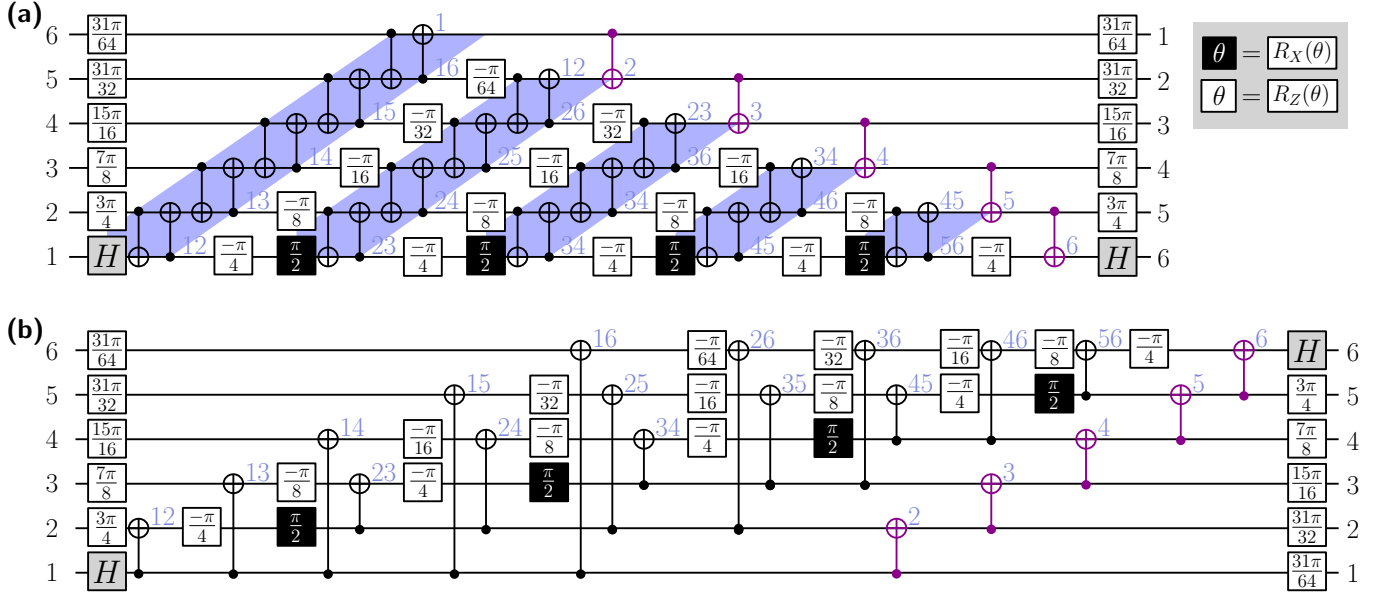


FIG. 11. QFT circuit implementation for LNN devices (a) and all-to-all connected devices (b). The blue numbers indicate the parity labels at the given circuit moments. Colored CNOT gates belong to a final cleanup step.

malism extends beyond complete graphs. As a first step in this direction we have proven that on LNN devices $\mu > 1$ for generator circuits of label sets with odd-body labels. More precisely, we have shown $\mu \geq 1 + \frac{1}{9}$ in this case but we have justified belief that this bound is not optimal. Finally, we have investigated applications of our formalism for the implementation of two important quantum routines: (i) the QAOA applied to QUBO and HUBO problems and (ii) the QFT and its approximation on all-to-all connected devices. On all investigated connectivity graphs, our approach significantly outperforms existing algorithms in gate count for both, QAOA and QFT. Simultaneously, the depth of our algorithms beats the best known approaches on the majority of platforms, where at most we are on par with existing algorithms. Our results indicate that full qubit connectivity is not necessarily required to obtain reasonably efficient implementations of quantum algorithms.

ACKNOWLEDGMENTS

This study was supported by the Austrian Research Promotion Agency (FFG Project No. FO999909249, FFG Basisprogramm) as well as funded in part by the Austrian Research Promotion Agency (FFG Project No. 884444, QFTE 2020), NextGenerationEU via FFG and Quantum Austria (FFG Project No. FO999896208) and the Horizon Europe programme HORIZON- CL4-2022-QUANTUM-02-SGA via the project 101113690 (PASQuanS2.1). Moreover, this publication has received funding by the Austrian Science Fund (FWF) SFB BeyondC Project No. F7108-N38, as well as funding within the QuantERA II Programme that is supported by the European Union's Horizon 2020 research and innovation programme under Grant Agreement No. 101017733. For the purpose of open access, the authors have applied a CC BY public copyright license to any Author Accepted Manuscript version arising from this submission. Furthermore, funding is acknowledged by the German Federal Ministry for Education and Research within ATIQ (Project No. 13N16127) and MuniQC-Atoms (Project No. 13N16080).

Appendix A: Notation and auxiliary results

This section presents the notations and auxiliary results that are used throughout the paper.

Definition A.1 (CNOT gate). Suppose that $n \geq 2$ and $i, j \in \{1, \dots, n\}$ with $i \neq j$. We denote by $\text{CX}_{i,j}: (\mathbb{C}^2)^{\otimes n} \rightarrow (\mathbb{C}^2)^{\otimes n}$ the unitary operator which is defined by $\text{CX}_{i,j}(|a_1 \dots a_n\rangle) := |b_1(a) \dots b_n(a)\rangle$ where

$$b_k(a) := \begin{cases} a_k, & k \neq j, \\ a_i \oplus a_j, & k = j. \end{cases}$$

for $a_1, \dots, a_n \in \{0, 1\}$. We call the operator *CNOT gate with control qubit i and target qubit j* .

Definition A.2 (Circuit). A (quantum) circuit C is a finite sequence which maps every time step - *moments* - enumerated from 1 to d to a set of non-overlapping gates. For a non-empty sequence, the number of elements of each set can be zero except for the set in the first and last moment. The *depth* of the circuit is d and denoted by $\text{depth}(C)$, and the *gate count* is the number of gates contained in the circuit which we denote by $\text{size}(C)$. For a set of non-overlapping gates C_1 , we also write for brevity C_1 for the circuit (C_1) which contains only the set C_1 . Note that we also call a circuit C a circuit for *complete graphs*. In general, if every gate in a circuit C can be implemented on a device with a certain connectivity graph, then we call the circuit C a circuit for that connectivity graph.

In this article, we propose *CNOT circuits* which are circuits where all gates are CNOT gates. To emphasize that a circuit C acts on n qubits we write $C^{(n)}$. If the circuits only acts on the qubits p, \dots, q , we write $C^{(p,q)}$. Furthermore, we also use $\text{CX}_{m,l}$ to denote the circuit $(\{\text{CX}_{m,l}\})$ which only contains the CNOT gate $\text{CX}_{m,l}$ for $m \neq l$.

Next, we introduce the term *reversed and adjoint circuit* as well as the *concatenation* of two circuits. These operations play a crucial role in reducing the depth of k -body generators, introduced below.

Definition A.3 (Reversed CNOT circuit). Let C be a CNOT circuit with depth d . Then, the *reversed circuit* \bar{C} of C is defined as the circuit with depth d where each moment m contains the reversed CNOT gates of the CNOT gates of the circuit C at the moment m . Here, the *reversed CNOT gate* $\bar{\text{CX}}_{i,j}$ of $\text{CX}_{i,j}$ with $1 \leq i, j \leq n$ and $i \neq j$ is defined as $\text{CX}_{n+1-i, n+1-j}$. We also write $\bar{C}^{(n)}$ to emphasize that the CNOT gates are reversed between all qubits $1, \dots, n$. Moreover, we also denote by $\bar{C}^{(p,q)}$ the circuit which reverses all CNOT gates of the circuit C between qubits p and q . In this case, every CNOT gate $\text{CX}_{i,j}$ for some $p \leq i, j \leq q$ with $i \neq j$ is replaced by $\text{CX}_{p+q-i, p+q-j}$.

Example A.4. Let $n = 7$ and C be the circuit on the left-hand side in Fig. 12. The corresponding reversed circuit $\bar{C}^{(2,6)}$ of C between qubits two and six is shown on the right-hand side in Fig. 12.

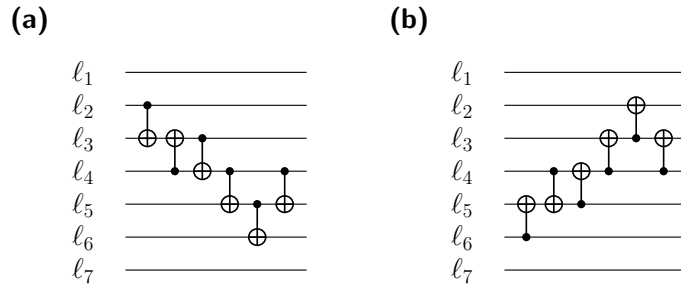


FIG. 12. Circuit C (a) and the reversed circuit $\bar{C}^{(2,6)}$ (b) in Example A.4.

Definition A.5 (Adjoint circuit). Let $C = (C_1, \dots, C_d)$ be a circuit where C_1, \dots, C_d denote the sets of non-overlapping gates. Then, the *adjoint circuit* of C is denoted by C^\dagger and defined as the sequence $(C_d^\dagger, \dots, C_1^\dagger)$ where C_l^\dagger denotes the set which contains the adjoint operators of all quantum gates in C_l for $l = 1, \dots, d$.

Definition A.6 (Shifted concatenation of circuits). For two circuits C_1 and C_2 we define the *concatenation*

$$C_1 \odot C_2$$

as the circuit which first contains all moments from C_1 and then all moments from C_2 . The *shifted concatenation by $s \geq 0$ moments*

$$C_1 \odot_s C_2$$

is the circuit which contains all moments of C_1 as-is and *in addition* all moments of C_2 but shifted by s moments to the right. Of course this is only well-defined if the resulting circuit does not contain overlapping gates. Similarly, we set

$$C_1 \odot_{-s} C_2$$

as the circuit which corresponds to the circuit $C_1 \odot C_2$ but with C_2 shifted to the left by s moments afterwards.

We emphasize that the subtle difference between positive and negative shifts is that positive shifts start at the left of the first circuit whereas negative shifts start at the right to determine the time moment where the first circuit is

concatenated with the second one. Moreover, we note that the concatenation operator is not an associative operation. Whenever we write

$$C_1 \odot_{s_1} C_2 \odot_{s_2} \cdots \odot_{s_{m-1}} C_m$$

for some circuits C_1, \dots, C_m with shifts $s_1, \dots, s_{m-1} \geq 0$, we mean the circuit

$$C_1 \odot_{s_1} (C_2 \odot_{s_2} (\cdots \odot_{s_{m-2}} (C_{m-1} \odot_{s_{m-1}} C_m))).$$

Figs. 13(a)-(c) show examples of concatenated circuits with six qubits. We observe that the depth of $C_1 \odot C_2 \odot C_3$ [see Fig. 13(a)] is nine whereas the depth of $C_1 \odot (C_2 \odot_2 C_3)$ [see Fig. 13(b)] and $C_1 \odot_2 (C_2 \odot_2 C_3)$ [see Fig. 13(c)] is seven and five, respectively, and their corresponding unitary operators are equal. This shows that finite sequences of valid sets of controlled-target qubit pairs with different depths can produce the same resulting unitary operators.

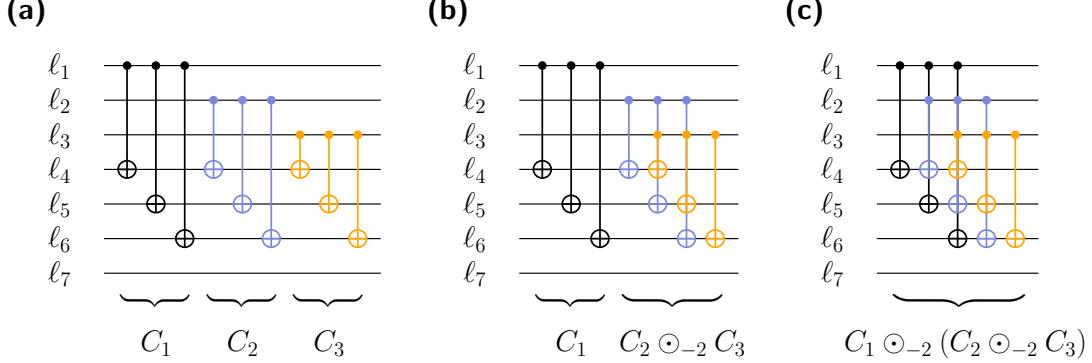


FIG. 13. (a) $C_1 \odot C_2 \odot C_3$. (b) $C_1 \odot (C_2 \odot_{-2} C_3)$. (c) $C_1 \odot_{-2} (C_2 \odot_{-2} C_3)$

To define k -body generators, the following definitions are necessary.

Definition A.7 (Parity label). Given a set of qubits $Q = \{1, \dots, n\}$ a *(parity) label* ℓ is a subset of Q . For two labels ℓ_1 and ℓ_2 we denote by $\ell_1 \ell_2 := \ell_1 \Delta \ell_2$ the *symmetric difference* of the two labels (all qubits which are contained in exactly one of the two labels), which is again a label. Moreover, we call the empty label the *trivial* (or *unphysical*) label. Note that the set of all labels over Q equipped with symmetric difference as an addition is a vector space over $\text{GF}(2)$. The zero vector is the trivial label.

Definition A.8 (Label action). Let C be a CNOT circuit on $n \geq 2$ qubits with depth d and ℓ_1, \dots, ℓ_n some labels.

(i) For $1 \leq i, j \leq n$ with $i \neq j$ the *right action of $\text{CX}_{i,j}$ on (ℓ_1, \dots, ℓ_n)* is defined as

$$(\ell_1, \dots, \ell_n) \text{CX}_{i,j} := (\ell_1, \dots, \ell_{j-1}, \ell_i \ell_j, \ell_{j+1}, \dots, \ell_n).$$

(ii) Let $C_m := \{\text{CX}_{i_1, j_1}, \dots, \text{CX}_{i_{k_m}, j_{k_m}}\}$ be the set of all non-overlapping CNOT gates at the moment m of the circuit C . Then, the *right action of C_m on (ℓ_1, \dots, ℓ_n)* is defined as

$$(\ell_1, \dots, \ell_n) C_m := (((\ell_1, \dots, \ell_n) \text{CX}_{i_1, j_1}) \cdots \text{CX}_{i_{k_m-1}, j_{k_m-1}}) \text{CX}_{i_{k_m}, j_{k_m}}.$$

(iii) Let C_1, \dots, C_d be the sets of all non-overlapping CNOT gates at every moment of the circuit C . Then, the *right action of the circuit C on (ℓ_1, \dots, ℓ_n)* is defined as

$$(\ell_1, \dots, \ell_n) C := (((\ell_1, \dots, \ell_n) C_1) \cdots C_{d-1}) C_d.$$

Remark A.9. Defining

$$G_n := \{C \mid C \text{ is a CNOT circuit with } n \text{ qubits}\} \quad \text{and} \quad M_n := \{(\ell_1, \dots, \ell_n) \mid \ell_1, \dots, \ell_n \text{ are labels}\},$$

it can be shown that the mapping

$$\cdot : M_n \times G_n \rightarrow M_n : (\ell, C) \mapsto \ell C$$

fulfills the properties of a right group action of G_n on M_n . However, note that assuming the empty sequence is the identity element, the set G_n together with the concatenation \odot does not form a group since there is no inverse element for any non-empty sequence.

Definition A.10 (Label generator). Consider n qubits and a set $L^{(n)}$ of non-trivial labels over these qubits. We say that a circuit $C^{(n)}$ generates the labels $L^{(n)}$ from a sequence of labels $\ell = (\ell_1, \dots, \ell_n)$ if the following holds: Let $C_{1,m}^{(n)}$ be the subcircuit which only contains the first m moments. Collect all labels occurring in each of the

$$\ell C_{1,m}^{(n)} \quad \text{for } m = 1, \dots, \text{depth}(C^{(n)})$$

into a set L' . If $L^{(n)}$ is a subset of L' , we say that the circuit generates $L^{(n)}$ from ℓ . Moreover, we say that $C^{(n)}$ generates some label $\hat{\ell}$ from ℓ if $\hat{\ell} \in L'$. In addition, we call $C^{(n)}$ *clean* if and only if $C^{(n)}$ generates the labels $L^{(n)}$ from ℓ and there exists a permutation $\pi: \{1, \dots, n\} \rightarrow \{1, \dots, n\}$ such that $\ell C^{(n)} = (\ell_{\pi(1)}, \dots, \ell_{\pi(n)})$.

This definition immediately leads us to the notion of k -body generators.

Definition A.11 (k -body generator). Let $C^{(n)}$ be a circuit with n qubits, $k \geq 2$ and $\ell = (\ell_1, \dots, \ell_n)$ with some labels ℓ_1, \dots, ℓ_n . We say that $C^{(n)}$ is a *k -body generator* if $C^{(n)}$ generates all k -body labels

$$\{\ell_{i_1} \ell_{i_2} \dots \ell_{i_k} \mid i_1 < \dots < i_k \leq n\}$$

from ℓ .

Next, we introduce a metric for CNOT circuits measuring the average CNOT count as well as the normalized depth for generating a certain set of labels.

Definition A.12 (Average CNOT count, normalized CNOT depth). Let $C^{(n)}$ be a CNOT circuit and suppose that $C^{(n)}$ generates the label set $L^{(n)}$ on n qubits. Then, we define

$$\mu_n(C^{(n)}, L^{(n)}) := \frac{\text{size}(C^{(n)})}{|L^{(n)}|} \quad \text{and} \quad \nu_n(C^{(n)}, L^{(n)}) := \frac{\text{depth}(C^{(n)}) n}{2 |L^{(n)}|}$$

as the *average CNOT count* and *normalized CNOT depth* of the circuit $C^{(n)}$ generating the label set $L^{(n)}$, respectively. Furthermore, we set

$$\mu(C, L) := \liminf_{n \rightarrow \infty} \mu_n(C^{(n)}, L^{(n)}) \quad \text{and} \quad \nu(C, L) := \liminf_{n \rightarrow \infty} \nu_n(C^{(n)}, L^{(n)})$$

as the *asymptotic average CNOT count* and *asymptotic normalized CNOT depth* of a family of circuits $C = (C^{(n)})_{n \geq m}$ and a family of label sets $L = (L^{(n)})_{n \geq m}$ starting from some natural number $m \geq 2$, respectively, where $C^{(n)}$ generates the label set $L^{(n)}$ for $n \geq m$.

Remark A.13. Let $C_k = (C_k^{(n)})_{n \geq k}$ be a family of k -body generators and $\mathcal{L}_k = (\mathcal{L}_k^{(n)})_{n \geq k}$ be the family of label sets $\mathcal{L}_k^{(n)}$ which contain all k -body labels on $n \geq k$ qubits.

(i) $\mu(C_k, \mathcal{L}_k) \geq 1$ and $\nu(C_k, \mathcal{L}_k) \geq 1$.

(ii) If $\text{size}(C_k^{(n)}) = cn^k + g(n)$ with $\lim_{n \rightarrow \infty} \frac{g(n)}{n^k} = 0$ and $c \geq 0$, then $c \geq \frac{1}{k!}$.

The statements from the above remark follow from the following lemma.

Lemma A.14 (Trivial size bound). Let $C^{(n)}$ be a CNOT circuit which generates a set $L^{(n)}$ of labels not containing the labels of the start sequence. Then the size of $C^{(n)}$ is at least $|L^{(n)}|$ and the depth of $C^{(n)}$ at least $|L^{(n)}|/(n/2)$.

Proof. Follows from the fact that each CNOT gate can only produce at most one new label and every moment of a circuit on n qubits can have at most $n/2$ CNOT gates. \square

As we observe from Remark A.13 (i), for every family of k -body generators we have that $\mu_{\text{CX}}(V_k) \geq 1$. The goal of the next sections is to construct families of k -body generators with an average CNOT count and a normalized depth as small as possible.

We conclude this section with the following two lemmas, which will be repeatedly applied to reduce the depth of the circuits presented in the next sections. The first lemma is utilized for the construction of our depth-optimized k -body generators [see Figs. 3(c), 4(a), for instance], while the application of the second lemma further reduces the depth of our QAOA circuits (see Fig. 10, for example).

Lemma A.15. Let $C^{(n)}$ be a CNOT circuit acting on n qubits with depth d and $\ell = (\ell_1, \dots, \ell_n)$ a sequence of labels. Then, it holds

$$\ell \overline{C}^{(n)} = \overline{\ell C^{(n)}}. \quad (\text{A1})$$

Here, for any sequence of labels $\ell = (\ell_1, \dots, \ell_n)$ we set $\bar{\ell} := (\ell_n, \ell_{n-1}, \dots, \ell_1)$. As a consequence, if $C^{(p,q)}$ is acting on qubits p, \dots, q , it holds

$$\ell \overline{C}^{(p,q)} = \overline{\ell C^{(p,q)}}, \quad (\text{A2})$$

where in this case $\bar{\ell} := (\ell_1, \dots, \ell_{p-1}, \ell_q, \ell_{q-1}, \dots, \ell_p, \ell_{q+1}, \dots, \ell_n)$. Moreover, if $C^{(p,q)}$ generates some label $\ell_{i_1} \ell_{i_2} \dots \ell_{i_m}$ with $1 \leq i_1 < \dots < i_m \leq n$ from ℓ , then $\overline{C}^{(p,q)}$ generates the label $\ell_{p+q-i_1} \ell_{p+q-i_2} \dots \ell_{i_{p+q-i_m}}$ from ℓ .

Proof. First, suppose that C contains only one CNOT gate, and let i the control and j the target qubit. Since $\ell_m = \ell_{n+1-m}$ for $m = 1, \dots, n$, we observe from the definition of the CNOT gate

$$\hat{\ell}_m = \begin{cases} \bar{\ell}_i \bar{\ell}_j, & \exists k \in \{1, \dots, n\} : m = j, \\ \bar{\ell}_m, & \text{else,} \end{cases}$$

where $(\hat{\ell}_1, \dots, \hat{\ell}_n) := \bar{\ell} \text{CX}_{i,j}$. Therefore, we have

$$\left(\overline{\ell \text{CX}_{i,j}} \right)_m = \hat{\ell}_{n+1-m} = \begin{cases} \bar{\ell}_i \bar{\ell}_j, & \exists k \in \{1, \dots, n\} : n+1-m = j, \\ \bar{\ell}_{n+1-m}, & \text{else,} \end{cases}$$

which equals

$$\begin{cases} \ell_{n+1-i} \ell_{n+1-j}, & \exists k \in \{1, \dots, n\} : m = n+1-j, \\ \ell_m, & \text{else,} \end{cases} = \left(\ell \overline{C}^{(n)} \right)_m.$$

Next, assume that the statement holds when the circuit has size $m \geq 1$ and let C be a circuit with size $m+1$. Then, we can find two circuits C_1 and C_2 of size at most m such that $\ell C = \ell(C_1 \odot C_2)$ for any sequence of labels ℓ . Thus, we have from our induction hypothesis

$$\ell \overline{C} = \ell \left(\overline{C_1} \odot \overline{C_2} \right) = \left(\overline{\ell C_1} \right) C_2 = \left(\overline{\ell C_1} \right) C_2.$$

Hence, applying our induction hypothesis again on the right-hand side yields

$$\overline{\left(\overline{\ell C_1} \right) C_2} = \overline{\ell \left(C_1 \odot C_2 \right)} = \overline{\ell C},$$

which shows desired relation. \square

Subsequently, for a label sequence $\ell = (\ell_1, \dots, \ell_n)$ and a set $I := \{i_1, \dots, i_m\}$ with $1 \leq i_1 < \dots < i_m \leq n$ we set $\ell_I := \ell_{i_1} \dots \ell_{i_m}$. Furthermore, for a set \mathcal{I} containing subsets of $\{1, \dots, n\}$ we set $L_{\mathcal{I}}^{(n)} := \{\ell_I \mid I \in \mathcal{I}\}$.

Lemma A.16. Let $C^{(n)}$ be a CNOT circuit acting on n qubits with depth d and $\ell = (\ell_1, \dots, \ell_n)$ a sequence of labels.

(i) The adjoint circuit $(C^{(n)})^\dagger$ generates the same labels as $C^{(n)}$ from the label sequence $\ell C^{(n)}$.

(ii) Let \mathcal{I} be a set of subsets of $\{1, \dots, n\}$ and suppose that $C^{(n)}$ generates $L_{\mathcal{I}}^{(n)}$ from ℓ as well as there exists a permutation $\pi: \{1, \dots, n\} \rightarrow \{1, \dots, n\}$ such that $\ell C^{(n)} = (\ell_{\pi(1)}, \dots, \ell_{\pi(n)})$. Then, the adjoint circuit $(C^{(n)})^\dagger$ generates $L_{\pi^{-1}(\mathcal{I})}^{(n)} := \{\ell_{\pi^{-1}(I)} \mid I \in \mathcal{I}\}$ from the label sequence ℓ .

Proof. (i) Let C_1, \dots, C_d be the sets of non-overlapping gates of the circuit $C^{(n)}$. Then, we observe that

$$\begin{aligned} \ell (C_1 \odot \dots \odot C_m) &= \ell \left(C_1 \odot \dots \odot C_m \odot C_{m+1} \odot \dots \odot C_d \odot C_d^\dagger \odot C_{d-1}^\dagger \odot \dots \odot C_{m+1}^\dagger \right) \\ &= \ell \left(C^{(n)} \odot C_d^\dagger \odot C_{d-1}^\dagger \odot \dots \odot C_{m+1}^\dagger \right) \\ &= \ell C^{(n)} \left(C_d^\dagger \odot C_{d-1}^\dagger \odot \dots \odot C_{m+1}^\dagger \right) \end{aligned}$$

for each $m = 1, \dots, d-1$. Since $C_d^\dagger, \dots, C_{m+1}^\dagger$ are the first $d-m$ moments of the circuit $(C^{(n)})^\dagger$, the above identity implies that $(C^{(n)})^\dagger$ generates the same labels as $C^{(n)}$ from the label sequence $\ell C^{(n)}$.

(ii) Define the label sequence $\ell' := (\ell_{\pi^{-1}(1)}, \dots, \ell_{\pi^{-1}(n)})$. Then, by applying (i) on the label sequence ℓ' we obtain that $(C^{(n)})^\dagger$ generates the label set

$$\{\ell'_I \mid I \in \mathcal{I}\} = \{\ell_{\pi^{-1}(I)} \mid I \in \mathcal{I}\} = L_{\pi^{-1}(\mathcal{I})}^{(n)}$$

from $\ell' C^{(n)} = (\ell'_{\pi(1)}, \dots, \ell'_{\pi(n)}) = \ell$, showing the desired result. \square

Note that in the following, whenever a circuit $C^{(n)}$ is defined for each number of qubits $n \geq 2$, we denote by $C^{(p,q)}$ the circuit which replaces the control qubit i and the target qubit j of each CNOT gate in the circuit $C^{(q-p+1)}$ by the control qubit $i+p-1$ and the target qubit $j+p-1$, respectively.

In the following, let $n \geq 2$ denote the number of qubits and $\ell = (\ell_1, \dots, \ell_n)$ be a finite sequence of some labels.

Appendix B: Main building blocks

In this section, we outline the main building blocks and its key properties that are being utilized for the construction of our k -body generators in the subsequent sections.

Definition B.1 (DCNOT gate, Parity Twine chain, CNOT chain). Let $1 \leq c, t \leq n$ with $c \neq t$.

- (i) The *DCNOT gate* is defined as $\text{DX}_{c,t} := \text{CX}_{t,c} \odot \text{CX}_{c,t}$
- (ii) The *Parity Twine chain* is defined as the circuit $\text{PTC}^{(n)} := \text{DX}_{1,2} \odot \dots \odot \text{DX}_{n-1,n}$. By $\text{PTC}^{(1)}$ we denote the empty sequence.
- (iii) The *CNOT chain* is the circuit defined as $\text{CXC}^{(n)} := \text{CX}_{1,2} \odot \text{CX}_{2,3} \odot \dots \odot \text{CX}_{n-1,n}$.
- (iv) The *modified CNOT chain* is the circuit defined as $\text{CXC}'^{(n)} := \text{CX}_{1,2} \odot_3 \text{CX}_{2,3} \odot_5 \dots \odot_{2(n-2)+1} \text{CX}_{n-1,n}$.

Remark B.2. (i) It holds $\ell \text{DX}_{c,t} = \hat{\ell}$ where $\hat{\ell}_i := \ell_i$ for $i \notin \{c, t\}$ as well as $\hat{\ell}_c := \ell_c \ell_t$ and $\hat{\ell}_t := \ell_c$.

- (ii) The Parity Twine chain satisfies $\ell \text{PTC}^{(n)} = (\ell_1(\ell_2 \dots \ell_n), \ell_1)$.

- (iii) We have for the CNOT chain $\ell \text{CXC}^{(n)} = (\ell_1, \ell_1 \ell_2, \ell_1 \ell_2 \ell_3, \dots, \ell_1 \ell_2 \dots \ell_n)$ and $\ell(\text{CXC}^{(n)})^\dagger = (\ell_1, \ell_1 \ell_2, \ell_2 \ell_3, \dots, \ell_{n-1} \ell_n)$. Obviously, the statement also holds for the modified CNOT chain.

Proof. Property (i) can be easily verified. For (ii) we use (i) to obtain

$$\begin{aligned} \ell \text{PTC}^{(n)} &= (\ell \text{DX}_{1,2}) (\text{DX}_{2,3} \odot \text{DX}_{3,4} \odot \dots \odot \text{DX}_{n-1,n}) \\ &= (\ell_1 \ell_2, \ell_1, \ell_3 \dots \ell_n) (\text{DX}_{2,3} \odot \text{DX}_{3,4} \odot \dots \odot \text{DX}_{n-1,n}). \end{aligned}$$

Consequently, using induction, we see that

$$\ell \text{PTC}^{(n)} = (\ell_1 \ell_2, \ell_1 \ell_3, \dots, \ell_1 \ell_n, \ell_1) = (\ell_1(\ell_2 \dots \ell_n), \ell_1).$$

Property (iii) can analogously be shown. \square

As we will later see, the following circuits are needed for our construction of k -body generators for arbitrary $k \geq 4$ in App. E and are used in a post-cleanup step in our circuits.

Definition B.3 (SWAP gate, SWAP chain). Let $1 \leq c, t \leq n$ with $c \neq t$.

- (i) The *SWAP gate* is defined as $\text{SW}_{c,t} := \text{CX}_{c,t} \odot \text{CX}_{t,c} \odot \text{CX}_{c,t}$
- (ii) The *SWAP chain* is defined as the circuit $\text{SWC}^{(n)} := \text{SW}_{1,2} \odot \text{SW}_{2,3} \odot \dots \odot \text{SW}_{n-1,n}$.

Remark B.4. (i) It holds $\ell \text{SW} = \hat{\ell}$ where $\hat{\ell}_i := \ell_i$ for $i \notin \{c, t\}$ as well as $\hat{\ell}_c := \ell_t$ and $\hat{\ell}_t := \ell_c$.

- (ii) The SWAP chain satisfies $\ell \text{SWC}^{(n)} = (\ell_2, \ell_3, \dots, \ell_n, \ell_1)$.

Next, we present our main results on k -body generators. We emphasize that some of the circuits in the subsequent sections are a concatenation of subcircuits with non-zero shifts. However, since these circuits produce the same labels as their counterparts where the shifts of the concatenated subcircuits are set to zero, we may assume that the shifts are zero when proving that the circuits generate a specific label set.

Appendix C: Two-body generators

In this section we quickly recap the circuit in Ref. [35] which generates all two-body labels for nearest neighbor connectivity graphs and introduce it with the help of a so-called *Parity Twine network of type I* which consists of a concatenation of Parity Twine chains.

Definition C.1 (Parity Twine network of type I). Define

$$\text{PTN}_l^{(n)} := \begin{cases} \text{PTC}^{(l)} \odot_4 \text{PTN}_{l-1}^{(n)}, & 3 \leq l \leq n \\ \text{PTC}^{(2)}, & l = 2. \end{cases}$$

for $2 \leq l \leq n$. Then, we denote by $\text{PTN}^{(n)} := \text{PTN}_{n-1}^{(n)}$ the *Parity Twine network of type I*.

Theorem C.2. *For the Parity Twine network of type I we have that*

$$\ell \text{PTN}^{(n)} = (\ell_{n-1} \ell_n, \dots, \ell_1 \ell_2, \ell_1). \quad (\text{C1})$$

and $\text{PTN}^{(n)}$ generates all two-body labels $\{\ell_i \ell_j \mid 1 \leq i < j \leq n\}$. Furthermore, $\text{size}(\text{PTN}^{(n)}) = n^2 - n$ and $\text{depth}(\text{PTN}^{(n)}) = 4n - 6$.

Proof. The case $n = 2$ is trivial. Assume that the statement holds for some $n - 1 \geq 2$. From Remark B.2 (ii) we see that $\text{PTN}^{(n)} = \text{PTC}^{(n)} \odot \text{PTN}^{(1, n-1)}$ is generating the labels $\{\ell_1 \ell_i \mid 1 < i \leq n\}$ and $\hat{\ell} := \ell \text{PTC}^{(n)} = (\ell_1 (\ell_2 \dots \ell_n), \ell_1)$. Finally, using the induction hypothesis, we have that

$$\hat{\ell} \text{PTN}^{(1, n-1)} = (\hat{\ell}_{n-2} \hat{\ell}_{n-1}, \dots, \hat{\ell}_1 \hat{\ell}_2, \hat{\ell}_1, \ell_1) = (\ell_{n-1} \ell_n, \dots, \ell_1 \ell_2, \ell_1)$$

and $\text{PTN}^{(n)}$ is generating the label set $\{\hat{\ell}_i \hat{\ell}_j \mid 1 \leq i < j \leq n - 1\} = \{\ell_i \ell_j \mid 2 \leq i < j \leq n\}$ from $\hat{\ell}$, which implies the required properties. The expression for the size of $\text{PTN}^{(n)}$ can be derived from the recursive definition of $\text{PTN}^{(n)}$

$$\text{size}(\text{PTN}^{(n)}) = \sum_{l=0}^{n-2} \text{size}(\text{PTC}^{(n-l)}) = \sum_{l=1}^n 2(l-1) = n^2 - n$$

Similarly, we get $\text{depth}(\text{PTN}^{(n)}) = 4(n-2) + 2$. □

Corollary C.3. *For $n \geq 3$ the circuit $\mathcal{G}_2^{(n)} := \text{PTN}^{(n)} \odot_{-(n-3)} \overline{\text{CXC}}^{(n)}$ is a two-body generator satisfying*

$$\ell \mathcal{G}_2^{(n)} = \bar{\ell} = (\ell_n, \ell_{n-1}, \dots, \ell_1)$$

as well as

$$\text{size}(\mathcal{G}_2^{(n)}) = n^2 - 1 \quad \text{and} \quad \text{depth}(\mathcal{G}_2^{(n)}) = 4n - 4.$$

Proof. The first identity follows from Theorem C.2, Remark B.2 (iii) and Lemma A.15. Moreover, from Theorem C.2 we deduce the relations $\text{size}(\mathcal{G}_2^{(n)}) = \text{size}(\text{PTN}^{(n)}) + \text{size}(\text{CXC}^{(n)}) = n^2 - 1$ and $\text{depth}(\mathcal{G}_2^{(n)}) = \text{depth}(\text{PTN}^{(n)}) + \text{depth}(\text{CXC}^{(n)}) - n + 3 = 4n - 4$. □

Appendix D: Three-body generators

As we have already seen in App. C, the repeated execution of Parity Twine chains replaces the encoded special label on each qubits with another one. The idea of the subsequent three-body generator is based on the two-body generator and involves linking the special labels to a fixed special label by using a CNOT gate at the beginning of each Parity Twine chain, thereby generating three-body labels. Thus, the Parity Twine chain is replaced by the so-called *modified Parity Twine chain*, which includes this additional CNOT gate prior to the Parity Twine chain. In the modified Parity Twine chain, the initial CNOT gate ensures (even with repeated usage of a modified Parity Twine chain) that the

fixed special label is contained on its initial qubit throughout the circuit. Applying this modification, the Parity Twine network of type I (introduced in the previous section) becomes a *Parity Twine network of type II*. In addition, this new network generates an output of labels that can be reused by another Parity Twine network of type II where the fixed special label is replaced by a new fixed label that has not previously been used. Thus, the concatenation of multiple Parity Twine network of type II ensures that all three-body labels are generated.

Throughout the whole section, we suppose that $n \geq 3$.

Definition D.1 (Modified Parity Twine chain, modified Parity Twine network of type I and Parity Twine network of type II).

- (i) The *modified Parity Twine chain* is defined as $\text{PTC}'^{(n)} := \text{CX}_{1,2} \odot \text{PTC}^{(2,n)}$.
- (ii) We set $\text{PTN}_{3,1}^{(n)} := \text{PTC}'^{(3)} \odot \text{CX}_{1,2}$ and $\text{PTN}_{3,l}^{(n)} := \text{PTC}'^{(l+2)} \odot_4 \text{PTN}_{3,l-1}^{(n)}$ for $2 \leq l \leq n-2$, and call $\text{PTN}'^{(n)} := \text{PTN}_{3,n-2}^{(n)}$ the *modified Parity Twine network of type I*.
- (iii) The *Parity Twine network of type II* is defined as $\text{PTN}_3^{(n)} := (\text{CX}_{2,3} \odot \text{CXC}'^{(3,n)}) \odot_1 \text{PTN}'^{(n)}$.

Theorem D.2. (i) The modified Parity Twine chain satisfies

$$\ell \text{PTC}'^{(n)} = (\ell_1, \ell_1 \ell_2 (\ell_3 \dots \ell_n), \ell_1 \ell_2). \quad (\text{D1})$$

(ii) It holds

$$\ell \text{PTN}'^{(n)} = (\ell_1, \ell_{n-1} \ell_n, \dots, \ell_3 \ell_4, \ell_2 \ell_3, \ell_1 \ell_2) \quad (\text{D2})$$

and $\text{PTN}'^{(n)}$ generates the labels $\{\ell_1 \ell_i \ell_j \mid 1 < i < j \leq n\}$ from ℓ . Moreover, we have that

$$\text{size}(\text{PTN}'^{(n)}) = n^2 - 2n + 1 \quad \text{and} \quad \text{depth}(\text{PTN}'^{(n)}) = 4n - 8 \quad (\text{D3})$$

(iii) For the Parity Twine network of type II we have that

$$(\ell_1, \ell_1 \ell_2, \ell_2 \ell_3, \dots, \ell_{n-1} \ell_n) \text{PTN}_3^{(n)} = (\ell_1, \ell_{n-1} \ell_n, \dots, \ell_3 \ell_4, \ell_2 \ell_3, \ell_1 \ell_2). \quad (\text{D4})$$

and $\text{PTN}_3^{(n)}$ generates the labels $\{\ell_1 \ell_i \ell_j \mid 1 < i < j \leq n\}$ from $(\ell_1, \ell_1 \ell_2, \ell_2 \ell_3, \dots, \ell_{n-1} \ell_n)$. Furthermore, it holds

$$\text{size}(\text{PTN}_3^{(n)}) = n^2 - n - 1 \quad \text{and} \quad \text{depth}(\text{PTN}_3^{(n)}) = 4n - 7. \quad (\text{D5})$$

Proof. (i) Applying $\text{CX}_{1,2}$ on ℓ and substituting ℓ with $(\ell_1, \ell_1, \ell_2, \ell_3, \dots, \ell_n)$ in Remark B.2 (ii) shows the first identity.

(ii) The case $n = 3$ can be easily verified. Suppose the statement holds for some $n-1 \geq 3$. From the definition of $\text{PTN}'^{(n)}$ and (i) we have that $\text{PTN}'^{(n)}$ is producing the label set $\{\ell_1 \ell_2 \ell_j \mid 2 < j \leq n\}$ from ℓ . Then, applying our induction hypothesis on $\text{PTN}'^{(n-1)}$ and the sequence $\hat{\ell} := \ell \text{PTC}'^{(n)} = (\ell_1, \ell_1 \ell_2 (\ell_3 \dots \ell_n), \ell_1 \ell_2)$ yields

$$\begin{aligned} \hat{\ell} \text{PTN}'^{(n-1)} &= (\hat{\ell}_1, \hat{\ell}_{n-2} \hat{\ell}_{n-1}, \dots, \hat{\ell}_3 \hat{\ell}_4, \hat{\ell}_2 \hat{\ell}_3, \hat{\ell}_2, \ell_1 \ell_2) \\ &= (\ell_1, \ell_{n-1} \ell_n, \dots, \ell_3 \ell_4, \ell_2 \ell_3, \ell_1 \ell_2) \end{aligned}$$

and $\text{PTN}'^{(n)}$ is generating the label set $\{\hat{\ell}_1 \hat{\ell}_i \hat{\ell}_j \mid 1 < i < j \leq n-1\} = \{\ell_1 \ell_i \ell_j \mid 2 < i < j \leq n\}$. This shows that the above statement holds true. The expressions for the depth and size can be derived as follows: From $\text{size}(\text{PTN}'^{(n)}) = \text{size}(\text{PTC}'^{(n)}) + \text{size}(\text{PTN}'^{(n-1)})$ for $n \geq 4$ and $\text{size}(\text{PTN}'^{(3)}) = 4$ we deduce

$$\text{size}(\text{PTN}'^{(n)}) = \sum_{l=0}^{n-4} \text{size}(\text{PTC}'^{(n-l)}) + 4 = 4 + \sum_{l=0}^{n-4} 2(n-l-2) + 1 = n^2 - 2n + 1.$$

Similarly, we have from $\text{depth}(\text{PTN}'^{(n)}) = 4 + \text{depth}(\text{PTN}'^{(n-1)})$ for $n \geq 4$ and $\text{depth}(\text{PTN}'^{(3)}) = 4$ the relation $\text{depth}(\text{PTN}'^{(n)}) = 4n - 8$.

(iii) Eq. (D4) and the property that $\text{PTN}_3^{(n)}$ is generating the label set $\{\ell_1 \ell_i \ell_j \mid 1 < i < j \leq n\}$ are derived from the relation $(\ell_1, \ell_1 \ell_2, \ell_2 \ell_3, \dots, \ell_{n-1} \ell_n)(\text{CX}_{2,3} \odot \text{CXC}'^{(3,n)}) = (\ell_1, \ell_1(\ell_2 \dots \ell_n))$ and applying (ii) on $\hat{\ell} := (\ell_1, \ell_1(\ell_2 \dots \ell_n))$. The expressions for the depth and size of $\text{PTN}_3^{(n)}$ follow from (ii). \square

Following the previous results, we now introduce our three-body generator and its properties.

Definition D.3 (Three-body generator). Let $W_3^{(n)} := \text{PTN}_3^{(n)} \odot_{s_{n-1}} \overline{W_3}^{(2,n)}$ with $W_3^{(3)} := \text{PTN}_3^{(3)}$ and

$$s_n := \begin{cases} -2(n-4), & \text{if } n > 4 \\ -1, & \text{if } n = 4, \\ 0, & \text{if } n = 3. \end{cases}$$

Then, we define the circuit

$$\mathcal{G}_3^{(n)} := (\text{CXC}^{(n)})^\dagger \odot W_3^{(n)} \odot \text{CX}_{c_n, t_n},$$

where (c_n, t_n) is $(\frac{n+1}{2} + 1, \frac{n+1}{2})$ if n is odd and $(\frac{n}{2}, \frac{n}{2} + 1)$ if n is even.

Theorem D.4. *The circuit $\mathcal{G}_3^{(n)}$ in Definition D.3 is a three-body generator satisfying*

$$\text{size}(\mathcal{G}_3^{(n)}) = \frac{n^3}{3} - \frac{n}{3} \quad \text{and} \quad \text{depth}(\mathcal{G}_3^{(n)}) = \begin{cases} n^2 + 5n - 19, & n \geq 5, \\ 18, & n = 4, \\ 8, & n = 3. \end{cases}$$

Moreover, it holds

$$\ell \mathcal{G}_3^{(n)} = (\ell_1, \ell_3, \dots, \ell_{o_n}, \ell_{e_n}, \dots, \ell_4, \ell_2),$$

where o_n and e_n denote the largest odd number and largest even number less or equal than n , respectively.

Proof. First, we show that $W_3^{(n)}$ generates all three-body labels from the sequence $(\ell_{n-1} \ell_n, \dots, \ell_1 \ell_2, \ell_1)$ and

$$(\ell_1, \ell_1 \ell_2, \ell_2 \ell_3, \dots, \ell_{n-1} \ell_n) W_3^{(n)} = (\ell_1, \ell_3, \dots, \ell_{\text{odd}}^{(n)}, \ell_{\text{even}}^{(n)}, \dots, \ell_2) \text{CX}_{c_n, t_n}.$$

The case $n = 3$ follows from Theorem D.2 (iii). Now, suppose that the statement holds for some $n - 1 \geq 3$. Then, we deduce from Theorem D.2 (iii) again and Eq. (A2)

$$\begin{aligned} (\ell_1, \ell_1 \ell_2, \ell_2 \ell_3, \dots, \ell_{n-1} \ell_n) W_3^{(n)} &= (\ell_1, \ell_{n-1} \ell_n, \dots, \ell_3 \ell_4, \ell_2 \ell_3, \ell_2) \overline{W_3}^{(2,n)} \\ &= \overline{(\ell_1, \ell_2, \ell_2 \ell_3, \ell_3 \ell_4, \dots, \ell_{n-1} \ell_n) W_3^{(2,n)}}. \end{aligned}$$

as well as $W_3^{(n)}$ is generating the label set $\{\ell_1 \ell_i \ell_j \mid 1 < i < j \leq n\}$. Then, applying our induction hypothesis and Lemma A.15 shows that $\overline{W_3}^{(2,n)}$ is generating the label set $\{\ell_i \ell_j \ell_r \mid 2 \leq i < j < r \leq n\}$ from $(\ell_1, \ell_{n-1} \ell_n, \dots, \ell_3 \ell_4, \ell_2 \ell_3, \ell_2)$ and therefore, $W_3^{(n)}$ is a three-body generator. Moreover, we also see that applying Eq. (A2) and the induction hypothesis yields that right-hand side equals

$$\overline{(\ell_1, \ell_2, \ell_4, \dots, \ell_{\text{even}}^{(n)}, \ell_{\text{odd}}^{(n)}, \dots, \ell_5, \ell_3) \text{CX}_{c_{n-1}+1, t_{n-1}+1}^{(2,n)}} = (\ell_1, \ell_3, \dots, \ell_{\text{odd}}^{(n)}, \ell_{\text{even}}^{(n)}, \dots, \ell_2) \overline{\text{CX}_{c_{n-1}+1, t_{n-1}+1}}^{(2,n)}.$$

and $W_3^{(n)}$ is generating the label set $\{\ell_2 \ell_i \ell_j \mid 2 < i < j \leq n\}$. Using that $\overline{\text{CX}_{c_{n-1}+1, t_{n-1}+1}}^{(2,n)} = \text{CX}_{c_n, t_n}$ and Remark B.2 (iii) shows desired statement.

Finally, we prove the statements on the depth and size of $\mathcal{G}_3^{(n)}$. Since $\text{size}(W_3^{(n)}) = \text{size}(\text{NCS}_3^{(n)}) + \text{size}(W_3^{(n-1)})$, we have from Theorem D.2 (iii)

$$\text{size}(W_3^{(n)}) = \sum_{l=0}^{n-3} \text{size}(\text{PTN}_3^{(n-l)}) = \sum_{l=1}^n l^2 - l - 1 = \frac{1}{3} n^3 - \frac{4}{3} n,$$

which shows the expression for the size of $\mathcal{G}_3^{(n)}$. To derive the expression for the depth of $\mathcal{G}_3^{(n)}$, we use the relations $\text{depth}(W_3^{(n)}) = \text{depth}(\text{PTN}_3^{(n)}) + s_{n-1} + \text{depth}(W_3^{(n-1)})$ for $n \geq 4$ and $\text{depth}(W_3^{(5)}) = 26$ as well as Theorem D.2 (iii) to obtain

$$\begin{aligned} \text{depth}(W_3^{(n)}) &= \text{depth}(W_3^{(5)}) + \sum_{l=0}^{n-6} \text{depth}(\text{PTN}_3^{(n-l)}) + s_{n-l-1} \\ &= -19 + \sum_{l=1}^n \text{depth}(\text{PTN}_3^{(l)}) + s_{l-1} \\ &= -19 + \sum_{l=1}^n 2l + 3 = n^2 + 4n - 19 \end{aligned}$$

for $n \geq 6$. For $n = 3, 4$ one can easily verify $\text{depth}(W_3^{(3)}) = 5$ and $\text{depth}(W_3^{(4)}) = 14$, implying the expression for the depth of $\mathcal{G}_3^{(n)}$. \square

Appendix E: Generators for arbitrary $k \geq 4$

Based on the previous sections, we now show that there exists a family of k -body generators $\mathcal{G}_k = (\mathcal{G}_k^{(n)})_{n \geq k}$ with $\mu(\mathcal{G}_k, \mathcal{L}_k) = 2$ and $\nu(\mathcal{G}_k, \mathcal{L}_k) = k$ for nearest neighbor connectivity graphs for all $k \geq 2$. For the construction of our k -body generator for $k \geq 4$, we first introduce a so-called *clean special four-body generator*, which generates all four-body labels with one fixed special label. The definition of the clean special four-body generator is motivated by the three-body generator in App. D and replaces Parity Twine networks of type II by *Parity Twine networks of type III*. The main difference between these two networks is that the latter applies an additional Parity Twine chain at beginning of the circuit which encodes the additional special label on the qubits. Additionally, the latter network incorporates a final pre-cleanup circuit that reverts the output labels to single labels. Based on the clean four-body generator, we present a constructive algorithm for establishing clean special k -body generators for arbitrary $k \geq 4$ which consequently allows the design of k -body generators for all $k \geq 4$. Throughout the whole section, we suppose that $n \geq 4$. The main theorem reads as follows:

Theorem E.1. *For all $k \geq 2$, there exists a family of k -body generators for nearest neighbor connectivity graphs $\mathcal{G}_k = (\mathcal{G}_k^{(n)})_{n \geq k}$ with size $(\mathcal{G}_k^{(n)}) = \frac{2n^k}{k!} + \mathcal{O}(n^{k-1})$ and depth $(\mathcal{G}_k^{(n)}) = \frac{2n^{k-1}}{(k-1)!} + \mathcal{O}(n^{k-2})$. As a consequence, $\mu(\mathcal{G}_k, \mathcal{L}_k) = 2$ and $\nu(\mathcal{G}_k, \mathcal{L}_k) = k$, where $\mathcal{L}_k = (\mathcal{L}_k^{(n)})_{n \geq k}$ is the family of labels sets $\mathcal{L}_k^{(n)}$ containing all k -body labels on $n \geq k$ qubits.*

As already mentioned, for the proof of Theorem E.1 we make use of so-called *special k -body generators* which are defined as follows.

Definition E.2 (Special k -body generator). Let $C^{(n)}$ be a circuit with n qubits, $k \geq 2$ and $\ell = (\ell_1, \dots, \ell_n)$ with some labels ℓ_1, \dots, ℓ_n . We say that $C^{(n)}$ is a *special k -body generator* if $C^{(n)}$ generates all k -body labels

$$\{\ell_1 \ell_{i_1} \ell_{i_2} \dots \ell_{i_{k-1}} \ell_n \mid 1 < i_1 < \dots < i_{k-1} \leq n\}$$

from ℓ and $\hat{\ell}_1 = \ell_1$ where $\hat{\ell} := \ell C^{(n)}$. Furthermore, we call ℓ_1 the *special label*.

Next, we introduce the *Parity Twine network of type III* as well as the *post-cleanup circuit* which are one of the key-ingredients for the proof of Theorem E.1.

Definition E.3 (Parity Twine network of type III, post-cleanup circuit). (i) The *Parity Twine network of type III* is defined as $\text{PTN}_4^{(n)} := \text{CXC}'^{(3,n)} \odot_{-2(n-3)} \text{PTC}^{(n)} \odot_5 \text{PTN}'^{(1,n-1)}$.

(ii) The post-cleanup circuit $\text{CL}^{(n)}$ is defined as

$$\text{CL}^{(n)} := \text{CX}_{c_n, t_n} \odot \text{OSC}^{(m_n, m_n+2)} \odot \text{PTC}^{(m_n+2, n)} \odot \overline{\text{SWC}}^{(m_n, n)} \odot \overline{\text{PTC}}^{(1, m_n)},$$

where $m_n := \lceil \frac{n-1}{2} \rceil$ and (c_n, t_n) is (m_n+1, m_n+2) if n is odd and (m_n+1, m_n) if n is even. Here, $\text{OSC}^{(m_n, m_n+2)}$ is defined as the circuit which is set to $\text{SWC}^{(m_n, m_n+2)}$ if n is odd and the empty sequence if n is even.

Theorem E.4. (i) For the Parity Twine network of type III we have that

$$(\ell_1, \ell_2, \ell_2\ell_3, \ell_3\ell_4, \dots, \ell_{n-1}\ell_n) \text{PTN}_4^{(n)} = (\ell_1\ell_2, \ell_{n-1}\ell_n, \ell_{n-2}\ell_{n-1}, \dots, \ell_3\ell_4, \ell_3, \ell_1). \quad (\text{E1})$$

and $\text{PTN}_4^{(n)}$ generates the labels $\{\ell_1\ell_2\ell_i\ell_j \mid 2 < i < j \leq n\}$ from $(\ell_1, \ell_2, \ell_2\ell_3, \ell_3\ell_4, \dots, \ell_{n-1}\ell_n)$. Furthermore, it holds

$$\text{size}(\text{PTN}_4^{(n)}) = n^2 - n - 1 \quad \text{and} \quad \text{depth}(\text{PTN}_4^{(n)}) = 4n - 7 \quad (\text{E2})$$

(ii) Define the sequence of labels $\ell_{\text{out}} := (\ell_1\ell_2, \ell_3\ell_4, \ell_3, \ell_1)$ for $n = 4$ and

$$\ell_{\text{out}} := (\ell_1(\ell_2, \ell_4, \dots, \ell_{e_n-2}), \hat{\ell}_1, \hat{\ell}_2, \hat{\ell}_3, (\ell_{o_n-2}, \ell_{o_n-4}, \dots, \ell_3)\ell_1)$$

where $(\hat{\ell}_1, \hat{\ell}_2, \hat{\ell}_3) := (\ell_{n-1}\ell_n, \ell_{n-1}, \ell_1)$ for even n and $(\hat{\ell}_1, \hat{\ell}_2, \hat{\ell}_3) := (\ell_1, \ell_{n-1}, \ell_{n-1}\ell_n)$ for odd n . Here, o_n and e_n denote again the largest odd number and largest even number less or equal than n , respectively. Then, the post-cleanup circuit $\text{CL}^{(n)}$ satisfies

$$\ell_{\text{out}} \text{CL}^{(n)} = (\ell_1, \ell_2, \ell_4, \dots, \ell_{e_n}, \ell_{o_n}, \dots, \ell_5, \ell_3).$$

Furthermore, it holds

$$\text{size}(\text{CL}^{(n)}) = \text{depth}(\text{CL}^{(n)}) = 5n - 3m_n - 5 + 6(n \bmod 2) = \frac{7}{2}n - 5 \left(-\frac{1}{2}\right)^{n \bmod 2}. \quad (\text{E3})$$

Proof. (i) From Remark B.2 (ii) and (iii) we deduce that

$$\begin{aligned} (\ell_1, \ell_2, \ell_2\ell_3, \ell_3\ell_4, \dots, \ell_{n-1}\ell_n) \text{PTN}_4^{(n)} &= (\ell_1, \ell_2, \ell_2(\ell_3 \dots \ell_n)) \left(\text{PTC}^{(n)} \odot \text{PTN}'^{(1, n-1)} \right) \\ &= (\ell_1\ell_2, \ell_1\ell_2(\ell_3 \dots \ell_n), \ell_1) \text{PTN}'^{(1, n-1)}. \end{aligned}$$

Therefore, applying Theorem D.2 (ii) on the label sequence $(\ell_1\ell_2, \ell_1\ell_2(\ell_3 \dots \ell_n), \ell_1)$ proves the first statement in (i). Moreover, using the expressions for the size and depth in Theorem D.2 (ii) we deduce $\text{size}(\text{PTN}_4^{(n)}) = 3n - 4 + \text{size}(\text{PTN}'^{(1, n-1)}) = n^2 - n$ as well as $\text{depth}(\text{PTN}_4^{(n)}) = 5 + \text{depth}(\text{PTN}'^{(1, n-1)}) = 4n - 7$.

(ii) Using Remark B.2 (ii), Remark B.4 (ii) and Lemma A.15, the statements in (ii) can be easily verified. \square

The definition of the Parity Twine network of type III and the post-cleanup circuit leads us immediately to the definition of the clean special four-body generator.

Definition E.5 (Clean special four-body generator). Let $W_4^{(n)} := \text{PTN}_4^{(n)} \odot_{s_{n-1}} \overline{W}_4^{(2, n)}$ with $W_4^{(4)} := \text{PTN}_4^{(4)}$ where and s_n is defined as in Definition D.3. Then, we define the circuit [see Fig. 4(a)]

$$\mathcal{SG}_4^{(n)} := (\text{CXC}^{(2, n)})^\dagger \odot W_4^{(n)} \odot \text{CL}^{(n)}.$$

Theorem E.6. The circuit $\mathcal{SG}_4^{(n)}$ in Definition E.5 is a clean special four-body generator satisfying

$$\begin{aligned} \text{size}(\mathcal{SG}_4^{(n)}) &= \frac{1}{3}n^3 + \frac{19}{6}n - 7 - 5 \left(-\frac{1}{2}\right)^{n \bmod 2} \quad \text{and} \\ \text{depth}(\mathcal{SG}_4^{(n)}) &= \begin{cases} n^2 + \frac{17}{2}n - 26 - 5 \left(-\frac{1}{2}\right)^{n \bmod 2}, & n \geq 5, \\ 20, & n = 4. \end{cases} \end{aligned}$$

Moreover, it holds

$$\ell \mathcal{SG}_4 = (\ell_1, \ell_2, \ell_4, \dots, \ell_{e_n}, \ell_{o_n}, \dots, \ell_5, \ell_3). \quad (\text{E4})$$

Proof. Using the same steps as in the proof of Theorem D.4 and applying Theorem E.4 (i), it can be verified that $W_4^{(n)}$ generates the labels $\{\ell_1 \ell_{i_1} \ell_{i_2} \ell_{i_3} \mid 1 < i_1 < i_2 < i_3 \leq n\}$ from the sequence $(\ell_1, \ell_2, \ell_2 \ell_3, \ell_3 \ell_4, \dots, \ell_{n-1} \ell_n)$ and

$$(\ell_1, \ell_2, \ell_2 \ell_3, \ell_3 \ell_4, \dots, \ell_{n-1} \ell_n) W_4^{(n)} = \ell_{\text{out}},$$

where ℓ_{out} is defined as in Theorem E.4 (ii). Therefore, using that $\ell(\text{CXC}^{(2,n)})^\dagger = (\ell_1, \ell_2, \ell_2 \ell_3, \ell_3 \ell_4, \dots, \ell_{n-1} \ell_n)$ and applying Theorem E.4 (ii) shows that $\mathcal{SG}_4^{(n)}$ is a clean special four-body generator satisfying Eq. (E4). Moreover, since $\text{size}(\text{PTN}_3^{(n)}) = \text{size}(\text{PTN}_4^{(n)})$ as well as $\text{depth}(\text{PTN}_3^{(n)}) = \text{depth}(\text{PTN}_4^{(n)})$ we have

$$\text{size}(W_4^{(n)}) = \text{size}(W_3^{(n)}) - \text{size}(\text{PTN}_3^{(3)}) = \text{size}(W_3^{(n)}) - 5$$

and similarly

$$\text{depth}(W_4^{(n)}) = \text{depth}(W_3^{(n)}) - 5.$$

Using the expression for $\text{depth}(W_3^{(n)})$ in the proof of Theorem D.4 as well as Eq. (E3) imply the remaining identities. \square

Subsequently to the clean special four-body generator in Definition E.5, we now show how arbitrary clean special k -body generator with $k \geq 4$ can be constructed.

Definition E.7 (Clean special k -body generator). Let $k_0 \geq 2$ and suppose that $\mathcal{SG}_{k_0}^{(n)}$ is a clean special k_0 -body generator. Then, we define for $k > k_0$

$$\mathcal{SG}_k^{(n)} := W_k^{(n)} \odot \text{CX}_{n-k+1, n-k+2} \odot \overline{\text{PTC}}^{(1, n-k+1)} \quad (\text{E5})$$

where $W_k^{(n)} := \text{CX}_{1,2} \odot \mathcal{SG}_{k-1}^{(2,n)} \odot \text{SW}_{1,2} \odot W_k^{(2,n)}$ with $W_k^{(k)} := \text{CX}_{1,2} \odot \mathcal{SG}_{k-1}^{(2,k)}$. Fig. 4(c) illustrates the circuit $\mathcal{SG}_k^{(n)}$.

Theorem E.8. Under the assumptions of Definition E.7, the circuit $\mathcal{SG}_k^{(n)}$ is a clean special k -body generator for each $k \geq k_0$. Moreover, if the clean special k_0 -body generator satisfies

$$\text{size}(\mathcal{SG}_{k_0}^{(n)}) = c_1 n^{k_0-1} + \mathcal{O}(n^{k_0-2}) \quad \text{and} \quad \text{depth}(\mathcal{SG}_{k_0}^{(n)}) = c_2 n^{k_0-2} + \mathcal{O}(n^{k_0-3})$$

where $c_1, c_2 > 0$ are some constants, then for every $k \geq k_0$ it holds

$$\text{size}(\mathcal{SG}_k^{(n)}) = c_1 \frac{(k_0-1)!}{(k-1)!} n^{k-1} + \mathcal{O}(n^{k-2}) \quad \text{and} \quad \text{depth}(\mathcal{SG}_k^{(n)}) = c_2 \frac{(k_0-2)!}{(k-2)!} n^{k-2} + \mathcal{O}(n^{k-3}).$$

Proof. (i) First, we show that $\mathcal{SG}_k^{(n)}$ is a clean special k -body generator for each $k \geq k_0$. To this end, suppose that $\mathcal{SG}_{k-1}^{(n)}$ is a clean-special $k-1$ -body generator for some $k-1 \geq k_0$. We prove that $W_k^{(n)}$ is a special k -body generator from ℓ and that there exists a permutation $\pi: \{1, \dots, n\} \rightarrow \{1, \dots, n\}$ with $\pi(1) = 1$ satisfying

$$\ell W_k^{(n)} = (\hat{\ell}_1 (\hat{\ell}_2 \dots \hat{\ell}_{n-k+1}), \hat{\ell}_1, \hat{\ell}_1 \hat{\ell}_{n-k+2}, \hat{\ell}_{n-k+3}, \dots, \hat{\ell}_n) \quad (\text{E6})$$

for $n > k$ and $\ell W_k^{(n)} = (\hat{\ell}_1, \hat{\ell}_1 \hat{\ell}_2, \hat{\ell}_3, \dots, \hat{\ell}_k)$ where $(\hat{\ell}_1, \dots, \hat{\ell}_n) := (\ell_{\pi(1)}, \dots, \ell_{\pi(n)})$. The remaining statement follows from the application of the label sequence on the right-hand side in Eq. (E6) on the circuits $\text{CX}_{k+1, n-k+2}$ and $\overline{\text{PTC}}^{(1, n-k+1)}$ given in Eq. (E5). The case $n = k$ can be easily verified. For $n > k$ we first observe that there exists a permutation $\pi_1: \{1, \dots, n-1\} \rightarrow \{1, \dots, n-1\}$ with $\pi_1(1) = 1$ such that

$$(\ell \text{CX}_{1,2}) \mathcal{SG}_{k-1}^{(2,n)} = (\ell_1, \ell_1 \ell_2, \ell_3, \dots, \ell_n) \mathcal{SG}_{k-1}^{(2,n)} = (\ell_1, \ell'_{\pi_1(1)}, \dots, \ell'_{\pi_1(n-1)}),$$

where $\ell'_1 := \ell_1 \ell_2$ and $\ell'_i := \ell_{i+1}$ for $2 \leq i \leq n-1$, and $\mathcal{SG}_{k-1}^{(2,n)}$ is generating the labels

$$\left\{ \ell'_1 \ell'_{i_1} \dots \ell'_{i_{k-2}} \mid 1 < i_1 < \dots < i_{k-2} \leq n \right\} = \left\{ \ell_1 \ell_2 \ell_{i_1} \dots \ell_{i_{k-2}} \mid 2 < i_1 < \dots < i_{k-2} \leq n \right\} \quad (\text{E7})$$

from $(\ell_1, \ell_1\ell_2, \ell_3, \dots, \ell_n)$. Furthermore, from our induction hypothesis we can imply that there exists a further permutation $\pi_2: \{1, \dots, n-1\} \rightarrow \{1, \dots, n-1\}$ with $\pi_2(1) = 1$ such that $W_k^{(2,n)}$ is generating the labels

$$\left\{ \ell_1 \ell'_{\pi_1(i_1+1)} \dots \ell'_{\pi_1(i_{k-1}+1)} \mid 1 < i_1 < \dots < i_{k-1} \leq n-1 \right\} = \left\{ \ell_1 \ell_{i_1} \dots \ell_{i_{k-1}} \mid 2 < i_1 < \dots < i_{k-1} \leq n \right\}$$

from the label sequence $\tilde{\ell} := (\ell \text{CX}_{1,2})(\mathcal{SG}_{k-1}^{(2,n)} \odot \text{SW}_{1,2}) = (\ell_1 \ell_2, \ell_1, \ell'_{\pi_1(2)}, \dots, \ell'_{\pi_1(n-1)})$ as well as

$$\begin{aligned} \tilde{\ell} W_k^{(2,n)} &= (\ell_1 \ell_2, \hat{\ell}_1 (\hat{\ell}_2 \dots \hat{\ell}_{n-k}), \hat{\ell}_1, \hat{\ell}_1 \hat{\ell}_{n-k+1}, \hat{\ell}_{n-k+2}, \dots, \hat{\ell}_{n-1})) \\ &= (\ell_1 \ell_2, \ell_1 (\ell_{\pi(2)+1} \dots \ell_{\pi(n-k)+1}), \ell_1, \ell_1 \ell_{\pi(n-k+1)+1}, \ell_{\pi(n-k+2)+1}, \dots, \ell_{\pi(n-1)+1}) \\ &= (\ell_{\sigma(1)} (\ell_{\sigma(2)} \dots \ell_{\sigma(n-k+1)}), \ell_1, \ell_1 \ell_{\sigma(n-k+2)}, \ell_{\sigma(n-k+3)}, \dots, \ell_{\sigma(n)}) \end{aligned}$$

where $(\hat{\ell}_1, \dots, \hat{\ell}_n) := (\ell_{\sigma_1}, \ell'_{\sigma(2)}, \dots, \ell'_{\sigma(n-1)})$ and $\pi := \pi_1 \circ \pi_2$. Here, $\sigma: \{1, \dots, n\} \rightarrow \{1, \dots, n\}$ denotes the permutation defined by $\sigma(1) := 1$, $\sigma(2) := 2$ and $\sigma(i) := \pi(i-1) + 1$. This shows together with Eq. (E7) that $W_k^{(n)}$ is a special k -body generator satisfying Eq. (E6).

(ii) We only prove the expression for the size of the circuit $\mathcal{SG}_k^{(n)}$. The expression for the depth of the circuit $\mathcal{SG}_k^{(n)}$ can be proven analogously. Assume that the statement holds for some $k-1 \geq k_0$. Then, our induction hypothesis implies

$$\text{size}(\mathcal{SG}_k^{(n)}) = \mathcal{O}(n) + \sum_{i=1}^{n-k} \text{size}(\mathcal{SG}_{k-1}^{(i+1,n)}) = \mathcal{O}(n) + c_1 \frac{(k_0-1)!}{(k-2)!} \sum_{i=1}^{n-2} i^{k-2} + \mathcal{O}(i^{k-3}).$$

Hence, applying Faulhaber's formula yields the above identity for the size of $\mathcal{SG}_k^{(n)}$. \square

Finally, based on clean special k -body generator we now establish k -body generators and derive their properties subsequently, completing the proof of Theorem E.1.

Definition E.9 (k -body generator). Let $k \geq 2$ and suppose that $\mathcal{SG}_k^{(n)}$ is a clean special k -body generator. Then, we set $\mathcal{G}_k^{(n)} := \mathcal{SG}_k^{(n)} \odot \mathcal{SG}_k^{(2,n)} \odot \dots \odot \mathcal{SG}_k^{(n-k+1,n)}$. Fig. 4(b) demonstrates an illustration of the circuit for the case $k=4$.

Theorem E.10. (i) Under the assumptions of Definition E.9, the circuit $\mathcal{G}_k^{(n)}$ is a k -body generator.

(ii) Let $k_0 \geq 2$ and $\mathcal{SG}_{k_0}^{(n)}$ be a clean special k_0 -body generator. Then, for every $k > k_0$ the circuit $\mathcal{SG}_k^{(n)}$ as defined in Definition E.7 is a clean special k -body generator and the circuit $\mathcal{G}_k^{(n)}$ as defined in Definition E.9 is a k -body generator. Moreover, if $\mathcal{SG}_{k_0}^{(n)}$ satisfies

$$\text{size}(\mathcal{SG}_{k_0}^{(n)}) = c_1 n^{k_0-1} + \mathcal{O}(n^{k_0-2}) \quad \text{and} \quad \text{depth}(\mathcal{SG}_{k_0}^{(n)}) = c_2 n^{k_0-2} + \mathcal{O}(n^{k_0-3}),$$

then it holds

$$\text{size}(\mathcal{G}_k^{(n)}) = c_1 \frac{(k_0-1)!}{k!} n^k + \mathcal{O}(n^{k-1}) \quad \text{and} \quad \text{depth}(\mathcal{G}_k^{(n)}) = c_2 \frac{(k_0-2)!}{(k-1)!} n^{k-1} + \mathcal{O}(n^{k-2}).$$

Proof. The statement in (i) can easily be proven by induction. The first statement in (ii) follows from Theorem E.8 and (i). The expressions for the depth and size of $\mathcal{G}_k^{(n)}$ can be similarly derived as the expressions for the depth and size of $\mathcal{SG}_k^{(n)}$ in the proof of Theorem E.8. \square

Proof of Theorem E.1. For $k=2$, the statement follows from the results presented [35]. The case $k=3$ follows from Theorem D.4. The case $k \geq 4$ is obtained by Theorem E.6 and Theorem E.10 (ii). \square

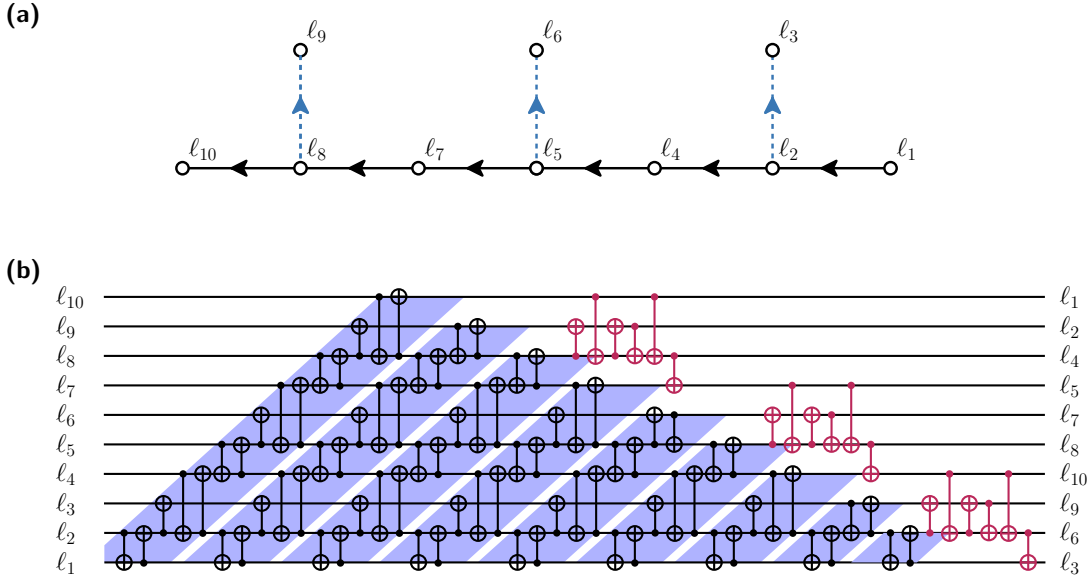


FIG. 14. (a) A Hamiltonian grid path for a sub-graph within a heavy-hexagon connectivity graph: Every other qubit has three immediate neighbors. (b) Implementation of a two-body generator $\mathcal{G}_{2,\text{hex}}^{(10)}$ based on the Hamiltonian grid path shown in (a) including a decoding circuit. CNOT gates depicted in red are attributed to the final decoding step.

Appendix F: Two-body generators for heavy-hexagon connectivity graphs

In this section, we investigate the heavy hexagon qubit layouts [21] and demonstrate how to utilize the strategy developed in Sec. IV C to build two-body generators. In contrast to the square grid connectivity graphs outlined in Sec. IV C, heavy hexagonal qubit layouts do not possess a Hamiltonian path. However, all qubits can be connected in a Hamiltonian grid path, where (roughly) every sixth qubit is a Hamiltonian grid path neighbor. In (the bulk of) a heavy hexagonal layout, every other qubit has three neighbors. Thus, Hamiltonian grid paths, based on sub-graphs of heavy hexagons, can have as many as 1/3 of the involved qubits as Hamiltonian grid neighbors. A corresponding Hamiltonian grid path is schematically shown in Fig. 14(a). Applying the principles of Sec. IV C along the Hamiltonian grid path of Fig. 14(a), we can immediately conclude the CNOT count of a two-body generator: Since one out of three qubits represents a Hamiltonian grid path neighbor, for generating three new two-body labels we require five CNOT gates (in contrast to the LNN case where we would require six). Thus, we expect to find an average asymptotic CNOT count of $\mu(\mathcal{G}_2, \mathcal{L}_2) = \frac{5}{3}$.

Fig. 14(b) illustrates the construction of $\mathcal{G}_{2,\text{hex}}^{(n)}$: shifted concatenations of adapted Parity Twine chains (PTC_{hex}, marked in blue) form a PTN_{hex}⁽ⁿ⁾ circuit. This is followed by a decoding circuit (marked in red) to restore single-labels. For the count and depth we obtain

$$\text{size} \left(\text{PTN}_{\text{hex}}^{(n)} \right) = \frac{5}{6} n^2 + \mathcal{O}(n)$$

$$\text{depth} \left(\text{PTN}_{\text{hex}}^{(n)} \right) = 5n + \mathcal{O}(1).$$

Note that, unlike for square grid connectivity graphs, here the lack of a Hamiltonian path complicates the decoding: Instead of a simple CNOT chain, here decoding requires $2n$ CNOT gates [compare Fig. 14(b)].

The two-body generators $\mathcal{G}_{2,\text{hex}}^{(n)}$ can be used for algorithms such as QFT and QAOA as discussed in Sec. V B and V A. For QAOA, shifted concatenation of $\mathcal{G}_{2,\text{hex}}^{(n)}$ and $(\mathcal{G}_{2,\text{hex}}^{(n)})^\dagger$ induces a depth reduction per QAOA layer by a factor of ~ 2 , resulting in a depth of $\frac{5}{2}n(1 + \frac{1}{p}) + \mathcal{O}(1)$ per QAOA layer given an odd number of QAOA cycles p . In case of an even number of cycles, the depth is slightly lower due to the asymmetry of the corresponding generators. In this case we find a depth of $\frac{5}{2}n(1 + \frac{2}{3p}) + \mathcal{O}(1)$.

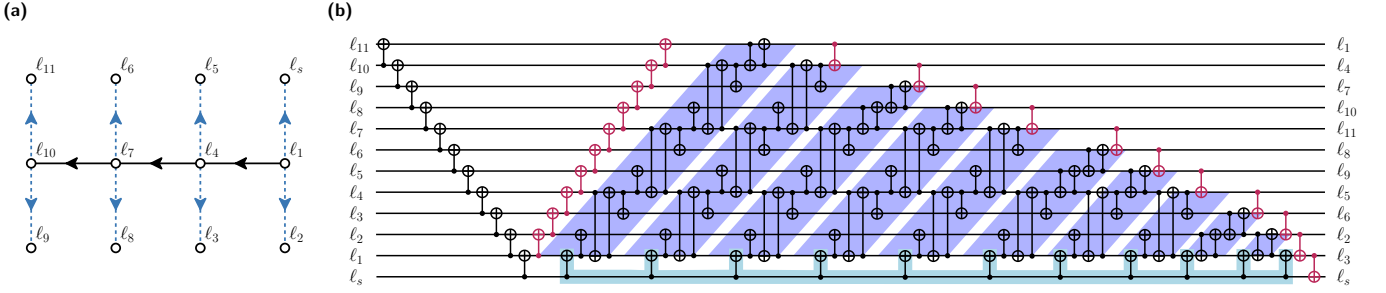


FIG. 15. (a) The Hamiltonian grid path used for the design of the adapted $\text{PTN}_{3,\text{grid}}$ circuit illustrated in (b) with 12 qubits. (b) The adapted special three-body generator $\text{PTN}_{3,\text{grid}}$ for the square grid connectivity graph pictured in (a).

Appendix G: k -body generators on complete and planar connectivity graphs

In this chapter, we discuss the size and depth scaling for the proposed k -body generators for complete and square grid connectivity graphs. However, rather than repeating extensive derivations, our focus is on the scaling up to leading order. We begin with the two-body generators.

1. Count and depth analysis of two-body generators

As discussed in the main text, for the construction of two-body generators on complete graphs, DCNOT gates can be replaced with CNOT gates resulting in half the number of gates as compared to the corresponding construction for nearest neighbor connectivity graphs. Since a two-body generator relies solely on DCNOT gates, we readily obtain

$$\text{size} \left(\text{PTN}_{\text{all-to-all}}^{(n)} \right) = \frac{1}{2} n^2 + \mathcal{O}(n).$$

A similar argument can be used to derive the depth: Since the count of each $\text{PTC}_{\text{all-to-all}}^{(n)}$ halves, so does the depth. Consequently, shifted concatenations of $\text{PTC}_{\text{all-to-all}}^{(n)}$ forming $\text{PTN}_{\text{all-to-all}}^{(n)}$ equivalently halve in depth resulting in

$$\text{depth} \left(\text{PTN}_{\text{all-to-all}}^{(n)} \right) = 2n + \mathcal{O}(1).$$

Fig. 6 illustrates the circuit for the two-body generator for complete graphs.

For square grid connectivity graphs, we observe that the Hamiltonian grid path consists of $\frac{1}{3}n + \mathcal{O}(\sqrt{n})$ qubits, resulting in $\frac{1}{3}n + \mathcal{O}(\sqrt{n})$ DCNOT gates, and $\frac{2}{3}n + \mathcal{O}(\sqrt{n})$ Hamiltonian grid path neighbors, corresponding to $\frac{2}{3}n + \mathcal{O}(\sqrt{n})$ CNOT gates. Hence, we deduce that $\text{size} \left(\text{PTC}_{\text{grid}}^{(n)} \right) = \frac{4}{3}n + \mathcal{O}(\sqrt{n})$. This implies that

$$\text{size} \left(\text{PTN}_{\text{grid}}^{(n)} \right) = \sum_{l=0}^{n-2} \text{size} \left(\text{PTC}_{\text{grid}}^{(n-l)} \right) = \sum_{l=2}^n \left(\frac{4}{3}l + \mathcal{O}(\sqrt{l}) \right) = \frac{2}{3}n^2 + \mathcal{O}(n^{3/2}).$$

Note that we also neglected the final pigeonhole circuit after each PTC_{grid} since they are of order $\mathcal{O}(1)$. The depth depends on the shifts introduced between consecutive PTC_{grid} circuits. From the circuit in Fig. 9, we observe that the square grid strategy requires a shift of six moments for a grid with three rows. Therefore, the depth is

$$\text{depth} \left(\text{PTN}_{\text{grid}}^{(n)} \right) = 6n + \mathcal{O}(\sqrt{n}).$$

2. Count and depth analysis of k -body generators

Next, we discuss the generalization to k -body generators by first considering complete graphs. The case $k = 3$ is not treated explicitly, but follows the same reasoning.

From Fig. 4(a) we observe that the only component of the clean special four-body generator circuit that determines the size to leading-order is the $\text{PTN}_4^{(n)}$ circuit. $\text{PTN}_{4,\text{all-to-all}}^{(n)}$ can be obtained similarly to $\text{PTN}_{\text{all-to-all}}^{(n)}$ and has half the size of $\text{PTN}_4^{(n)}$. This readily yields

$$\text{size} \left(\mathcal{SG}_{4,\text{all-to-all}}^{(n)} \right) = \mathcal{O}(n) + \sum_{l=0}^{n-4} \text{size} \left(\text{PTN}_{4,\text{all-to-all}}^{(n-l)} \right) = \frac{1}{6} n^3 + \mathcal{O}(n^2).$$

Together with Theorem E.10, we find $\mu(\mathcal{G}_{k,\text{all-to-all}}, \mathcal{L}_k) = 1$.

For the depth scaling of the circuit construction for complete graphs, we again refer to Fig. 4(a), now focusing on the shifts between circuit components. As outlined in App. G 1 similar to the count, also the depth of respective two-body generators for complete graphs halves with respect to nearest neighbor connectivity graphs. Now there are two extra components to be considered for special four-body generators: the initial CNOT chains of the PTN_4 circuits and the initial CNOT gates of the modified Parity Twine chains. These components consist of CNOT gates with shifts of two and four moments, respectively, which can also be halved. Therefore, we have

$$\text{depth} \left(\mathcal{SG}_{4,\text{all-to-all}}^{(n)} \right) = \frac{1}{2} n^2 + \mathcal{O}(n).$$

Finally, combining this with Theorem E.10 we find $\nu(\mathcal{G}_{k,\text{all-to-all}}, \mathcal{L}_k) = k/2$.

Similar arguments can be applied to the size scaling of respective circuits adapted to square grids. The main size contribution for building the clean special four-body generator still arises from the concatenated $\text{PTN}_{4,\text{grid}}$ circuits, which can be obtained just as the PTN_{grid} circuits. Therefore, using $\text{size} \left(\text{PTC}_{\text{grid}}^{(n)} \right) = \frac{4}{3}n + \mathcal{O}(\sqrt{n})$ and applying Theorem E.10, we conclude

$$\mu(\mathcal{G}_{k,\text{grid}}, \mathcal{L}_k) = \frac{4}{3}.$$

For the depth analysis, we observe that the PTN_{grid} circuit forms a “triangle” (compare to the circuit diagram of Fig. 9) with a relatively long right side (measured in circuit moments), unlike the symmetric “triangle” used for the circuit construction for nearest neighbor connectivity graphs. In the main text, we discuss a strategy useful for QAOA using shifted concatenations of PTN_{grid} and $(\overline{\text{PTN}}_{\text{grid}})^\dagger$ to optimize depth. However, since $\text{PTN}_{4,\text{grid}}$ is not clean, utilizing the adjoint is not possible because the special label creates an asymmetry between the input and output label sequences. Consequently, when building a clean special four-body generator, we can only use reversed circuits for subsequent special $\text{PTN}_{4,\text{grid}}$ circuits. This allows shifted concatenations with an overlap of $\frac{4}{3}n + \mathcal{O}(\sqrt{n})$ leading to

$$\text{depth} \left(\mathcal{SG}_{4,\text{grid}}^{(n)} \right) = \mathcal{O}(n) + \sum_{l=4}^{n-1} \left(6l - \frac{4}{3}l + \mathcal{O}(\sqrt{l}) \right) = \frac{7}{3} n^2 + \mathcal{O}(n\sqrt{n}).$$

Combining this result with Theorem E.10 yields $\nu(\mathcal{G}_{k,\text{grid}}, \mathcal{L}_k) = \frac{7}{3}k$. For the analogous construction for heavy-hexagon connectivity graphs we obtain $\mu(\mathcal{G}_{k,\text{hex}}, \mathcal{L}_k) = \frac{5}{3}$ and $\nu(\mathcal{G}_{k,\text{hex}}, \mathcal{L}_k) = \frac{5}{3}k$ for $k \geq 3$.

The above results, in particular the increased depth scaling, emerges from the alignment mismatch of the corresponding generators. This is especially pronounced in the case of square grid connectivity graph and, in fact, is expected to worsen with increased connectivity. However, for the case of $k = 3$, these issues can be partially circumvented using adapted generator building blocks to yield further depth reductions. The main idea of this approach is as follows: Instead of applying the initial CNOT chain solely before the first $\text{PTN}_{3,\text{grid}}$ circuit, we apply it before every $\text{PTN}_{3,\text{grid}}$ circuit. Moreover, we add an additional CNOT chain after each $\text{PTN}_{3,\text{grid}}$ circuit (see Fig. 15). The resulting modified $\text{PTN}_{3,\text{grid}}$ circuit maps a sequence of single labels to a sequence of single labels while generating all three-body labels with the special label ℓ_s . As a consequence, this enables us to use Lemma A.16 and concatenate $\text{PTN}_{3,\text{grid}}$ and $(\overline{\text{PTN}}_{3,\text{grid}})^\dagger$ (instead of $\text{PTN}_{3,\text{grid}}$ and $\overline{\text{PTN}}_{3,\text{grid}}$). Then, consecutive $\text{PTN}_{3,\text{grid}}$ $[(\overline{\text{PTN}}_{3,\text{grid}})^\dagger]$ can be shifted with overlaps alternating between $6n - 4/3n + \mathcal{O}(\sqrt{n}) = 14/3n + \mathcal{O}(\sqrt{n})$ and $n + \mathcal{O}(1)$ which reduces the depth as we circumvent the alignment mismatch. However, individual modified $\text{PTN}_{3,\text{grid}}$ blocks possess an increased depth of $7n$, so that in total the depth of the three-body generator designed in this way sums up to $\frac{25}{12}n^2 + \mathcal{O}(n^{3/2})$. In principle, this approach can also be applied to heavy-hexagon connectivity graphs. However, there, the corresponding alignment mismatch is less dramatic [see Fig. 14(b)]. As a consequence the modification of the $\text{PTN}_{3,\text{grid}}$ as outlined for square grid connectivity graphs does not lead to a depth reduction. In general, we expect this method to achieve depth reductions for layouts with sufficient connectivity with the effect getting more pronounced for increasing connectivity.

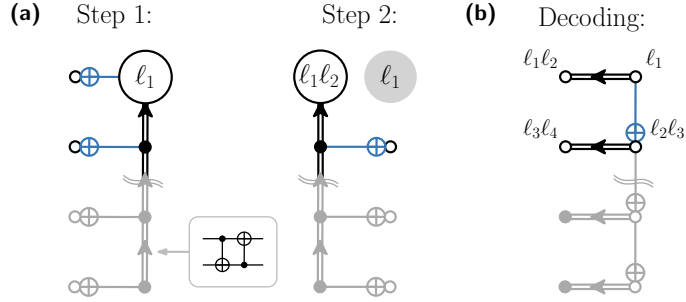


FIG. 16. (a) Schematic of the first two consecutive Parity Twine chains adapted to a ladder connectivity graph, illustrating how labels are transported along two distinct Hamiltonian grid paths. (b) Schematic of the decoding procedure, which begins with a single DCNOT gate and is followed by one CNOT gate. This sequence is then applied repeatedly from top to bottom. The resulting decoding step contributes only in sub-leading order to both the circuit size and depth.

Appendix H: Optimizing depth for planar connectivity graphs

In Sec. IV C we have introduced a robust strategy to reduce the gate count of k -body generator algorithms by efficiently implementing them on a given connectivity graph. Simultaneously, this comes at the expense of a depth increase compared to the corresponding construction for nearest neighbor connectivity graphs. If we aim to improve both, size and depth, several additional considerations are necessary. Specifically, achieving lower depth (as compared to implementations for nearest neighbor connectivity graphs) requires stricter connectivity requirements on the hardware, which is why in the main text we focus on a more practical, ready-to-implement strategy.

The overall size of our algorithm implementations is largely determined by the size of the DCNOT gates which constitutes the most prominent component. Meanwhile, the depth depends on the required shift between the constituent circuit components, in particular the shifts between subsequent Parity Twine chains. Conceptually, we can interpret the minimal shift between Parity Twine chains as the number of moments one Parity Twine chain needs to transport a corresponding label far enough so that it does not interfere with the label transported by the subsequent Parity Twine chain. To reduce these shifts, faster label transportation is essential. One way to achieve this is by using multiple Hamiltonian grid paths for label transport. The corresponding Hamiltonian paths must not intersect, collectively cover all qubits and an edge must exist that connects labels that have traveled m moments on one path with those that have traveled m moments on another. We also note that k -body generator algorithms for $k > 2$ require implementing a special version of Parity Twine chains. This imposes an additional hardware requirement: the special label must connect to the starting position of each Hamiltonian grid path.

Finally, we demonstrate how the above strategy can be applied to construct a two-body generator on a ladder connectivity graph (see Fig. 16) that reduces both size and depth compared to the two-body generator for nearest neighbor connectivity graphs. A ladder layout naturally provides two Hamiltonian grid paths that meet all the requirements for a two-body generator as outlined above. With this strategy, we achieve

$$\text{size} \left(\text{PTN}_{\text{ladder}}^{(n)} \right) = \frac{3}{4} n^2 + \mathcal{O}(n)$$

$$\text{depth} \left(\text{PTN}_{\text{ladder}}^{(n)} \right) = 3n + \mathcal{O}(1).$$

Interestingly, these scaling factors lie midway between our constructions for complete and nearest neighbor connectivity graphs, yet require only a moderate increase in connectivity compared to nearest neighbor connectivity graphs (see Tabs. I and II). To adapt this approach for k -body generators while preserving the improved depth scaling, one would need to introduce ‘‘checkerboard connectivity’’ - that is, diagonal couplings between qubits that are already connected in the vertical and horizontal directions.

Appendix I: Proof of a non-trivial lower bound for μ

In this section, we derive a non-trivial lower bound for the asymptotically average CNOT count for nearest neighbor connectivity graphs.

Theorem I.1. *Consider a family $L = (L^{(n)})_n$ of label sets (n being the number of qubits) with the following two properties:*

(i) For all $\ell_1, \ell_2 \in L^{(n)}$ we have $\ell_1 \ell_2 \notin L^{(n)}$.

(ii) We have $\lim_{n \rightarrow \infty} \frac{|L^{(n)}|}{n} = \infty$.

Let $C = (C^{(n)})_n$ be a family of CNOT-circuits for nearest neighbor connectivity graphs so that $C^{(n)}$ generates $L^{(n)}$. Then

$$\mu(C, L) \geq 1 + \gamma,$$

for some absolute constant $\gamma > 0$.

Remark I.2. The largest γ for which the theorem holds is not known to us. In the proof below we give a simple argument to see that $\gamma = \frac{1}{43}$ works. A slightly more involved argument pushes this to $\gamma = \frac{1}{9}$. But we have no reason to assume that this is optimal.

Proof. Consider an arbitrary family of labels and a corresponding family of generator circuits as described *but* with the property that

$$\frac{\text{size}(C^{(n)})}{|L^{(n)}|} \leq 1 + \delta \quad (\text{I1})$$

for an infinite number of n . In order to prove the theorem we have to show that necessarily $\delta \geq \gamma$. Below we always assume that n is set to one of the values for which the above inequality holds. Moreover we consider the limit for large n whenever we utilize Landau-notation like $o(1)$.

Without loss of generality we may assume that every moment of the circuits contains exactly one CNOT gate. We may also assume that none of the single body labels is an element of $L^{(n)}$ (due to property (ii)).

Let us define a few things. For a moment m and qubit i we call (i, m) a *spacetime point*. Next we define the notion of a *good* spacetime point which basically tracks where new labels occur. We do this recursively by looking through the following list of rules and apply the first one which matches:

- Initialization: spacetime point $(i, 1)$ is *bad* (meaning *not good*) for all i ,
- Spawning good: (i, m) is good if qubit i is a target (of a CNOT gate) at moment m and the resulting label is in $L^{(n)}$ and occurs for the first time (did not occur in an earlier moment at any of the qubits),
- Spawning bad: (i, m) is bad if qubit i is a target at moment m and the previous case did not apply.
- Propagation: (i, m) is good if qubit i is not a target in moment m and $(i, m - 1)$ is good. The same rule applies to bad spacetime points.

We say that a CNOT gate (of the circuit) at moment m with target at t is *successful* if spacetime point (t, m) is good. Finally, let us say that a CNOT gate at moment m with target t is *typical* if it is successful, $m > 1$, and spacetime point $(t, m - 1)$ was already good. That is, the qubit which is targeted by a typical gate already supported a new label before the CNOT was applied and again got a new one after applying the gate. Fig. 17 shows a summary of these definitions.

In what follows we try to count the number of untypical gates in two different ways. We will obtain a contradiction if δ is too small.

a. *Counting untypical gates - part 1.* For a moment m let $\text{good}(m)$ be the number of good spacetime points in that moment. Clearly $0 \leq \text{good}(m) \leq n$. Moreover, $\text{good}(m) - \text{good}(m - 1) \in \{-1, 0, +1\}$ for all $m > 1$ (recall our assumption that each moment contains exactly one CNOT gate). Observe that (c.f. Fig. 17):

- If g is typical we have $\text{good}(m) - \text{good}(m - 1) = 0$.
- If g is untypical and successful we have $\text{good}(m) - \text{good}(m - 1) = 1$.
- If g is unsuccessful (hence untypical) we have $\text{good}(m) - \text{good}(m - 1) \in \{-1, 0\}$.

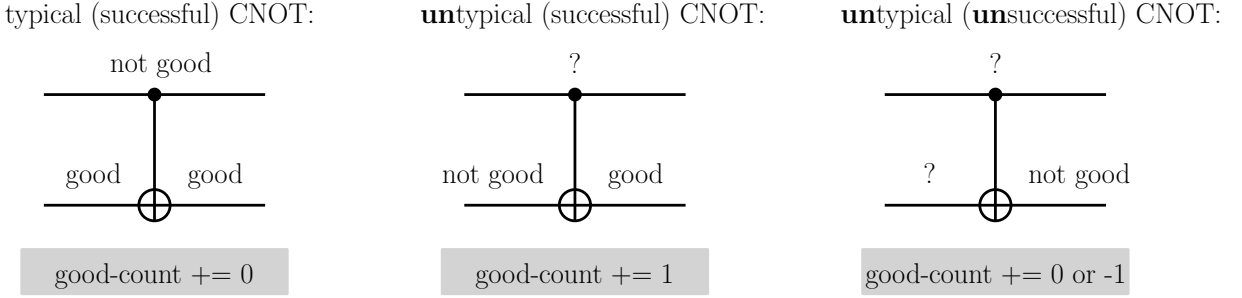


FIG. 17. A *successful* gate is a gate which produces a good spacetime point on its target (it contains one of the desired labels for the first time). A *typical* gate is successful and in addition its target was already succeeded by a good spacetime point. Interestingly, the control of a typical gate never occupies a good spacetime point. This is a consequence of the property (i) of the label sets we consider and is crucial for the proof.

Clearly we have exactly $|L^{(n)}|$ successful gates. Hence, we have at most $\delta |L^{(n)}|$ unsuccessful gates (see Eq. (I1)). Furthermore, from the above listing and the fact that the good-function is bounded by n we deduce that

$$\begin{aligned}
 & \left| \left\{ g \mid g \text{ is an untypical and a successful gate in } C^{(n)} \right\} \right| = \sum_{\substack{m=2 \\ \text{good}(m)-\text{good}(m-1)=1}}^{\text{depth}(C^{(n)})} 1 \\
 &= \sum_{m=2}^{\text{depth}(C^{(n)})} \text{good}(m) - \text{good}(m-1) - \sum_{\substack{m=2 \\ \text{good}(m)-\text{good}(m-1)\neq 1}}^{\text{depth}(C^{(n)})} \text{good}(m) - \text{good}(m-1) \\
 &\leq n + \left| \left\{ g \mid g \text{ is an unsuccessful gate in } C^{(n)} \right\} \right|.
 \end{aligned}$$

This and (ii) implies that there are at most $(\delta + o(1)) |L^{(n)}|$ untypical successful gates. Hence,

$$\text{there are at most } (2\delta + o(1)) |L^{(n)}| \text{ untypical gates} \quad (\text{I2})$$

or more precisely,

$$\text{there are at least } (1 - \delta - o(1)) |L^{(n)}| \text{ typical gates.} \quad (\text{I3})$$

b. *Counting untypical gates - part 2.* For subsets G of gates from $C^{(n)}$ let us define the partial function pred' by

$$\text{pred}'(G) := \text{the latest } g \text{ in } C^{(n)} \text{ before } G \text{ which targets one of the qubits of } G.$$

It is a partial function because such a g must not necessarily exist. With *qubits of* G we just mean the union of all controls and targets of the gates in G . That g comes *before* G means that every gate in G lives in a later moment than g . Let us define another partial function pred_3 , this time defined on the gates g of $C^{(n)}$ by

$$\text{pred}_3(g) = (g_1, g_2, g_3)$$

where $g_1 = \text{pred}'(\{g\})$ and $g_{i+1} = \text{pred}'(\{g, g_1, \dots, g_i\})$ for $i = 1, 2$. The intuition behind this is that $\text{pred}_3(g)$ gives us the first three gates *immediately* before g which have some influence on the label produced by g (if this many predecessor gates exist).

We call a gate g *super-typical* if it is typical and $\text{pred}_3(g)$ exists.

It is not hard to see that the number of gates for which pred_3 is *not* defined is at most $3(n-1) = o(1) |L^{(n)}|$ (using property (ii)). Therefore, we deduce from (I3) that

$$\text{there are at least } (1 - \delta - o(1)) |L^{(n)}| \text{ super-typical gates.} \quad (\text{I4})$$

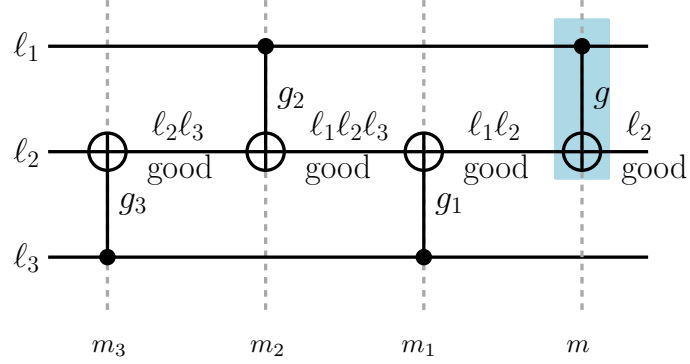


FIG. 18. Under the assumption that all of the four gates g , g_1 , g_2 , and g_3 are typical the gates have to be arranged in some alternating fashion as shown. This on the other hand is also not possible because the middle label present at spacetime point $(k+1, m_3-1)$ would be regenerated by g , which is not possible if g is typical. Let us note here that the definition of pred_3 ensures that we can ignore all other gates for the things that matter in our analysis. Indeed, it can happen that e.g. between moments m_3 and m other gates are applied. But by definition of the g_i they do not target relevant qubits. E.g. it can happen that there is a gate with control at k and target at $k-1$ somewhere between moments m_3 and m . But this is irrelevant for our analysis.

Finally let us define yet another partial function U by

$$U(g) := \text{the first gate in } \text{pred}_3(g) \text{ which is untypical.}$$

The intuition behind it is that for "some" typical gates it finds us an untypical gate. This in turn will help us to count untypical gates in a second way. Let us state two important claims

- Claim 1: $U(g)$ is defined for all super-typical g .
- Claim 2: There exists an absolute constant N such that for each untypical gate u the pre-image $U^{-1}(\{u\})$ contains at most N elements. An easy argument shows that $N = 21$ works. A more involved one shows that $N = 4$ works too.

Before we prove those two claims let us finish the main part of the proof: We are now in the position to prove the following chain of inequalities:

$$\begin{aligned} (2\delta + o(1)) |L^{(n)}| &\geq |\{g \mid g \text{ is untypical}\}| \\ &\geq |\{U(g) \mid g \text{ is super-typical}\}| = \sum_{g \in \{g \mid g \text{ is super-typical}\}} \frac{1}{|U^{-1}(\{U(g)\})|} \\ &\geq \frac{1}{N} |\{g \mid g \text{ is super-typical}\}| \\ &\geq \frac{1}{N} (1 - \delta - o(1)) |L^{(n)}|. \end{aligned}$$

The first line is just (I2). The second line follows from claim 1 and the third line from claim 2. The fourth line follows from (I4). From this we deduce that

$$\delta \geq \frac{1}{2N+1}$$

Using $N = 21$ implies the theorem and the proof is complete (up to the two claims).

c. *Proof of claim 1:* The claim basically just says that for any typical gate g for which $\text{pred}_3(g) = (g_1, g_2, g_3)$ exists, at least one of the g_i is untypical. We prove this by contradiction: Let us assume that there was a typical g , for which $\text{pred}_3(g) = (g_1, g_2, g_3)$ exists so that all g_i are typical too.

Let m be the moment in which g acts and m_i the moment in which g_i acts. By definition we have $m > m_1 > m_2 > m_3$. Let us assume that the control qubit of g is k and the target qubit $k+1$ (without loss of generality we can assume that the target has a higher index, otherwise we can just mirror the situation).

Let us make a short intermezzo to make a crucial observation: Consider a CNOT gate at moment m and with control and target at c and t . Assume it is typical. Then, the spacetime point (c, m) is necessarily *bad*. This follows from property (i) of the family of label sets $(L^{(n)})_n$ (two of the desired labels cannot be combined to another desired label).

Using this crucial observation it is not hard to see that the gates of g_i have to be placed as drawn in Fig. 18. To see this, let us start by proving that g_1 has control at $k+2$ and target at $k+1$. By definition of g_1 it has to target either k or $k+1$ (the qubits of g). There are four possible cases under a linear connectivity constraint:

- (i) control at $k-1$, target at k .
- (ii) control at k , target at $k+1$.
- (iii) control at $k+1$, target at k .
- (iv) control at $k+2$, target at $k+1$.

The first case is not possible because typicality of g_1 would imply that the spacetime points (k, m_1) to (k, m) are good which in turn contradicts g being typical due to our crucial observation. In the second case, the spacetime points $(k+1, m_1-1)$ and $(k+1, m)$ would contain the same label, again contradicting typicality of g . In the third case, the spacetime point $(k, m-1)$ would be good, which is not possible due to the same reasons as in the first case. Hence, only the last case remains - as desired. The arguments for the other two gates are basically the same.

Hence, the gates are positioned as shown in Fig. 18. On the other hand, this implies that the spacetime points $(k+1, m_3-1)$ and $(k+1, m)$ have the same label - contradicting typicality of g . This shows the first claim.

d. *Proof of claim 2:* Given an untypical gate u we have to find an absolute upper bound N on the number of typical gates g such that $U(g) = u$. Assume that the support of u (control and target) is $\{k, k+1\}$. Then any g with $U(g) = u$ must be supported on $\{k-3, \dots, k+4\}$. More precisely its support is one of seven possibilities $\{k-3, k-2\}$, $\{k-2, k-1\}$, ..., $\{k+3, k+4\}$. But for each of these seven supports there can only be at most three corresponding g with $U(g) = u$ (the fourth one would have all of the other three gates in the way towards u). Hence in total there are at most three times seven (i.e. 21) g with $U(g) = u$. In other words, $N = 21$ is an upper bound as desired.

e. *Improving the bound N in claim 2:* The preceding argument is rather crude and merely serves as a simple argument to see the existence of N . One may ask what the optimal value for N is to ultimately find a better bound for γ . But note that the optimal γ might still be larger than the optimal N suggests (we believe that this is indeed the case).

Again consider an untypical u . Using the fact that typical gates come at an alternating pattern (see Fig. 18) we can see that there can be at most five gates g such that $U(g) = u$.

In Fig. 19 we show a *hypothetical* scenario for which $u = U(g^{(i)})$ for $i \in \{1, \dots, 5\}$. Up to certain trivial changes this is actually the only scenario for which $U^{-1}(u)$ has (at most) five elements.

There are still two cases to consider: The gate g can either be present or not. Although we have $U(g) \neq u$ the presence of this gate can in principle influence the pre-image. Interestingly both cases are not possible! If the gate g is not present it is easy to see that $g^{(1)}$ cannot be typical (which would imply $U(g^{(2)}) = g^{(1)} \neq u$). In fact, label ℓ_3 would be regenerated by $g^{(1)}$. If g is present $g^{(2)}$ cannot be typical because it would regenerate ℓ_3 .

Hence we showed that four is an upper bound for N and hence the theorem holds for $\gamma = \frac{1}{9}$. \square

[1] F. Arute, K. Arya, R. Babbush, D. Bacon, J. C. Bardin, R. Barends, R. Biswas, S. Boixo, F. G. S. L. Brandao, D. A. Buell, B. Burkett, Y. Chen, Z. Chen, B. Chiaro, R. Collins, W. Courtney, A. Dunsworth, E. Farhi, B. Foxen, A. Fowler, C. Gidney, M. Giustina, R. Graff, K. Guerin, S. Habegger, M. P. Harrigan, M. J. Hartmann, A. Ho, M. Hoffmann, T. Huang, T. S. Humble, S. V. Isakov, E. Jeffrey, Z. Jiang,

D. Kafri, K. Kechedzhi, J. Kelly, P. V. Klimov, S. Knysh, A. Korotkov, F. Kostritsa, D. Landhuis, M. Lindmark, E. Lucero, D. Lyakh, S. Mandrà, J. R. McClean, M. McEwen, A. Megrant, X. Mi, K. Michelsen, M. Mohseni, J. Mutus, O. Naaman, M. Neeley, C. Neill, M. Y. Niu, E. Ostby, A. Petukhov, J. C. Platt, C. Quintana, E. G. Rieffel, P. Roushan, N. C. Rubin, D. Sank, K. J. Satzinger, V. Smelyanskiy, K. J. Sung, M. D. Tre

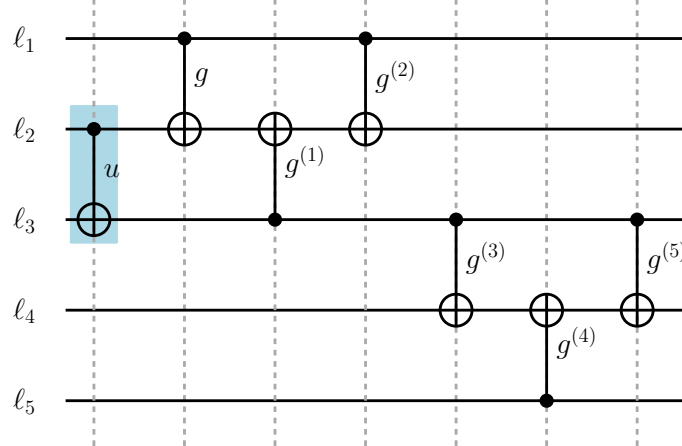


FIG. 19. The only *hypothetically* possible scenario for an untypical gate u for which $U^{-1}(u) (= \{g^{(i)} \mid i = 1, \dots, 5\})$ has (at most) five elements. The gate g can either be present or not. In both cases, using label tracking we see that this scenario is not possible concluding that $U^{-1}(u)$ has at most four elements for any untypical u .

vithick, A. Vainsencher, B. Villalonga, T. White, Z. J. Yao, P. Yeh, A. Zalcman, H. Neven, and J. M. Martinis, Quantum supremacy using a programmable superconducting processor, [Nature 574, 505 \(2019\)](#).

[2] S. A. Moses, C. H. Baldwin, M. S. Allman, R. Arconia, L. Ascarrunz, C. Barnes, J. Bartolotta, B. Bjork, P. Blanchard, M. Bohn, J. G. Bohnet, N. C. Brown, N. Q. Burdick, W. C. Burton, S. L. Campbell, J. P. Campora, C. Carron, J. Chambers, J. W. Chan, Y. H. Chen, A. Chernoguzov, E. Chertkov, J. Colina, J. P. Curtis, R. Daniel, M. DeCross, D. Deen, C. Delaney, J. M. Dreiling, C. T. Ertsgaard, J. Esposito, B. Estey, M. Fabrikant, C. Figgatt, C. Foltz, M. Foss-Feig, D. Francois, J. P. Gaebler, T. M. Gatterman, C. N. Gilbreth, J. Giles, E. Glynn, A. Hall, A. M. Hankin, A. Hansen, D. Hayes, B. Higashi, I. M. Hoffman, B. Horning, J. J. Hout, R. Jacobs, J. Johansen, L. Jones, J. Karcz, T. Klein, P. Lauria, P. Lee, D. Liefer, S. T. Lu, D. Lucchetti, C. Lytle, A. Malm, M. Matheny, B. Mathewson, K. Mayer, D. B. Miller, M. Mills, B. Neyenhuis, L. Nugent, S. Olson, J. Parks, G. N. Price, Z. Price, M. Pugh, A. Ransford, A. P. Reed, C. Roman, M. Rowe, C. Ryan-Anderson, S. Sanders, J. Sedlacek, P. Shevchuk, P. Siegfried, T. Skripka, B. Spaun, R. T. Sprenkle, R. P. Stutz, M. Swallows, R. I. Tobey, A. Tran, T. Tran, E. Vogt, C. Volin, J. Walker, A. M. Zolot, and J. M. Pino, A race-track trapped-ion quantum processor, [Phys. Rev. X 13, 041052 \(2023\)](#).

[3] Y. Kim, A. Eddins, S. Anand, K. X. Wei, E. van den Berg, S. Rosenblatt, H. Nayfeh, Y. Wu, M. Zaletel, K. Temme, and A. Kandala, Evidence for the utility of quantum computing before fault tolerance, [Nature 618, 500 \(2023\)](#).

[4] D. Bluvstein, S. J. Evered, A. A. Geim, S. H. Li, H. Zhou, T. Manovitz, S. Ebadi, M. Cain, M. Kalinowski, D. Hangleiter, J. P. Bonilla Ataides, N. Maskara, I. Cong, X. Gao, P. Sales Rodriguez, T. Karolyshyn, G. Semeghini, M. J. Gullans, M. Greiner, V. Vuletić, and M. D. Lukin, Logical quantum processor based on reconfigurable atom arrays, [Nature 626, 58 \(2024\)](#).

[5] R. Acharya, D. A. Abanin, L. Aghababaie-Beni, I. Aleiner, T. I. Andersen, M. Ansmann, F. Arute, K. Arya, A. Asfaw, N. Astrakhantsev, J. Atalaya, R. Babbush, D. Bacon, B. Ballard, J. C. Bardin, J. Bausch, A. Bengtsson, A. Bilmes, S. Blackwell, S. Boixo, G. Bortoli, A. Bourassa, J. Bovaird, L. Brill, M. Broughton, D. A. Browne, B. Buehea, B. B. Buckley, D. A. Buell, T. Burger, B. Burkett, N. Bushnell, A. Cabrera, J. Campero, H.-S. Chang, Y. Chen, Z. Chen, B. Chiaro, D. Chik, C. Chou, J. Claes, A. Y. Cleland, J. Cogan, R. Collins, P. Conner, W. Courtney, A. L. Crook, B. Curtin, S. Das, A. Davies, L. De Lorenzo, D. M. Debroy, S. Demura, M. Devoret, A. Di Paolo, P. Donohoe, I. Drozdov, A. Dunsworth, C. Earle, T. Edlich, A. Eickbusch, A. M. Elbag, M. Elzouka, C. Erickson, L. Faoro, E. Farhi, V. S. Ferreira, L. F. Burgos, E. Forati, A. G. Fowler, B. Foxen, S. Gajjam, G. Garcia, R. Gosula, A. G. Dau, D. Graumann, A. Greene, J. A. Gross, S. Habegger, J. Hall, M. C. Hamilton, M. Hansen, M. P. Harrigan, S. D. Harrington, F. J. H. Heras, S. Heslin, P. Heu, O. Higgott, G. Hill, J. Hilton, G. Holland, S. Hong, H.-Y. Huang, A. Huff, W. J. Huggins, L. B. Ioffe, S. V. Isakov, J. Iveland, E. Jeffrey, Z. Jiang, C. Jones, S. Jordan, C. Joshi, P. Juhas, D. Kafri, H. Kang, A. H. Karamlou, K. Kechedzhi, J. Kelly, T. Khaire, T. Khattar, M. Khezri, S. Kim, P. V. Klimov, A. R. Klots, B. Kobrin, P. Kohli, A. N. Korotkov, F. Kostritsa, R. Kothari, B. Kozlovskii, J. M. Kreikebaum, V. D. Kurilovich, N. Lacroix, D. Landhuis, T. Lange-Dei, B. W. Langley, P. Laptev, K.-M. Lau, L. Le Guevel, J. Ledford, J. Lee, K. Lee, Y. D. Lensky, S. Leon, B. J. Lester, W. Y. Li, Y. Li, A. T. Lill, W. Liu, W. P. Livingston, A. Locharla, E. Lucero, D. Lundahl, A. Lunt, S. Madhuk, F. D. Malone, A. Maloney, S. Mandrà, J. Manyika, L. S. Martin, O. Martin, S. Martin, C. Maxfield, J. R. McClean, M. McEwen, S. Meeks, A. Megrant, X. Mi, K. C. Miao, A. Mieszala, R. Molavi, S. Molina, S. Montazeri, A. Morvan, R. Movassagh, W. Mruczkiewicz, O. Naaman, M. Neeley, C. Neill, A. Nersisyan, H. Neven, M. Newman, J. H. Ng, A. Nguyen, M. Nguyen, C.-H. Ni, M. Y. Niu, T. E. O'Brien, W. D. Oliver, A. Opremcak, K. Ottosson, A. Petukhov, A. Pizzuto, J. Platt, R. Potter, O. Pritchard, L. P. Pryadko, C. Quintana, G. Ramachandran, M. J. Reagor, J. Redding,

D. M. Rhodes, G. Roberts, E. Rosenberg, E. Rosenfeld, P. Roushan, N. C. Rubin, N. Saei, D. Sank, K. Sankaragomathi, K. J. Satzinger, H. F. Schurkus, C. Schuster, A. W. Senior, M. J. Shearn, A. Shorter, N. Shutty, V. Shvarts, S. Singh, V. Sivak, J. Skruzny, S. Small, V. Smelyanskiy, W. C. Smith, R. D. Somma, S. Springer, G. Sterling, D. Strain, J. Suchard, A. Szasz, A. Sztein, D. Thor, A. Torres, M. M. Torunbalci, A. Vaishnav, J. Vargas, S. Vdovichev, G. Vidal, B. Villalonga, C. V. Heidweiller, S. Waltman, S. X. Wang, B. Ware, K. Weber, T. Weidel, T. White, K. Wong, B. W. K. Woo, C. Xing, Z. J. Yao, P. Yeh, B. Ying, J. Yoo, N. Yosri, G. Young, A. Zalcman, Y. Zhang, N. Zhu, N. Zobrist, G. Q. AI, and Collaborators, Quantum error correction below the surface code threshold, *Nature* (2024).

[6] K. L. Brown, W. J. Munro, and V. M. Kendon, Using quantum computers for quantum simulation, *Entropy* **12**, 2268 (2010).

[7] H. Bernien, S. Schwartz, A. Keesling, H. Levine, A. Omran, H. Pichler, S. Choi, A. S. Zibrov, M. Endres, M. Greiner, V. Vuletić, and M. D. Lukin, Probing many-body dynamics on a 51-atom quantum simulator, *Nature* **551**, 579 (2017).

[8] Y. Cao, J. Romero, J. P. Olson, M. Degroote, P. D. Johnson, M. Kieferová, I. D. Kivlichan, T. Menke, B. Peropadre, N. P. D. Sawaya, S. Sim, L. Veis, and A. Aspuru-Guzik, Quantum chemistry in the age of quantum computing, *Chemical Reviews* **119**, 10856 (2019).

[9] R. Orús, S. Mugel, and E. Lizaso, Quantum computing for finance: Overview and prospects, *Reviews in Physics* **4**, 100028 (2019).

[10] E. Farhi, J. Goldstone, S. Gutmann, and M. Sipser, Quantum computation by adiabatic evolution, *arXiv:quant-ph/0001106* (2000).

[11] F. E., J. Goldstone, and S. Gutmann, A quantum approximate optimization algorithm, *arXiv:1411.4028* (2014).

[12] M. Cerezo, A. Arrasmith, R. Babbush, S. C. Benjamin, S. Endo, K. Fujii, J. R. McClean, K. Mitarai, X. Yuan, L. Cincio, and P. J. Coles, Variational quantum algorithms, *Nature Reviews Physics* **3**, 625 (2021).

[13] J. Preskill, Quantum Computing in the NISQ era and beyond, *Quantum* **2**, 79 (2018).

[14] L. Gyongyosi and S. Imre, Circuit depth reduction for gate-model quantum computers, *Scientific Reports* **10**, 11229 (2020).

[15] C. Zhang, A. B. Hayes, L. Qiu, Y. Jin, Y. Chen, and E. Z. Zhang, Time-optimal qubit mapping, in *Proceedings of the 26th ACM International Conference on Architectural Support for Programming Languages and Operating Systems*, ASPLOS '21 (Association for Computing Machinery, New York, NY, USA, 2021) p. 360–374.

[16] A. Holmes, S. Johri, G. G. Guerreschi, J. S. Clarke, and A. Y. Matsuura, Impact of qubit connectivity on quantum algorithm performance, *Quantum Science and Technology* **5**, 025009 (2020).

[17] C. Gidney, Halving the cost of quantum addition, *Quantum* **2**, 74 (2018).

[18] P. Schindler, D. Nigg, T. Monz, J. T. Barreiro, E. Martinez, S. X. Wang, S. Quint, M. F. Brandl, V. Nebendahl, C. F. Roos, M. Chwalla, M. Hennrich, and R. Blatt, A quantum information processor with trapped ions, *New Journal of Physics* **15**, 123012 (2013).

[19] C. Piltz, T. Sriarunothai, S. S. Ivanov, S. Wölk, and C. Wunderlich, Versatile microwave-driven trapped ion spin system for quantum information processing, *Science Advances* **2**, e1600093 (2016).

[20] B. Rempfer and K. Oberland, Comparison of superconducting NISQ architectures (2024), *arXiv:2409.02063* [quant-ph].

[21] C. Chamberland, G. Zhu, T. J. Yoder, J. B. Hertzberg, and A. W. Cross, Topological and subsystem codes on low-degree graphs with flag qubits, *Phys. Rev. X* **10**, 011022 (2020).

[22] M. Dupont, B. Evert, M. J. Hodson, B. Sundar, S. Jeffrey, Y. Yamaguchi, D. Feng, F. B. Maciejewski, S. Hadfield, M. S. Alam, Z. Wang, S. Grabbe, P. A. Lott, E. G. Rieffel, D. Venturelli, and M. J. Reagor, Quantum-enhanced greedy combinatorial optimization solver, *Science Advances* **9**, eadi0487 (2023).

[23] G. E. Crooks, Performance of the quantum approximate optimization algorithm on the maximum cut problem (2018), *arXiv:1811.08419* [quant-ph].

[24] I. D. Kivlichan, J. McClean, N. Wiebe, C. Gidney, A. Aspuru-Guzik, G. K.-L. Chan, and R. Babbush, Quantum simulation of electronic structure with linear depth and connectivity, *Phys. Rev. Lett.* **120**, 110501 (2018).

[25] B. O'Gorman, W. J. Huggins, E. G. Rieffel, and K. B. Whaley, Generalized swap networks for near-term quantum computing (2019), *arXiv:1905.05118* [quant-ph].

[26] A. Hashim, R. Rines, V. Omole, R. K. Naik, J. M. Kreikebaum, D. I. Santiago, F. T. Chong, I. Siddiqi, and P. Gokhale, Optimized swap networks with equivalent circuit averaging for qaoa, *Phys. Rev. Res.* **4**, 033028 (2022).

[27] J. Weidenfeller, L. C. Valor, J. Gacon, C. Tornow, L. Bello, S. Woerner, and D. J. Egger, Scaling of the quantum approximate optimization algorithm on superconducting qubit based hardware, *Quantum* **6**, 870 (2022).

[28] S. Z. Pei Yuan, Full characterization of the depth overhead for quantum circuit compilation with arbitrary qubit connectivity constraint, *arXiv:2402.02403* (2024).

[29] V. Kaushal, B. Lekitsch, A. Stahl, J. Hilder, D. Pijn, C. Schmiegelow, A. Bermudez, M. Müller, F. Schmidt-Kaler, and U. Poschinger, Shuttling-based trapped-ion quantum information processing, *AVS Quantum Science* **2**, 014101 (2020).

[30] D. Bluvstein, H. Levine, G. Semeghini, T. T. Wang, S. Ebadi, M. Kalinowski, A. Keesling, N. Maskara, H. Pichler, M. Greiner, V. Vuletić, and M. D. Lukin, A quantum processor based on coherent transport of entangled atom arrays, *Nature* **604**, 451 (2022).

[31] A. Zwerver, S. Amitonov, S. de Snoo, M. Madzik, M. Rimbach-Russ, A. Sammak, G. Scappucci, and L. Vandersypen, Shuttling an electron spin through a silicon quantum dot array, *PRX Quantum* **4**, 030303 (2023).

[32] M. Künne, A. Willmes, M. Oberländer, C. Gorjaew, J. D. Teske, H. Bhardwaj, M. Beer, E. Kammerloher, R. Otten, I. Seidler, R. Xue, L. R. Schreiber, and H. Bluhm, The spinbus architecture for scaling spin qubits with electron shuttling, *Nature Communications* **15**, 4977 (2024).

[33] A. T. Schmitz, N. P. Sawaya, S. Johri, and A. Y. Matsuura, Graph optimization perspective for low-depth trotter-suzuki decomposition, *arXiv:2103.08602* (2021).

[34] A. Meijer-van de Griend and S. Meng Li, Dynamic qubit routing with cnot circuit synthesis for quantum compilation, *Journal Electronic Proceedings in Theoretical Computer Science, EPTCS* **394**, 363 (2023).

[35] B. Klaver, S. Rombouts, M. Fellner, A. Messinger, K. Ender, K. Ludwig, and W. Lechner, Swap-less implementation of quantum algorithms (2024), [arXiv:2408.10907 \[quant-ph\]](https://arxiv.org/abs/2408.10907).

[36] A. Cowtan, S. Dilkes, R. Duncan, W. Simmons, and S. Sivarajah, Phase Gadget Synthesis for Shallow Circuits, *EPTCS* **318**, 213 (2020).

[37] W. Lechner, P. Hauke, and P. Zoller, A quantum annealing architecture with all-to-all connectivity from local interactions, *Science Advances* **1**, e1500838 (2015).

[38] M. Fellner, A. Messinger, K. Ender, and W. Lechner, Universal parity quantum computing, *Phys. Rev. Lett.* **129**, 180503 (2022).

[39] M. Fellner, A. Messinger, K. Ender, and W. Lechner, Applications of universal parity quantum computation, *Phys. Rev. A* **106**, 042442 (2022).

[40] B. Park and D. Ahn, Reducing CNOT count in quantum Fourier transform for the linear nearest-neighbor architecture, *Scientific Reports* **13**, 8638 (2023).

[41] B. Cheng, X.-H. Deng, X. Gu, Y. He, G. Hu, P. Huang, J. Li, B.-C. Lin, D. Lu, Y. Lu, C. Qiu, H. Wang, T. Xin, S. Yu, M.-H. Yung, J. Zeng, S. Zhang, Y. Zhong, X. Peng, F. Nori, and D. Yu, Noisy intermediate-scale quantum computers, *Frontiers of Physics* **18**, 21308 (2023).

[42] D. Collins, N. Linden, and S. Popescu, Nonlocal content of quantum operations, *Phys. Rev. A* **64**, 032302 (2001).

[43] Y. Sung, L. Ding, J. Braumüller, A. Vepsäläinen, B. Kannan, M. Kjaergaard, A. Greene, G. O. Samach, C. McNally, D. Kim, A. Melville, B. M. Niedzielski, M. E. Schwartz, J. L. Yoder, T. P. Orlando, S. Gustavsson, and W. D. Oliver, Realization of high-fidelity cz and zz-free iswap gates with a tunable coupler, *Phys. Rev. X* **11**, 021058 (2021).

[44] K. X. Wei, I. Lauer, E. Pritchett, W. Shanks, D. C. McKay, and A. Javadi-Abhari, Native two-qubit gates in fixed-coupling, fixed-frequency transmons beyond cross-resonance interaction, *PRX Quantum* **5**, 020338 (2024).

[45] M. P. Harrigan, K. J. Sung, M. Neeley, K. J. Satzinger, F. Arute, K. Arya, J. Atalaya, J. C. Bardin, R. Barends, S. Boixo, M. Broughton, B. B. Buckley, D. A. Buell, B. Burkett, N. Bushnell, Y. Chen, Z. Chen, Ben Chiaro, R. Collins, W. Courtney, S. Demura, A. Dunsworth, D. Eppens, A. Fowler, B. Foxen, C. Gidney, M. Giustina, R. Graff, S. Habegger, A. Ho, S. Hong, T. Huang, L. B. Ioffe, S. V. Isakov, E. Jeffrey, Z. Jiang, C. Jones, D. Kafri, K. Kechedzhi, J. Kelly, S. Kim, P. V. Klimov, A. N. Korotkov, F. Kostritsa, D. Landhuis, P. Laptev, M. Lindmark, M. Leib, O. Martin, J. M. Martinis, J. R. McClean, M. McEwen, A. Megrant, X. Mi, M. Mohseni, W. Mruczkiewicz, J. Mutus, O. Naaman, C. Neill, F. Neukart, M. Y. Niu, T. E. O'Brien, B. O'Gorman, E. Ostby, A. Petukhov, H. Putterman, C. Quintana, P. Roushan, N. C. Rubin, D. Sank, A. Skolik, V. Smelyanskiy, D. Strain, M. Streif, M. Szalay, A. Vainsencher, T. White, Z. J. Yao, P. Yeh, A. Zalcman, L. Zhou, H. Neven, D. Bacon, E. Lucero, E. Farhi, and R. Babbush, Quantum approximate optimization of non-planar graph problems on a planar superconducting processor, *Nature Physics* **17**, 332 (2021).

[46] D. Bluvstein, H. Levine, G. Semeghini, T. T. Wang, S. Ebadi, M. Kalinowski, A. Keesling, N. Maskara, H. Pichler, M. Greiner, V. Vuletić, and M. D. Lukin, A quantum processor based on coherent transport of entangled atom arrays, *Nature* **604**, 451 (2022).

[47] K. Blekos, D. Brand, A. Ceschini, C.-H. Chou, R.-H. Li, K. Pandya, and A. Summer, A review on quantum approximate optimization algorithm and its variants, *Physics Reports* **1068**, 1 (2024), a review on Quantum Approximate Optimization Algorithm and its variants.

[48] N. Sachdeva, G. S. Hartnett, S. Maity, S. Marsh, Y. Wang, A. Winick, R. Dougherty, C. D., Y. Q. Chong, M. Hush, P. S. Mundada, C. D. B. Bentley, M. J. Biercuk, and Y. Baum, Quantum optimization using a 127-qubit gate-model ibm quantum computer can outperform quantum annealers for nontrivial binary optimization problems, [arXiv:2406.01743](https://arxiv.org/abs/2406.01743) (2024).

[49] E. Pelofske, A. Bärtschi, L. Cincio, J. Golden, and S. Eidenbenz, Scaling whole-chip QAOA for higher-order Ising spin glass models on heavy-hex graphs, *npj Quantum Information* **10**, 109 (2024).

[50] P. Shor, Algorithms for quantum computation: discrete logarithms and factoring, in *Proceedings 35th Annual Symposium on Foundations of Computer Science* (1994) pp. 124–134.

[51] A. Y. Kitaev, Quantum measurements and the abelian stabilizer problem, [arXiv:quant-ph/9511026](https://arxiv.org/abs/quant-ph/9511026) (1999).

[52] T. G. Draper, Addition on a quantum computer, [arXiv:quant-ph/0008033](https://arxiv.org/abs/quant-ph/0008033) (2000).

[53] L. Ruiz-Perez and J. C. Garcia-Escartin, Quantum arithmetic with the quantum Fourier transform, *Quantum Information Processing* **16**, 152 (2017).

[54] A. W. Harrow, A. Hassidim, and S. Lloyd, Quantum algorithm for linear systems of equations, *Phys. Rev. Lett.* **103**, 150502 (2009).

[55] D. Maslov, Linear depth stabilizer and quantum Fourier transformation circuits with no auxiliary qubits in finite-neighbor quantum architectures, *Phys. Rev. A* **76**, 052310 (2007).

[56] Y. Jin, X. Gao, M. Guo, H. Chen, F. Hua, C. Zhang, and E. Z. Zhang, Quantum Fourier transformation circuits compilation, [arXiv:2312.16114](https://arxiv.org/abs/2312.16114) (2023).

[57] X. Gao, Y. Jin, M. Guo, H. Chen, and E. Z. Zhang, Linear depth qft over ibm heavy-hex architecture (2024), [arXiv:2402.09705 \[quant-ph\]](https://arxiv.org/abs/2402.09705).

[58] E. Bäumer, V. Tripathi, A. Seif, D. Lidar, and D. S. Wang, Quantum Fourier transform using dynamic circuits, [arXiv:2403.09514](https://arxiv.org/abs/2403.09514) (2024).

[59] Y. Takahashi, N. Kunihiro, and K. Ohta, The quantum Fourier transform on a linear nearest neighbor architecture, *Quantum Information & Computation* **7**, 383 (2007).